

# Synthesis of Responsive Polymer Brushes for Sensing Applications

THÈSE N° 5077 (2011)

PRÉSENTÉE LE 30 JUIN 2011

À LA FACULTÉ SCIENCES ET TECHNIQUES DE L'INGÉNIEUR

LABORATOIRE DES POLYMÈRES

PROGRAMME DOCTORAL EN SCIENCE ET GÉNIE DES MATÉRIAUX

ÉCOLE POLYTECHNIQUE FÉDÉRALE DE LAUSANNE

POUR L'OBTENTION DU GRADE DE DOCTEUR ÈS SCIENCES

PAR

Nicolas Bertrand SCHÜWER

acceptée sur proposition du jury:

Prof. D. Damjanovic, président du jury

Prof. H.-A. Klok, directeur de thèse

Prof. E. Bakker, rapporteur

Prof. A. Kilbinger, rapporteur

Prof. P. Mural, rapporteur



ÉCOLE POLYTECHNIQUE  
FÉDÉRALE DE LAUSANNE

Suisse  
2011



The work described in this Thesis has been performed at the École Polytechnique Fédérale de Lausanne from May 2007 until May 2011 under the supervision of Prof. Harm-Anton Klok.

This work was financially supported by the European Commission (Mobesens Project) and the Competence Centre for Materials Science and Technology (CCMX).



*Szeretett feleségemnek és csodálatos lányomnak*



## Acknowledgments

I would like to sincerely thank Prof. Harm-Anton Klok for giving the opportunity to perform the work presented in this Thesis in his laboratory. I am thankful for his motivation, enthusiasm, guidance, support and also his patience. And I am especially grateful for the freedom he offered me to express my own ideas and curiosity.

I would like to express my gratitude to my thesis jury, Prof. Eric Bakker, Prof. Andreas Kilbinger, Prof. Paul Muralt, and Prof. Dragan Damjanovic for taking the time to review and evaluate my work.

In addition, I thank Thomas Geue from the Paul Scherrer Institute for his help with the neutron reflectivity measurements, as well as Mary-Lou Tercier-Waeber from Geneva University for her great help with the voltammetric measurements.

Furthermore, I would like to thank all my colleagues from the Laboratoire des Polymères for the great time. I owe a special thank to the “brush subgroup”: Raph, Sorin, JP, Rich and Solenne and to my lab mate Duško, Caroline, Arda, Carl, Laurent, Tugba and Oxana for the great atmosphere/music in the lab. Many thanks to the other lab members: Bojana, Maarten (special thanks to Maarten for the peptide synthesis), Görkem, Ana, Marie-Hélène, Béatrice, Sanhao, Zuzana, Vitaliy, Nadja, Guillaume, Marc, Matt, Harald, Fred, Tuan, Philippe, Maude, Cindy & Cindy.

I also would like to take the opportunity to thank my colleagues from the IMX Institute; Nicolas Xanthopoulos and Dr. Vincent Laporte for the XPS analysis, and the ATMX team for their great help.

Last, I wish to thank my family, my wife and my daughter for their support, understanding, patience and all the great moments all along these years.





---

## Table of contents

<b>List of Abbreviations</b> .....	<b>iii</b>
<b>Summary</b> .....	<b>1</b>
<b>Résumé</b> .....	<b>5</b>
<b>1. Synthesis and Characterization of Polymer Brushes</b> .....	<b>7</b>
1.1. Introduction .....	7
1.2. Synthesis of Polymer Brushes via SI-ATRP .....	9
1.3. Characterization of polymer brushes .....	12
1.4. References .....	18
<b>2. Responsive Surfaces Based on Polymer Brushes</b> .....	<b>25</b>
2.1. Introduction .....	25
2.2. Solvent Responsive Polymer Brushes .....	25
2.3. Thermoresponsive Polymer Brushes .....	30
2.4. pH and Ion Responsive Polymer brushes .....	35
2.4.1. pH Sensitive Polymer Brushes .....	36
2.4.2. Ions Sensitive Polymer Brushes .....	38
2.5. References .....	40
<b>3. Tuning the pH Sensitivity of Poly(methacrylic acid) Brushes</b> .....	<b>45</b>
3.1. Introduction .....	45
3.2. Results and discussion .....	46
3.2.1. Polymer brush synthesis .....	46
3.2.2. Swelling properties of dense PMAA brushes .....	49
3.2.3. Influence of the polymer brush density on the swelling behavior .....	51
3.2.4. Post-polymerization modification and study of the resulting brushes .....	52
3.3. Conclusions .....	57
3.4. Experimental .....	59
3.4.1. Materials .....	59
3.4.2. Methods .....	59
3.4.3. Procedures .....	60
3.5. References .....	63
3.6. Supporting Information .....	65
<b>4. A Potassium-Selective Quartz Crystal Microbalance Sensor Based on Crown-Ether Functionalized Polymer Brushes</b> .....	<b>71</b>

4.1.	Introduction .....	71
4.2.	Results and discussion .....	72
4.3.	Conclusions .....	77
4.4.	Experimental.....	79
4.4.1.	Materials.....	79
4.4.2.	Methods.....	79
4.4.3.	Precedures .....	80
4.5.	References .....	82
4.6.	Supporting Information .....	84
<b>5.</b>	<b>Peptide Functionalized Polymer Brushes for Voltammetric Based Mercury (II)</b>	
	<b>Detection .....</b>	<b>87</b>
5.1.	Introduction .....	87
5.2.	Results and discussion .....	88
5.2.1.	Synthesis of the Hg <sup>2+</sup> sensitive polymer brush.....	88
5.2.2.	Cyclic voltammetry experiments.....	90
5.2.3.	Square wave voltammetry experiments.....	93
5.3.	Conclusions .....	94
5.4.	Experimental.....	95
5.4.1.	Materials.....	95
5.4.2.	Methods.....	95
5.4.3.	Procedure.....	96
5.5.	References .....	99
5.6.	Supporting Information .....	101
<b>6.</b>	<b>Neutron Reflectivity Study on the Post-Polymerization Modification of Poly(2-hydroxyethyl methacrylate) Brushes.....</b>	<b>105</b>
6.1.	Introduction .....	105
6.2.	Results and discussion .....	106
6.3.	Conclusions .....	113
6.4.	Experimental.....	113
6.4.1.	Materials.....	113
6.4.2.	Methods.....	114
6.4.3.	Procedure.....	115
6.5.	References .....	117
<b>7.</b>	<b>Conclusions and Perspectives.....</b>	<b>119</b>

---

## List of Abbreviations

$\Delta f$	change in resonance frequency
AA	acrylic acid
Abs.	Absorbance
AFM	atomic force microscopy
A(R)GET	activators (re)generated by electron transfer
ATRP	atom transfer radical polymerization
bpy	2,2'-bipyridyl
CDCl <sub>3</sub>	deuterated chloroform
Cu <sup>I</sup> Br	copper (I) bromide
Cu <sup>I</sup> Cl	copper (I) chloride
Cu <sup>II</sup> Br <sub>2</sub>	copper (II) bromide
DMAP	4-(dimethylamino)pyridine
DLS	dynamic light scattering
EBiB	ethyl $\alpha$ -bromoisobutyrate
EDC	<i>N</i> -(3-dimethylaminopropyl)- <i>N'</i> -ethylcarbodiimide hydrochloride
FTIR	Fourier transform infrared
GMA	glycidyl methacrylate
GPC	gel permeation chromatography
h	dry thickness of the polymer brush
H	wet thickness of the polymer brush
HEMA	2-hydroxyethyl methacrylate
HMTETA	1,1,4,7,10,10-hexamethyltriethylene tetramine
GMA	glycidyl methacrylate
LCST	lower critical solution temperature
MBAM	<i>N,N'</i> -methylenebisacrylamide
MMA	methyl methacrylate
$M_n$	number-average molecular weight of the polymer chains
NaMA	sodium methacrylate
NEXAFS	near edge X-ray absorption fine structure analysis
NHS	<i>N</i> -hydroxysuccinimide
NIPAM	<i>N</i> -isopropylacrylamide
NPC	<i>p</i> -nitrophenyl chloroformate
NR	neutron reflectivity
PAA	poly(acrylic acid)
PAM	polyacrylamide
PBMA	poly( <i>n</i> -butyl methacrylate)
PCBMA	poly(carboxybetaine methacrylate)
PCDMA	poly(cadmium dimethacrylate)
PCS	photon correlation spectroscopy
PDEAEMA	poly(2-(diethylamino)ethyl methacrylate)
PPEGMA	poly(poly(ethylene glycol) methacrylate)

PPEGMEMA	poly(poly(ethylene glycol) methyl ether methacrylate)
PPEGMEMA <sub>2</sub>	poly(di(ethylene glycol) methyl ether methacrylate)
PPEGMEMA <sub>3</sub>	poly(tri(ethylene glycol) methyl ether methacrylate)
PDMAEA	poly(2-(dimethylamino) ethyl acrylate)
PDMAEMA	poly(2-(dimethylamino)ethyl methacrylate)
PDMAM	poly( <i>N,N</i> -dimethylacrylamide)
PGMA	poly(glycidyl methacrylate)
PHDFDA	poly(heptadecafluorodecyl acrylate)
PHEMA	poly(2-hydroxyethyl methacrylate)
PHFA	poly(heptadecafluorodecyl acrylate)
PMA	poly(methyl acrylate)
PMAA	poly(methacrylic acid)
PMBAM	poly( <i>N,N'</i> -methylenebisacrylamide)
PMEP	poly(2-methacryloyloxyethyl phosphate)
PMMA	poly(methyl methacrylate)
PNIPAM	poly( <i>N</i> -isopropyl acrylamide)
PNVI	poly( <i>N</i> -vinylimidazole)
PPFA	poly(pentafluoropropyl acrylate)
PPFS	poly(2,3,4,5,6-pentafluorostyrene)
PPFPA	poly(pentafluoropropyl acrylate)
PS	polystyrene
PSBMA	poly(sulfobetaine methacrylate)
PSEMA	poly(2-sulfatoethyl methacrylate)
PSS(Na)	poly(sodium 4-styrenesulfonate)
PTFA	poly(trifluoroethyl acrylate)
P4VP	poly(4-vinylpyridine)
PVB(Na)	poly(sodium 4-vinylbenzoate)
q	scattering vector
QCM	quartz crystal microbalance
QCM-D	quartz crystal microbalance with dissipation
QELS	quasi-elastic light scattering
SI-ATRP	surface-initiated atom transfer radical polymerization
SI-CRP	surface-initiated controlled radical polymerization
SI-NMP	surface-initiated nitroxide-mediated polymerization
SI-PIMP	surface-initiated photoiniferter-mediated polymerization
SI-RAFT	surface-initiated reversible-addition fragmentation chain transfer
SLD	scattering length density
SPM	scanning probe microscopy
SPR	surface plasmon resonance
TGA	thermogravimetric analysis
TOF-SIMS	time-of-flight secondary ion mass spectroscopy
UCST	upper critical solution temperature
WCA	water contact angle

XPS	X-ray photoelectron spectroscopy
XRR	X-ray reflectivity
$z$	distance form the surface
$\sigma$	grafting density of the polymer brush
$\rho$	density of the polymer
$\rho_D$	SLD of the post-modified PHEMA at the brush-air interface
$\rho_{\text{HEMA}}$	SLD of PHEMA
$\rho(z)$	SLD at the distance $z$ of the surface
$\phi(z)$	volume fraction of deuterated at a distance $z$ form the surface
$\mu$ -GISAXS	microfocus grazing incidence small-angle X-ray scattering



## Summary

During the past decades the field of sensors has been subject to much attention due to an increased demand for (bio)sensors and environmental monitoring. The efforts have been concentrated to create sensors which are reliable, highly sensitive and selective, small and fast responding. Surface modification by polymer coating has been proven an excellent method to introduce selectivity on actuators. Among the various techniques that allow the formation of polymer thin film, polymer brushes have gained attention along the past decades due to their unique structure and the possibility offered by controlled/"living" surface-initiated radical polymerization technique to generate polymer thin film with precisely controlled thickness, composition and architecture.

Polymer brushes have found numerous applications including nonbiofouling surfaces and cell adhesive surfaces, protein binding and immobilization, chromatography supports, membrane functionalization, responsive surface, antibacterial coatings or low friction surfaces. Despite their interesting properties and the numerous reports describing the potential of polymer brush as responsive surface, their use for "real" sensing applications has received little or no attention so far. This Thesis describes how polymer brushes can be employed as selective surface modification for sensing application. We aimed at synthesizing polymer thin film able to detect analytes of interest, with a particular focus on low detection limit and high selectivity.

After a short introduction to the field of polymer brushes (**Chapter 1**), **Chapter 2** presents a review of the work accomplished in the field of responsive polymer brushes with an emphasis on solvent responsive, thermoresponsive, pH- and ion-sensitive polymer brushes.

The pH-induced swelling and collapse of surface-tethered, weak polyelectrolyte brushes is of interest not only for the development of responsive surface coatings but also for the pH controlled transport or adsorption. **Chapter 3** discusses results of an extensive series of quartz crystal microbalance (QCM) experiments that aimed at further understanding the influence of brush thickness and density on the pH-responsiveness of poly(methacrylic acid) (PMAA) brushes and developing strategies that allow to engineer the pH responsiveness and dynamic response range of PMAA based brushes. It was observed that due to their high grafting density, the apparent pKa of surface-tethered PMAA differs from that of the corresponding free polymer in solution and also covers a broader pH range. The pKa of the PMAA brushes was found to depend both on brush

thickness and density; thicker brushes showed a higher pKa value and brushes of higher density started to swell at higher pH. The second part of this section demonstrates the feasibility of the *N*-hydroxysuccinimide-mediated post-polymerization modification to engineer the pH responsiveness of the PMAA brushes. By using appropriate amine functionalized acids, it was possible to tune both the pH of maximum response as well as the dynamic response range of these PMAA based polyelectrolyte brushes.

In **Chapter 4**, benzo-15-crown-5 functionalized polymer brushes prepared via surface-initiated atom transfer radical polymerization were used as the active layer in a potassium-selective QCM sensor. The polymer brushes allowed the selective detection of potassium ions, even in the presence of a large excess of sodium ions and the sensitivity of the sensor could be tuned by varying the brush thickness.

**Chapter 5** demonstrates the possibility to use peptide functionalized polymer brush, prepared via surface-initiated atom transfer radical polymerization (SI-ATRP), to probe heavy metal ions via voltammetric based methods. The polymer brush enhanced the mercury (II) ions sensitivity as compared to the bar electrode and allowed the detection of mercury down to the nanomolar concentration range. Furthermore it was demonstrated that the heavy metal recognition is a reversible and reproducible process.

Post-polymerization modification reactions are widely employed to prepare functional polymer brushes. Relatively little is known, however, about the distribution of functional groups in such post-modified brushes. Using neutron reflectivity and UV-visible spectroscopy as principal tools, **Chapter 6** investigates the *p*-nitrophenyl chloroformate (NPC) mediated post-polymerization modification of poly(2-hydroxyethyl methacrylate) (PHEMA) brushes, prepared via surface-initiated atom transfer radical polymerization, with D-10 leucine and D-3 serine. The neutron reflectivity experiments indicate that the post-polymerization modification depends both on the brush thickness and density. Whereas, for dense brushes, post-polymerization modification with D-10 leucine is limited to the top  $\sim 200$  Å of the brush, independently of the brush thickness, the extent of post-modification can be significantly extended by decreasing brush density, or by using the more hydrophilic and sterically less demanding D-3 serine, which reflects the ability of this amino acid to more readily penetrate the brush. UV-vis. experiment revealed that the NPC activation is also non-uniform, but brush thickness and density dependent, which adds to brush thickness, density and the nature of the amino acid as another of a complex set of variables that determine the final distribution of functional groups in post-modified brushes.



**Keywords:** polymer brush, controlled radical polymerization (CRP), surface-initiated polymerization (SIP), surface-initiated atom transfer radical polymerization (SI-ATRP), post-polymerization modification, responsive surface, sensor, crown-ether, mercury (II) detection, potassium sensing, pH responsiveness, cyclic voltammetry, square wave voltammetry, quartz crystal microbalance, neutron reflectivity.



## Résumé

Au cours des dernières décennies, le domaine des capteurs a été le sujet de nombreuses recherches en raison d'une demande accrue pour les (bio)capteurs et la surveillance environnementale. Les efforts se sont concentrés sur le développement de capteurs fiables, à haute sensibilité et sélectivité, ainsi que sur la miniaturisation des systèmes. La modification de capteurs par des couches minces de polymères est une méthode efficace pour introduire une sélectivité de détection. Parmi les différentes techniques qui permettent la formation de couches minces de polymères, la polymérisation initiée à partir de la surface a été l'objet de nombreuses études au cours de la dernière décennie en raison des possibilités uniques offertes par cette méthode pour la création de couches minces de polymères au sein desquelles toutes les chaînes sont attachées par l'une de leur extrémité à la surface (structure dite en "brosse"). Ce genre de revêtement polymérique a trouvé de nombreuses applications dans de différents domaines tel que la chromatographie, la fonctionnalisation de membranes, la synthèse de revêtement sensible, ainsi que dans le monde biomédicale.

Cette thèse décrit l'utilisation de couches minces de polymères, synthétisés par polymérisation radicalaire contrôlée, pour la détection sélective d'ions. Le but visé par ce travail est la synthèse de couches minces capables de détecter sélectivement un analyte, avec un accent particulier pour des limites de détection basses et une haute sélectivité. Après une brève introduction au domaine des revêtements polymériques ayant une structure en "brosse" (**Chapitre 1**); le **Chapitre 2** se concentre sur le travail accompli dans le domaine des couches minces de polymères sensibles aux pH, ions, température et solvants. L'influence du pH sur la conformation de couches minces de polyelectrolytes faibles contenant des groupes carboxyliques est traitée dans le **Chapitre 3**. Le comportement de différentes couches d'acide polyméthacrylique a été étudié en détails, et l'influence de l'épaisseur de la couche et de la densité de greffage des chaînes de polymères, au sein du revêtement, sur le pKa apparent a été étudié. En outre il a été démontré que la sensibilité au pH peut être ajustée en utilisant des réactions simples de couplage. Dans le **Chapitre 4**, les propriétés de couches minces de polymères contenant des éthers couronnes sont étudiées à l'aide d'une microbalance à quartz. Ces revêtements permettent la détection sélective des ions potassium, même en présence d'un grand excès d'ions d'interférence et la sensibilité du capteur peut être réglée en faisant varier l'épaisseur de la couche de polymère. Le **Chapitre 5** est dédié à l'utilisation de "brosse"

de polymères, fonctionnalisées avec un peptide, pour mesurer la concentration de métaux lourds en milieu aqueux. Dans cette étude, la réponse des couches de polymères a été mesurée par des méthodes voltamétriques. Le système synthétisé présente une sensibilité accrue au mercure en comparaison d'une électrode simple sans polymère. Par ailleurs, il a été démontré que la reconnaissance des ions mercure (II) est un procédé électrochimique réversible et reproductible. Le dernier chapitre (**Chapitre 6**) traite d'une question plus fondamentale. Utilisant la réflectométrie de neutron, la répartition de molécules deutérées, introduite par réaction de couplage, dans des couches minces de polymères a été déterminée en utilisant le contraste élevé entre la diffusion de neutrons par l'hydrogène et le deutérium. L'influence de la longueur des chaînes de polymères et de la densité de greffage (distance entre les chaînes de polymères) sur la répartition finale des molécules deutérées a été étudiée.

**Mots-clés:** brosses de polymères, polymérisation radicalaire contrôlée, polymérisation depuis une surface, couplage post-polymérisation, surface sensible, capteur, éther-couronne, détection du mercure (II), mesure de la concentration d'ions potassium, pH, voltamétrie cyclique, microbalance à cristal de quartz, réflectivité de neutrons.

# 1. Synthesis and Characterization of Polymer Brushes

## 1.1. Introduction

Surface modification is a key field in materials science since surface chemistry drives the interaction of an object with its surrounding environment and thus the application of materials. Standard surface-coating techniques encompass evaporation based methods, spin- and dip-coating, drop-casting or Langmuir-Blodgett deposition. Even if these techniques are well-established, they are subject to several limitations originating from the weak physical interactions between the substrate and the coated specie. Therefore the films created by the above mentioned methods usually suffer from desorption during solvent exposure; displacement by molecules which have a stronger interaction with the surface, or dewetting and delamination. These issues have pushed researchers to look for covalently bound materials in order to enhance the stability of polymer coatings.

Anchoring polymer chains to a surface and/or an interface can be accomplished by two methods, the “grafting to” approach (Figure 1A) and the “grafting from” approach (Figure 1B). In the “historic” grafting to strategy, the surface is modified with preformed polymer chains either via physisorption or chemisorption. Physisorption is achieved by self-assembly of block copolymers in which at least one block has a preferential adsorption for the surface. The efficiency of this technique is driven by solvent-polymer interaction, as well as hydrophobic/hydrophilic and/or columbic interaction between the surface and the polymer. In this method the polymer chains are reversibly attached to the substrate and can be cleaved off from the surface via solvent exchange, thermal treatment and competitive absorption. This non covalent attachment of the polymer chains strongly limits the stability of the assembly and restricts the use and application of such coatings. Surface-tethered polymer chains assembly of enhanced stability can be obtained by chemisorption of an ends functional polymer chains onto a complementary surface. This method presents the advantage to form a covalent linkage between the polymer chain and the surface, contrary to the physisorption route. Although they present a relative experimental simplicity, due to steric hindrance of the coiled polymer chains, both physisorption and chemisorption approaches do not allow the synthesis of densely packed

arrangement of surface grafted polymer chains. Only limited amount of polymer chains can be tethered with these methods, since the polymer chain need to diffuse through the already formed polymer layer in order to react with the surface. Thus, the “grafting to” method is only able to generate polymer layers of low densities and as a direct consequence the film thicknesses obtained by this protocol are restricted to few nanometers.<sup>1,2</sup>

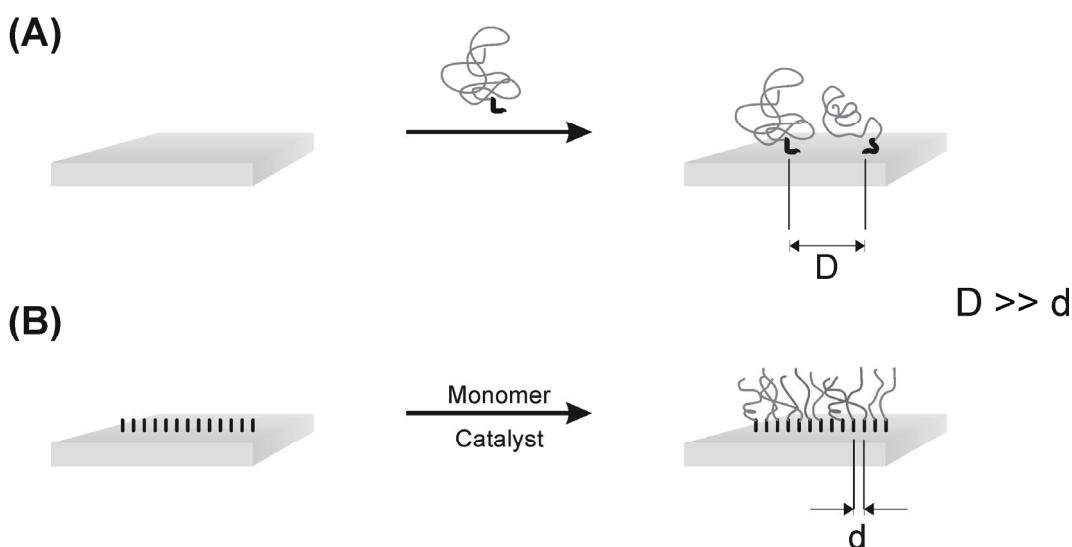


**Figure 1.** Synthetic strategies to surface-anchored polymer chains assembly. (A) Physisorption of a preformed polymers (“grafting to” approach); (B) polymer brushes grown via surface-initiated polymerization techniques (“grafting from” approach). “D” and “d” represent the two different grafting densities.

The “grafting from” approach represents a powerful tool to generate polymer tethered layers in which all polymer chains are attached covalently with one of their chain ends to the substrate. This densely packed arrangement of surface grafted polymer chains is refer to as polymer brush.<sup>3</sup> In a polymer brush the grafting density is such that steric repulsions force the chains to stretch out from the surface in order to avoid overlapping. Polymer brushes are grown from a surface via a two steps surface-initiated polymerization. First, the substrate is modified with a polymerization initiator (or a polymerization active molecule), followed by the direct surface-initiated polymerization of the monomer. The thickness of the film is thus controlled by the polymerization condition and can be accurately controlled via the polymerization reaction time. The use of controlled/“living” surface-initiated radical polymerization techniques allows to precisely control the

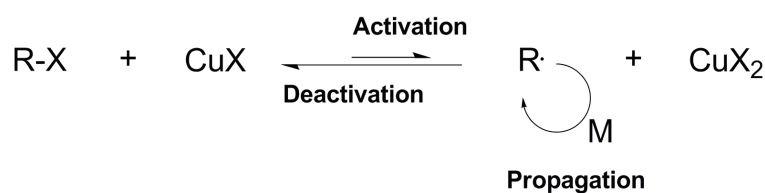
thickness, composition and architecture of polymer brushes, which makes them very attractive coatings to control the surface properties of a broad range of materials. Contrary to the “grafting to” approach, surface-initiated polymerization allows the synthesis polymer layer with high and controlled densities; and film thicknesses up to 700 nm can be achieved.<sup>4</sup>

## 1.2. Synthesis of Polymer Brushes via Surface-Initiated Atom Transfer Radical Polymerization

Due to their advantages in terms of compatibility with both aqueous and organic media as well as a high tolerance towards a wide range of functional groups, controlled/“living” radical-based polymerization have been most frequently used as compared to other polymerization techniques (*i.e.* ionic polymerization). In the scope of this Thesis, we will only focus on surface-initiated atom transfer radical polymerization (SI-ATRP). The other surface-initiated controlled radical polymerization (SI-CRP); namely surface-initiated reversible-addition fragmentation chain transfer (SI-RAFT), surface-initiated nitroxide-mediated polymerization (SI-NMP), surface-initiated photoiniferter-mediated polymerization (SI-PIMP), will not be discussed. The interested reader can refer to references 2,5-8 for more details on the other (SI)-CRP techniques.

Amongst the different controlled radical polymerization techniques that are available, atom transfer radical polymerization (ATRP) has been most extensively used to produce polymer brushes due to its high versatility and robustness. ATRP was first reported, in solution, in 1995<sup>9-11</sup> and has been extensively reviewed since.<sup>12-16</sup> The commonly accepted mechanism for atom transfer radical polymerization is displayed in Scheme 1. This polymerization technique relies on the reversible redox activation of a dormant alkyl halide-terminated polymer chain end by a halogen transfer to a transition metal complex (most frequently copper based). The homolytic cleavage of the carbon-halogen bond generates a free and active carbon-centered radical species at the polymer chain end. This activation step is based on a single electron transfer from the transition metal complex to the halogen atom, which leads to the oxidation of the transition metal complex. Then, in a fast, reversible reaction, the oxidized form of the catalyst reconverts the propagating

radical chain end to the corresponding halogen-capped dormant species (deactivation). The controlled nature of the ATRP comes from the equilibrium between activate/dormant species (highly shifted toward the deactivated form), which induces low propagating radical concentrations. This mechanism contrasts with free-radical polymerization in which the radicals propagate in a free manner until complete conversion of the monomer or termination.



**Scheme 1.** Schematic representation of the mechanism for atom transfer radical polymerization.

Many parameters, such as ligand to transition metal ratio,  $\text{Cu}^{\text{II}}$  to  $\text{Cu}^{\text{I}}$  ratio, chemical structure of the ligand, counterion, solvent or initiator, influence the performance of (SI)-ATRP, and thus offer the possibility to fine tune the reaction.<sup>17-25</sup>

Surface-initiated atom transfer radical polymerization (SI-ATRP) was first reported in 1997 by Huang and Wirth who successfully grafted poly(acrylamide) (PAM) brushes from benzylchloride-derivatized silica particles.<sup>26</sup> The main difference between ATRP in solution and SI-ATRP is that in the latter case the polymerization initiator is immobilized of the surface (Scheme 2). The mechanism of the polymerization, however, is assumed to be similar for both solution and surface-initiated polymerization.

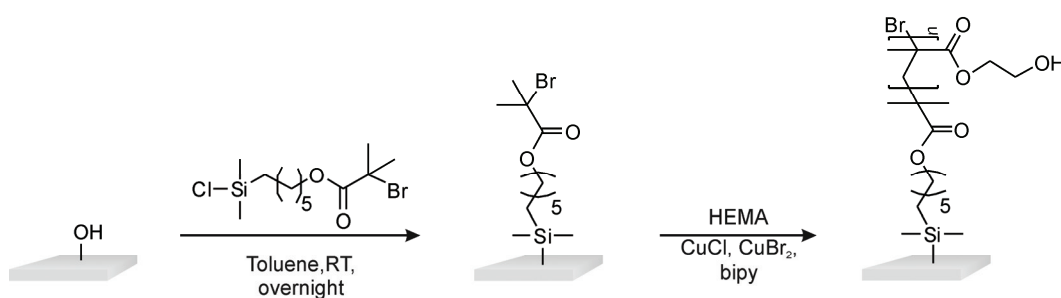
SI-ATRP has been demonstrated to be a versatile method to prepare polymer brushes grafted from various substrates, including silicon, silicon oxide, metal oxide, clay, gold, metal and semiconductor, carbon or polymer surfaces. This polymerization technique also allows the precisely control the density and architecture of the polymer layer and allows the formation of block, gradient and random copolymer, as well as hyperbranched, comb-shaped and/or cross-linked polymer brushes.<sup>8</sup>

It was observed that addition of free, sacrificial initiator was necessary to achieve a controlled polymerization. In the absence of sacrificial initiator, the initiator concentration, and related to this, the concentration of the deactivating  $\text{Cu}^{\text{II}}$  species, was too low to allow a controlled polymerization.<sup>27</sup> Instead of adding a sacrificial initiator, another strategy to overcome the insufficient deactivator concentration that results from



surface-confined ATRP is to add the deactivating  $\text{Cu}^{\text{II}}$  species directly to the polymerization solution.<sup>28</sup>

A significant increase in the rate of SI-ATRP was observed for polymerizations carried out in polar solvent and in particular aqueous media.<sup>19,22,29,30</sup> Jones *et al.* synthesized 50 nm-thick PMMA brushes in a controlled fashion within 4 hours of polymerization time using a  $\text{Cu}^{\text{I}}\text{Br}/2,2'$ -bipyridine (bpy) catalyst system in water/methanol mixture as solvent.<sup>31</sup> A purely aqueous-based system was used by Huang *et al.* for the preparation of 700 nm-thick poly(2-hydroxyethyl methacrylate) (PHEMA) brushes via “water-accelerated” SI-ATRP using a mixed halide  $\text{Cu}^{\text{I}}\text{Cl}/\text{Cu}^{\text{II}}\text{Br}_2/\text{bpy}$  catalyst system.<sup>32</sup> As described by Matyjaszewski *et al.*, the use of such mixed halide systems represents, because of the higher free energy of dissociation of the C-Cl bond compared to C-Br bond, a valuable tool to shift the equilibrium between dormant and propagating radical species on the side of dormant species, which leads to an increase over the control of the polymerization.<sup>33</sup>



**Scheme 2.** Surface-initiated atom transfer radical polymerization of 2-hydroxyethyl methacrylate.

The (possible) presence of residual amounts of the metal catalyst in polymers prepared via (SI)-ATRP often raises concerns, in particular with the use of these materials in (bio)medical applications. Matyjaszewski and coworkers have developed an ATRP variant that allows to overcome these concerns and which makes it possible to reduce the concentration of the copper catalyst to a few ppm and increases the tolerance towards oxygen or other radical traps in the polymerization system. This ATRP variant is referred to as activators (re)generated by electron transfer ATRP or A(R)GET ATRP.<sup>34-38</sup> A(R)GET ATRP involves the use of reducing agents, such as ascorbic acid,  $\text{Sn}^{\text{II}}$  2-

ethylhexanoate or  $\text{Cu}^0$ , to continuously restore  $\text{Cu}^I$  from  $\text{Cu}^{II}$  and has also been successfully applied to surface-initiated polymerization.<sup>39-45</sup>

Summarizing, SI-ATRP has been proven an excellent technique to prepare polymer brushes. ATRP is chemically versatile, compatible with a large assortment of monomers and functional groups and tolerates a relatively high degree of impurities. In particular, ATRP is relatively insensitive towards small residual traces of oxygen, which are readily removed by oxidation of the ATRP catalyst. The fact that most of the standard ATRP catalyst systems, as well as surface immobilizable initiators are commercially available in ready-to-use quality, or can be synthesized relatively easily, also makes ATRP an attractive technique from an experimental point of view. SI-ATRP, however, also has limitations. In particular, the controlled polymerization of monomers that can complex or react with the metal catalyst, such as pyridine-containing or acidic monomers, can be challenging. For pyridinic monomers, this problem can be partially overcome by using highly coordinative tri- or tetradentate ligands to form the catalytic transition metal complex.<sup>46,47</sup> The preparation of acidic polymer brushes has been accomplished via ATRP of the corresponding sodium salts.<sup>48-54</sup> An interesting exception has been reported in a recent publication by Jain *et al.*, who reported the first example of successful direct SI-ATRP of a protonated acidic monomer, 2-(methacryloyloxy)ethyl succinate (MES).<sup>54</sup> Another limitation of (SI)-ATRP is related to the transition metal catalyst, which can be difficult to remove. Residual traces of catalysts in the final polymer brushes might have undesirable consequences for applications, such as in biomedical or electronic industry. However, some methods, in particular A(R)GET ATRP, have been developed that allow to reduce the amount of copper to the level of a few ppm.<sup>16</sup>

### 1.3. Characterization of polymer brushes

The characterization of polymer brushes can be a challenging task since many of the analytical tools in polymer science are solution-based techniques. Table 1 provides an overview of the different techniques that have been used to characterize polymer brushes. For a broad variety of polymer brush properties, Table 1 lists the analytical methods that are available to study that particular property. Instead of discussing the technical details of all the analytical techniques, this section will highlight how some of the most

prominent properties of a polymer brush can be studied with the analytical tools that are currently available.

**Table 1.** Overview of analytical techniques that are available for the characterization of polymer brushes.

Property	Methods														
	SPM	Optical and electron microscopy	Electrochemistry	Ellipsometry	Infrared spectroscopy	Contact angle measurement	SPR	TOF-SIMS	QCM(-D)	XPS	XRR	TGA	NR	GPC	NEXAFS
Chemical composition and structure					x	x		55,56		x					57
Thickness	58,59	60		x							61,62	50,63	x		
Molecular weight and molecular weight distribution	64,65													2,66	
Brush density <sup>a</sup>	x			x								67		x	
Topography and surface structure	x	68,69				x		70		71,72	61,62				
Stiffness	x									x					
Conformation and swelling	73,74		75,76	77,78	x	x	73,79		80,81				x		82
Polymerization kinetics	x			x											83,84
Electronic and electrochemical properties			85,86												

<sup>a</sup>: To determine the density of a polymer brush, a combination of different methods has to be used. SPM: scanning probe microscopy; SPR: surface plasmon resonance; TOF-SIMS: time-of-flight secondary ion mass spectroscopy; QCM(-D): quartz crystal microbalance (with dissipation monitoring); XPS: X-ray photoelectron spectroscopy; XRR: X-ray reflectivity; TGA: thermogravimetric analysis; NR: neutron reflectivity; GPC: gel permeation chromatography; NEXAFS: near edge X-ray absorption fine structure analysis.

A wide range of techniques can be used to probe the chemical composition and structure of a polymer brush. IR spectroscopy is a useful tool to qualitatively provide evidence for the presence of certain functional groups. For the characterization of very thin films, the sensitivity can be improved by using special techniques such as grazing-angle reflection-absorption infrared spectroscopy.<sup>87</sup> XPS can provide quantitative information about the chemical composition of a polymer brush and can also give insight into the chemical structure of the analyzed material. Depending on the sample that is investigated, the penetration depth of the X-ray beam varies from 2 to 10 nm. One of the attractive features of XPS is that it also allows depth profiling<sup>88</sup> and mapping analysis.<sup>71,89</sup> Time-of-flight secondary ion mass spectroscopy (TOF-SIMS) has also been used by different groups.<sup>55</sup> This method gives information on the chemical surface composition and also allows depth profiling analysis<sup>56</sup> and surface mapping.<sup>70</sup> Auger electron spectroscopy (AES) can also be used to determine chemical composition but, in contrast to XPS, this technique requires conducting samples.<sup>90</sup> Near-edge X-ray absorption fine structure (NEXAFS) analysis provides information on bond-type and molecular orientation of the chemical groups populating the top 3 nm of a polymer brush-covered substrate.<sup>57</sup>

Ellipsometry is a convenient and accurate tool to determine the thickness of an initiator monolayer or a polymer brush. Alternatively, AFM can also be used, but this requires the use of patterned brushes or mechanically removing (scratching) part of the polymer brush coating prior to the analysis. It has been observed, however, that under high load conditions, the AFM tip can compress the brush, leading to an underestimation of the film thickness.<sup>58,59,91,92</sup> Other techniques that have been used to determine brush thickness include X-ray reflectivity (XRR)<sup>61,62</sup> and, for brushes grafted on particles, transmission electron microscopy (TEM),<sup>60</sup> dynamic light scattering (DLS)<sup>50,93,94</sup> and thermogravimetric analysis (TGA).<sup>50,63</sup>

In principle, information about the molecular weight and molecular weight distribution of the surface-attached polymer chains can be obtained by GPC analysis after cleavage of the brush from the substrate.<sup>2,66</sup> In practice, however, this requires high surface area substrates (*e.g.* silica particles) that can provide sufficient material for GPC analysis as well as special linkers that facilitate brush cleavage. The use of strong acids such as hydrochloric acid<sup>95</sup> or hydrofluoric acid<sup>96</sup> to cleave the brush bears the possible risk of undesired side-reactions. An alternative approach that is frequently used to assess the molecular weight of surface-grafted polymers is based on the addition of a sacrificial

initiator to the polymerization reaction. Marutani *et al.* found that the molecular weight of the polymer generated in solution from the sacrificial initiator was in good agreement with that of the polymer chains that were cleaved from the particle surface.<sup>96</sup> However, in spite of these encouraging results, the validity of comparing the results of a solution/bulk polymerization with that of a surface-initiated polymerization remains a matter of debate. As reported by Bruening, Baker and coworkers, surface-initiated polymerizations are inherently heterogeneous processes and the diffusion of monomer, catalyst or ligands to the surface may be a limiting factor. Therefore, the rate-limiting steps and kinetics for surface-initiated polymerizations may be different compared to homogeneous solution/bulk processes.<sup>18</sup> Moreover, the substrate geometry was shown to drastically affect the molecular weight and polydispersity of surface-tethered chains. Gorman, Petrie and Genzer studied the effect of confinement on polymer growth and compared the molecular weight and polydispersity of PMMA prepared in solution with that obtained from polymerization from flat and concave substrates. These authors concluded that introducing confinement induces a dramatic decrease of the molecular weight of the surface-attached polymer chains.<sup>97</sup> In addition to GPC, AFM can also be used to obtain information about the molecular weight and molecular weight distribution of polymer brushes. By analyzing the extension profiles of poly(*N,N*-dimethylacrylamide) and poly(*N*-isopropyl acrylamide) brushes grown via SI-ATRP, Goodman *et al.* obtained contour length distributions from which molecular weights were calculated that corresponded well with results obtained by GPC.<sup>64,65</sup>

The number-average molecular weight of the surface-grafted polymer chains can be used to calculate the grafting density ( $\sigma$ ) of the brush. From the dry thickness of the polymer brush ( $h$ ), the density of the polymer ( $\rho$ ) and the number-average molecular weight of the grafted polymer chains ( $M_n$ ),  $\sigma$  can be calculated according to:<sup>98,99</sup>

$$\sigma = (h \cdot \rho N_a) / M_n$$

For polymer brushes grafted from particles, the dry brush thickness that is needed to calculate the grafting density cannot be obtained from ellipsometry. In this case, however, grafting density can be determined from the weight loss observed upon thermogravimetric analysis in combination with the number-average molecular weight of the grafted polymer chains and the specific surface area of the particle substrate.<sup>67</sup> It is of interest to compare the grafting density of a polymer brush with the surface concentration of initiator/iniferter groups since it can provide information about the efficiency of the

initiation step of the SI-CRP process. The surface concentration of polymerization initiators/iniferters can be determined using XPS,<sup>100,101</sup> in particular when the polymerization active group contains a halogen atom, as it is the case for ATRP initiators.<sup>61,102</sup> Other techniques that have been used to determine initiator surface concentrations include TGA<sup>63</sup> and elemental analysis.<sup>103,104</sup> The initiation efficiency of surface-attached initiators has been reported to vary from 5 to 30 %, depending on the shape of the substrate, the type of surface-tethered initiator and the polymerization conditions.<sup>105-109</sup>

The topography and surface structure of polymer brushes has been investigated by AFM,<sup>71</sup> optical microscopy,<sup>68</sup> scanning electron microscopy (SEM),<sup>69</sup> fluorescence microscopy,<sup>110</sup> XPS “mapping”,<sup>71,72</sup> and X-ray reflectivity.<sup>61,62</sup>

The mechanical and viscoelastic properties of a polymer brush do not only depend on the chemical composition of the brush, but also on the conformation of the surface-tethered polymer chains and changes therein (swelling, collapse). QCM (quartz crystal microbalance) and QCM-D (quartz crystal microbalance with dissipation monitoring) are useful tools to *in situ* monitor such conformational changes.<sup>80,81,111</sup> Ellipsometry has also been used to study conformational changes in polymer brushes.<sup>77,78</sup> Scanning probe microscopy is attractive since the behavior of surface-attached polymer chains can be studied as a function of temperature,<sup>112</sup> in liquid media<sup>73-75,91,113</sup> or in controlled vapor atmosphere.<sup>114</sup> Scanning probe microscopy has not only been used to visualize conformational changes. By covering the back-side of a cantilever with a polymer brush, changes in the cantilever deflection can also be used as a read-out to monitor conformational transitions.<sup>115-117</sup> Yim *et al.* and Zhang *et al.* used neutron reflectivity experiments to probe temperature-dependent conformational changes in PNIPAM brushes that were prepared using SI-ATRP.<sup>118,119</sup> Several other techniques have been used to probe the swelling and collapse of polymer brushes. Wu *et al.*, for example, used NEXAFS analysis to study the spatial concentration of surface-tethered PAA chains at different ionic strengths.<sup>82</sup> Aoki *et al.* used fluorescence depolarization experiments to study nanosecond dynamics of PMMA brushes in both poor and good solvents.<sup>120</sup> In another study on solvent responsive polymer brushes, microfocus grazing incidence small-angle X-ray scattering ( $\mu$ -GISAXS) measurements were performed to elucidate the behavior of PMMA brush-backcoated micromechanical cantilevers.<sup>121</sup> Surface plasmon resonance (SPR)<sup>79</sup> and SPR-related methods<sup>73</sup> can also be used to probe conformational changes of polymer brushes. Li *et al.* showed that collapse/swelling of P4VP brushes

grafted from gold nanoparticles resulted in a shift of the SPR peak.<sup>73</sup> <sup>1</sup>H-NMR spectroscopy cannot be used to study brushes grown from planar substrates but is a useful technique to characterize brushes grafted from nanoobjects, such as nanotubes or nanoparticles, that can be dispersed in solvent.<sup>70,122,123</sup>

The kinetics of SI-CRP are typically monitored by preparing a series of brushes with different polymerization times and subsequently measuring the brush thickness with AFM or ellipsometry. In addition to these *ex situ* methods, SI-CRP can also be monitored *in situ* using QCM.<sup>25,42,83,84,124-126</sup>

Electrochemical methods, including electrochemical impedance spectroscopy (EIS),<sup>76,127</sup> chronoamperometry<sup>128</sup> and cyclic voltammetry (CV)<sup>86,129</sup> have been used to probe electronic properties such as the resistance, capacitance, charge as well as the redox properties of polymer brushes. It was demonstrated that those methods can be used to monitor the swelling/collapse of polymer brushes upon ion exchange<sup>75,76</sup> or ionic strength variations.<sup>128</sup> Furthermore, based on electrochemical impedance spectroscopy measurements, Jennings and coworkers developed an equivalent electronic circuit model for polymer brush coated substrate.<sup>85,130</sup>

## 1.4. References

1. Brittain, W. J.; Minko, S. *Journal of Polymer Science Part a-Polymer Chemistry* **2007**, *45*, 3505-3512.
2. Zhao, B.; Brittain, W. J. *Progress in Polymer Science* **2000**, *25*, 677-710.
3. Milner, S. T. *Science* **1991**, *251*, 905-914.
4. Huang, W. X.; Kim, J.-B.; Bruening, M. L.; Baker, G. L. *Macromolecules* **2002**, *35*, 1175-1179.
5. Edmondson, S.; Osborne, V. L.; Huck, W. T. S. *Chemical Society Reviews* **2004**, *33*, 14-22.
6. Tsujii, Y.; Ohno, K.; Yamamoto, S.; Goto, A.; Fukuda, T. *Advances in Polymer Science* **2006**, *197*, 1-45.
7. Braunecker, W. A.; Matyjaszewski, K. *Progress in Polymer Science* **2007**, *32*, 93-146.
8. Barbey, R.; Lavanant, L.; Paripovic, D.; Schüwer, N.; Sugnaux, C.; Tugulu, S.; Klok, H.-A. *Chemical Reviews* **2009**, *109*, 5437-5527.
9. Wang, J.-S.; Matyjaszewski, K. *Journal of the American Chemical Society* **1995**, *117*, 5614-5615.
10. Kato, M.; Kamigaito, M.; Sawamoto, M.; Higashimura, T. *Macromolecules* **1995**, *28*, 1721-1723.
11. Percec, V.; Barboiu, B. *Macromolecules* **1995**, *28*, 7970-7972.
12. Patten, T. E.; Matyjaszewski, K. *Advanced Materials* **1998**, *10*, 901-915.
13. Patten, T. E.; Matyjaszewski, K. *Accounts of Chemical Research* **1999**, *32*, 895-903.
14. Matyjaszewski, K.; Xia, J. H. *Chemical Reviews* **2001**, *101*, 2921-2990.
15. Kamigaito, M.; Ando, T.; Sawamoto, M. *Chemical Reviews* **2001**, *101*, 3689-3745.
16. Tsarevsky, N. V.; Matyjaszewski, K. *Chemical Reviews* **2007**, *107*, 2270-2299.
17. Matyjaszewski, K.; Göbels, B.; Paik, H.-J.; Horwitz, C. P. *Macromolecules* **2001**, *34*, 430-440.
18. Kim, J. B.; Huang, W. X.; Miller, M. D.; Baker, G. L.; Bruening, M. L. *Journal of Polymer Science Part a-Polymer Chemistry* **2003**, *41*, 386-394.
19. Nanda, A. K.; Matyjaszewski, K. *Macromolecules* **2003**, *36*, 599-604.
20. Nanda, A. K.; Matyjaszewski, K. *Macromolecules* **2003**, *36*, 1487-1493.



21. Tang, W.; Nanda, A. K.; Matyjaszewski, K. *Macromolecular Chemistry and Physics* **2005**, *206*, 1171-1177.
22. Matyjaszewski, K.; Nanda, A. K.; Tang, W. *Macromolecules* **2005**, *38*, 2015-2018.
23. Tang, W.; Tsarevsky, N. V.; Matyjaszewski, K. *Journal of the American Chemical Society* **2006**, *128*, 1598-1604.
24. Tang, W.; Matyjaszewski, K. *Macromolecules* **2006**, *39*, 4953-4959.
25. Cheng, N.; Azzaroni, O.; Moya, S.; Huck, W. T. S. *Macromolecular Rapid Communications* **2006**, *27*, 1632-1636.
26. Huang, X. Y.; Wirth, M. J. *Analytical Chemistry* **1997**, *69*, 4577-4580.
27. Ejaz, M.; Yamamoto, S.; Ohno, K.; Tsujii, Y.; Fukuda, T. *Macromolecules* **1998**, *31*, 5934-5936.
28. Matyjaszewski, K.; Miller, P. J.; Shukla, N.; Immaraporn, B.; Gelman, A.; Luokala, B. B.; Siclovan, T. M.; Kickelbick, G.; Vallant, T.; Hoffmann, H.; Pakula, T. *Macromolecules* **1999**, *32*, 8716-8724.
29. Wang, X.-S.; Lascelles, S. F.; Jackson, R. A.; Armes, S. P. *Chemical Communications* **1999**, 1817-1818.
30. Wang, X.-S.; Armes, S. P. *Macromolecules* **2000**, *33*, 6640-6647.
31. Jones, D. M.; Huck, W. T. S. *Advanced Materials* **2001**, *13*, 1256-1259.
32. Huang, W. X.; Kim, J. B.; Bruening, M. L.; Baker, G. L. *Macromolecules* **2002**, *35*, 1175-1179.
33. Matyjaszewski, K.; Shipp, D. A.; Wang, J.-L.; Grimaud, T.; Patten, T. E. *Macromolecules* **1998**, *31*, 6836-6840.
34. Jakubowski, W.; Matyjaszewski, K. *Macromolecules* **2005**, *38*, 4139-4146.
35. Min, K.; Gao, H. F.; Matyjaszewski, K. *Journal of the American Chemical Society* **2005**, *127*, 3825-3830.
36. Jakubowski, W.; Matyjaszewski, K. *Angewandte Chemie-International Edition* **2006**, *45*, 4482-4486.
37. Jakubowski, W.; Min, K.; Matyjaszewski, K. *Macromolecules* **2006**, *39*, 39-45.
38. Matyjaszewski, K.; Jakubowski, W.; Min, K.; Tang, W.; Huang, J. Y.; Braunecker, W. A.; Tsarevsky, N. V. *Proceedings of the National Academy of Sciences of the United States of America* **2006**, *103*, 15309-15314.
39. Zhao, H. Y.; Kang, X. L.; Liu, L. *Macromolecules* **2005**, *38*, 10619-10622.

40. Bombalski, L.; Min, K.; Dong, H. C.; Tang, C. B.; Matyjaszewski, K. *Macromolecules* **2007**, *40*, 7429-7432.
41. Esteves, A. C. C.; Bombalski, L.; Trindade, T.; Matyjaszewski, K.; Barros-Timmons, A. *Small* **2007**, *3*, 1230-1236.
42. He, J.; Wu, Y. Z.; Wu, J.; Mao, X.; Fu, L.; Qian, T. C.; Fang, J.; Xiong, C. Y.; Xie, J. L.; Ma, H. W. *Macromolecules* **2007**, *40*, 3090-3096.
43. Matyjaszewski, K.; Dong, H. C.; Jakubowski, W.; Pietrasik, J.; Kusumo, A. *Langmuir* **2007**, *23*, 4528-4531.
44. Wischerhoff, E.; Uhlig, K.; Lankenau, A.; Börner, H. G.; Laschewsky, A.; Duschl, C.; Lutz, J.-F. *Angewandte Chemie-International Edition* **2008**, *47*, 5666-5668.
45. Okelo, G. O.; He, L. *Biosensors & Bioelectronics* **2007**, *23*, 588-592.
46. Bao, Z.; Bruening, M. L.; Baker, G. L. *Journal of the American Chemical Society* **2006**, *128*, 9056-9060.
47. Ayres, N.; Cyrus, C. D.; Brittain, W. J. *Langmuir* **2007**, *23*, 3744-3749.
48. Ashford, E. J.; Naldi, V.; O'Dell, R.; Billingham, N. C.; Armes, S. P. *Chemical Communications* **1999**, 1285-1286.
49. Wang, X.-S.; Jackson, R. A.; Armes, S. P. *Macromolecules* **2000**, *33*, 255-257.
50. Chen, X. Y.; Randall, D. P.; Perruchot, C.; Watts, J. F.; Patten, T. E.; von Werne, T.; Armes, S. P. *Journal of Colloid and Interface Science* **2003**, *257*, 56-64.
51. Osborne, V. L.; Jones, D. M.; Huck, W. T. S. *Chemical Communications* **2002**, 1838-1839.
52. Tugulu, S.; Barbey, R.; Harms, M.; Fricke, M.; Volkmer, D.; Rossi, A.; Klok, H.-A. *Macromolecules* **2007**, *40*, 168-177.
53. Sankhe, A. Y.; Husson, S. M.; Kilbey, S. M., II. *Journal of Polymer Science Part a-Polymer Chemistry* **2007**, *45*, 566-575.
54. Jain, P.; Dai, J. H.; Baker, G. L.; Bruening, M. L. *Macromolecules* **2008**, *41*, 8413-8417.
55. Kim, Y. P.; Lee, B. S.; Kim, E.; Choi, I. S.; Moon, D. W.; Lee, T. G.; Kim, H. S. *Analytical Chemistry* **2008**, *80*, 5094-5102.
56. Navarro, M.; Benetti, E. M.; Zapotoczny, S.; Planell, J. A.; Vancso, G. J. *Langmuir* **2008**, *24*, 10996-11002.
57. Andruzzi, L.; Senaratne, W.; Hexemer, A.; Sheets, E. D.; Ilic, B.; Kramer, E. J.; Baird, B.; Ober, C. K. *Langmuir* **2005**, *21*, 2495-2504.

58. Farhan, T.; Azzaroni, O.; Huck, W. T. S. *Soft Matter* **2005**, *1*, 66-68.
59. Kidoaki, S.; Ohya, S.; Nakayama, Y.; Matsuda, T. *Langmuir* **2001**, *17*, 2402-2407.
60. Dey, T. *Journal of Nanoscience and Nanotechnology* **2006**, *6*, 2479-2483.
61. Yu, K.; Wang, H. F.; Xue, L. J.; Han, Y. C. *Langmuir* **2007**, *23*, 1443-1452.
62. Yu, K.; Wang, H. F.; Han, Y. C. *Langmuir* **2007**, *23*, 8957-8964.
63. Babu, K.; Dhamodharan, R. *Nanoscale Research Letters* **2008**, *3*, 109-117.
64. Goodman, D.; Kizhakkedathu, J. N.; Brooks, D. E. *Langmuir* **2004**, *20*, 6238-6245.
65. Goodman, D.; Kizhakkedathu, J. N.; Brooks, D. E. *Langmuir* **2004**, *20*, 3297-3303.
66. Prucker, O.; Ruhe, J. *Macromolecules* **1998**, *31*, 592-601.
67. Bartholome, C.; Beyou, E.; Bourgeat-Lami, E.; Chaumont, P.; Lefebvre, F.; Zydowicz, N. *Macromolecules* **2005**, *38*, 1099-1106.
68. Azzaroni, O.; Zheng, Z. J.; Yang, Z. Q.; Huck, W. T. S. *Langmuir* **2006**, *22*, 6730-6733.
69. Ward, J. H.; Bashir, R.; Peppas, N. A. *Journal of Biomedical Materials Research, Part A* **2001**, *56*, 351-360.
70. Fan, X. W.; Lin, L. J.; Dalsin, J. L.; Messersmith, P. B. *Journal of the American Chemical Society* **2005**, *127*, 15843-15847.
71. Zhou, F.; Zheng, Z. J.; Yu, B.; Liu, W. M.; Huck, W. T. S. *Journal of the American Chemical Society* **2006**, *128*, 16253-16258.
72. Slim, C.; Tran, Y.; Chehimi, M. M.; Garraud, N.; Roger, J.-P.; Combellas, C.; Kanoufi, F. *Chemistry of Materials* **2008**, *20*, 6677-6685.
73. Li, D. X.; He, Q.; Cui, Y.; Li, J. B. *Chemistry of Materials* **2007**, *19*, 412-417.
74. Kaholek, M.; Lee, W. K.; Ahn, S. J.; Ma, H. W.; Caster, K. C.; LaMattina, B.; Zauscher, S. *Chemistry of Materials* **2004**, *16*, 3688-3696.
75. Choi, E. Y.; Azzaroni, O.; Cheng, N.; Zhou, F.; Kelby, T.; Huck, W. T. S. *Langmuir* **2007**, *23*, 10389-10394.
76. Yu, B.; Zhou, F.; Hu, H.; Wang, C. W.; Liu, W. M. *Electrochimica Acta* **2007**, *53*, 487-494.
77. Li, J.; Chen, X. R.; Chang, Y. C. *Langmuir* **2005**, *21*, 9562-9567.
78. Tu, H.; Heitzman, C. E.; Braun, P. V. *Langmuir* **2004**, *20*, 8313-8320.

79. Lee, B. S.; Chi, Y. S.; Lee, K. B.; Kim, Y. G.; Choi, I. S. *Biomacromolecules* **2007**, *8*, 3922-3929.
80. Moya, S. E.; Azzaroni, O.; Kelby, T.; Donath, E.; Huck, W. T. S. *Journal of Physical Chemistry B* **2007**, *111*, 7034-7040.
81. Kurosawa, S.; Aizawa, H.; Talib, Z. A.; Atthoff, B.; Hilborn, J. *Biosensors & Bioelectronics* **2004**, *20*, 1165-1176.
82. Wu, T.; Gong, P.; Szleifer, I.; Vlcek, P.; Subr, V.; Genzer, J. *Macromolecules* **2007**, *40*, 8756-8764.
83. Nakayama, Y.; Matsuda, T. *Macromolecules* **1999**, *32*, 5405-5410.
84. Fu, L.; Chen, X. N.; He, J. N.; Xiong, C. Y.; Ma, H. W. *Langmuir* **2008**, *24*, 6100-6106.
85. Brantley, E. L.; Jennings, G. K. *Macromolecules* **2004**, *37*, 1476-1483.
86. Fulghum, T. M.; Estillore, N. C.; Vo, C. D.; Armes, S. P.; Advincula, R. C. *Macromolecules* **2008**, *41*, 429-435.
87. Yamamoto, S.; Ejaz, M.; Tsujii, Y.; Fukuda, T. *Macromolecules* **2000**, *33*, 5608-5612.
88. LeMieux, M. C.; Peleshanko, S.; Anderson, K. D.; Tsukruk, V. V. *Langmuir* **2007**, *23*, 265-273.
89. Slim, C.; Tran, Y.; Chehimi, M. M.; Garraud, N.; Roger, J.-P.; Combellas, C.; Kanoufi, F. *Chemistry of Materials* **2008**, *20*, 6677-6685.
90. Azzaroni, O.; Brown, A. A.; Huck, W. T. S. *Angewandte Chemie-International Edition* **2006**, *45*, 1770-1774.
91. Azzaroni, O.; Moya, S.; Farhan, T.; Brown, A. A.; Huck, W. T. S. *Macromolecules* **2005**, *38*, 10192-10199.
92. Pyun, J.; Kowalewski, T.; Matyjaszewski, K. *Macromolecular Rapid Communications* **2003**, *24*, 1043-1059.
93. Zhang, M. M.; Liu, L.; Zhao, H. Y.; Yang, Y.; Fu, G. Q.; He, B. L. *Journal of Colloid and Interface Science* **2006**, *301*, 85-91.
94. Li, D.; He, Q.; Yang, Y.; Möhwald, H.; Li, J. *Macromolecules* **2008**, *41*, 7254-7256.
95. Raghuraman, G. K.; Dhamodharan, R. *Journal of Nanoscience and Nanotechnology* **2006**, *6*, 2018-2024.
96. Marutani, E.; Yamamoto, S.; Ninjbadgar, T.; Tsujii, Y.; Fukuda, T.; Takano, M. *Polymer* **2004**, *45*, 2231-2235.

97. Gorman, C. B.; Petrie, R. J.; Genzer, J. *Macromolecules* **2008**, *41*, 4856-4865.
98. Biesalski, M.; Ruhe, J. *Macromolecules* **2002**, *35*, 499-507.
99. Sanjuan, S.; Tran, Y. *Macromolecules* **2008**, *41*, 8721-8728.
100. Tugulu, S.; Barbey, R.; Harms, M.; Fricke, M.; Volkmer, D.; Rossi, A.; Klok, H. A. *Macromolecules* **2007**, *40*, 168-177.
101. Ma, H.; Wells, M.; Beebe, T. P., Jr.; Chilkoti, A. *Advanced Functional Materials* **2006**, *16*, 640-648.
102. Xu, D.; Yu, W. H.; Kang, E. T.; Neoh, K. G. *Journal of Colloid and Interface Science* **2004**, *279*, 78-87.
103. Nagase, K.; Kobayashi, J.; Kikuchi, A.; Akiyama, Y.; Kanazawa, H.; Okano, T. *Biomacromolecules* **2008**, *9*, 1340-1347.
104. Nagase, K.; Kobayashi, J.; Kikuchi, A. I.; Akiyama, Y.; Kanazawa, H.; Okano, T. *Langmuir* **2008**, *24*, 511-517.
105. Jones, D. M.; Brown, A. A.; Huck, W. T. S. *Langmuir* **2002**, *18*, 1265-1269.
106. Shah, R. R.; Merreceyes, D.; Husemann, M.; Rees, I.; Abbott, N. L.; Hawker, C. J.; Hedrick, J. L. *Macromolecules* **2000**, *33*, 597-605.
107. Bao, Z. Y.; Bruening, M. L.; Baker, G. L. *Macromolecules* **2006**, *39*, 5251-5258.
108. Kobayashi, M.; Matsuno, R.; Otsuka, H.; Takahara, A. *Science and Technology of Advanced Materials* **2006**, *7*, 617-628.
109. Liu, Y.; Klep, V.; Zdyrko, B.; Luzinov, I. *Langmuir* **2004**, *20*, 6710-6718.
110. Dong, R.; Krishnan, S.; Baird, B. A.; Lindau, M.; Ober, C. K. *Biomacromolecules* **2007**, *8*, 3082-3092.
111. Jhon, Y. K.; Bhat, R. R.; Jeong, C.; Rojas, O. J.; Szeleifer, I.; Genzer, J. *Macromolecular Rapid Communications* **2006**, *27*, 697-701.
112. Cui, Y.; Tao, C.; Zheng, S. P.; He, Q.; Ai, S. F.; Li, J. B. *Macromolecular Rapid Communications* **2005**, *26*, 1552-1556.
113. Ryan, A. J.; Crook, C. J.; Howse, J. R.; Topham, P.; Jones, R. A. L.; Geoghegan, M.; Parnell, A. J.; Ruiz-Perez, L.; Martin, S. J.; Cadby, A.; Menelle, A.; Webster, J. R. P.; Gleeson, A. J.; Bras, W. *Faraday Discussions* **2005**, *128*, 55-74.
114. Zhou, F.; Huck, W. T. S. *Chemical Communications* **2005**, 5999-6001.
115. Abu-Lail, N. I.; Kaholek, M.; LaMattina, B.; Clark, R. L.; Zauscher, S. *Sensors and Actuators B-Chemical* **2006**, *114*, 371-378.
116. Zhou, F.; Shu, W. M.; Welland, M. E.; Huck, W. T. S. *Journal of the American Chemical Society* **2006**, *128*, 5326-5327.

117. Zhou, F.; Biesheuvel, P. M.; Chol, E. Y.; Shu, W.; Poetes, R.; Steiner, U.; Huck, W. T. S. *Nano Letters* **2008**, *8*, 725-730.
118. Yim, H.; Kent, M. S.; Mendez, S.; Balamurugan, S. S.; Balamurugan, S.; Lopez, G. P.; Satija, S. *Macromolecules* **2004**, *37*, 1994-1997.
119. Zhang, J. M.; Nylander, T.; Campbell, R. A.; Rennie, A. R.; Zauscher, S.; Linse, P. *Soft Matter* **2008**, *4*, 500-509.
120. Aoki, H.; Kitamura, M.; Ito, S. *Macromolecules* **2008**, *41*, 285-287.
121. Wolkenhauer, M.; Bumbu, G. G.; Cheng, Y.; Roth, S. V.; Gutmann, J. S. *Applied Physics Letters* **2006**, *89*.
122. Wei, Q. S.; Ji, J.; Shen, J. C. *Macromolecular Rapid Communications* **2008**, *29*, 645-650.
123. Kong, H.; Li, W. W.; Gao, C.; Yan, D. Y.; Jin, Y. Z.; Walton, D. R. M.; Kroto, H. W. *Macromolecules* **2004**, *37*, 6683-6686.
124. Moya, S. E.; Brown, A. A.; Azzaroni, O.; Huck, W. T. S. *Macromolecular Rapid Communications* **2005**, *26*, 1117-1121.
125. Ma, H.; Textor, M.; Clark, R. L.; Chilkoti, A. *Biointerphases* **2006**, *1*, 35-39.
126. Dobbelin, M.; Arias, G.; Loinaz, I.; Llarena, I.; Mecerreyes, D.; Moya, S. *Macromolecular Rapid Communications* **2008**, *29*, 871-875.
127. Zhou, F.; Hu, H. Y.; Yu, B.; Osborne, V. L.; Huck, W. T. S.; Liu, W. M. *Analytical Chemistry* **2007**, *79*, 176-182.
128. Spruijt, E.; Choi, E. Y.; Huck, W. T. S. *Langmuir* **2008**, *24*, 11253-11260.
129. Sakakiyama, T.; Ohkita, H.; Ohoka, M.; Ito, S.; Tsujii, Y.; Fukudal, T. *Chemistry Letters* **2005**, *34*, 1366-1367.
130. Bantz, M. R.; Brantley, E. L.; Weinstein, R. D.; Moriarty, J.; Jennings, G. K. *Journal of Physical Chemistry B* **2004**, *108*, 9787-9794.

## 2. Responsive Surfaces Based on Polymer Brushes

### 2.1. Introduction

Depending on the architecture and chemical composition of the surface-attached polymer chains, the conformation and structure of a polymer brush can be manipulated using a variety of external stimuli. These responsive properties potentially provide the basis for the development of “smart” surfaces. In the following sections, the influence of solvent, temperature, pH and ions on the conformation, structure and properties of polymer brushes prepared via SI-CRP will be discussed.

### 2.2. Solvent Responsive Polymer Brushes

The conformation of polymer brushes is highly dependent on the solvent. In the presence of a good solvent, the polymer chains will try to maximize the polymer/solvent contacts and swell, while in a poor solvent the brush will collapse in order to reduce polymer/solvent interactions. This section will successively discuss the influence of solvent on the structure and properties of homopolymer, diblock copolymer and triblock copolymer brushes, as well as binary polymer brushes.

Chen *et al.* used AFM and ellipsometry to study the behavior of PMMA brushes in water and THF, which are poor, respectively, good solvents for this polymer.<sup>1</sup> Upon immersion in water, a decrease in layer thickness and a reduction of surface roughness was observed, indicating the collapse of the brush. Other studies looked at the behavior of PMMA brushes using a micromechanical cantilever, which was coated on one side with a PMMA brush. Upon changing the solvent from isopropanol (a poor solvent) to ethyl acetate (a good solvent), a deflection of the cantilever was observed.<sup>2-4</sup> When going back to isopropanol the deflection reached its initial value. The swelling or the collapse of the polymer chains induces a mechanical stress and results in the bending of the cantilever.



When the brush was exposed to an isopropanol/ethyl acetate mixture that contains a small amount of ethyl acetate, the brush showed an intermediate behavior that was related to the fact that solvent only absorbed in the top layer.<sup>2</sup> This special regime was found to be very quickly and fully reversible, because the trapped solvent molecules can easily leave the polymer chains. Similar swelling behavior was observed when a PMMA brush was alternatively exposed to nitrogen and saturated toluene vapor.<sup>4</sup> Aoki *et al.* used fluorescence depolarization to study the dynamic swelling properties of PMMA brushes in benzene (a good solvent) and acetonitrile (a bad solvent).<sup>5</sup> It was observed that the thickness of the polymer layer was around two times lower in acetonitrile than in benzene. Furthermore, the motion of the polymer chains was faster in the good solvent. The authors also studied the influence of brush density on the swelling properties. For low density polymer brushes, in which the polymer chains could easily change their conformation, a fast response to solvent-exchange was observed. On the other hand, in case of high density brushes, the layer was found to be almost non-responsive to solvent-exchange. Aoki *et al.* proposed that due to their high density, the polymer chains interact strongly with each other and adopt a stretched conformation, even in a poor solvent. An example of an application of solvent responsive homopolymer brushes was reported by Li *et al.* who demonstrated that carbon nanotubes coated with poly(*n*-butyl acrylate) or poly(acrylic acid) brushes can be used as gas sensors.<sup>6</sup> The electrical resistance of the polymer brush-coated carbon nanotubes increased upon exposure to organic vapor. The polymer brush-coated carbon nanotubes showed a good sensitivity to organic vapors such as acetone, chloroform, methanol or toluene with a fast and reproducible response. The chemoselectivities and maximum response values of the polymer brush-modified nanotubes towards organic vapors were found to correlate with the solubility of the pure polymers in the respective solvents.

The response of a diblock copolymer brush to changes in solvent quality is more complex than that of a simple homopolymer brush. This is schematically illustrated in Figure 1. In the presence of solvent B, which is a good solvent for both blocks, the system will be fully extended. In contact with solvent A, which is a good solvent for the lower part of the brush but a poor solvent for the upper part, the lower block will swell while the upper block will collapse and eventually (depending on the nature of the lower segment) penetrate the other block in order to minimize as much as possible its contact with the solvent. Depending on the interaction parameter between the two blocks, this can lead to the formation of nanosized surface patterns.



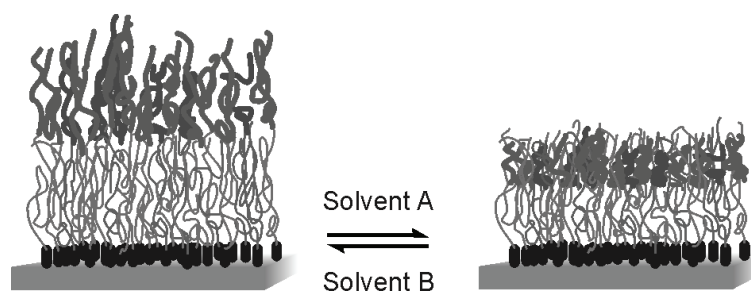


**Figure 1.** Structural changes in a diblock copolymer brush upon variations in solvent quality; solvent B is a good solvent for both blocks, while solvent A is a good solvent for the lower block but a non-solvent for the upper block.

Granville *et al.* studied the behavior of different semi-fluorinated diblock copolymer brushes (PS-*b*-PPFS, PS-*b*-PHFA, PS-*b*-PPFA, PS-*b*-PTFA, PMA-*b*-PPFS, PMA-*b*-PHFA, PMA-*b*-PPFA and PMA-*b*-PTFA).<sup>7</sup> Rowe *et al.* performed similar studies on PS-*b*-PAA, PS-*b*-PNIPAM and PMA-*b*-PDMAEA diblock copolymer brushes.<sup>8</sup> In these studies, the brushes were first exposed to a good solvent for both blocks. After that the brushes were exposed to a poor solvent for the outer block and a good solvent for the inner block. The contact angle of the brush after this second step was close to the value expected for the inner block, indicating a swelling of the inner block and a strong collapse of the outer one (reversible rearrangement). These observations were confirmed by XPS measurements, which revealed a change in the surface atomic composition upon the solvent treatment. Similar behavior was observed by Yu *et al.* for PS-*b*-(PMMA-*co*-PCDMA) diblock copolymer brushes.<sup>9</sup>

Xu *et al.* investigated the wetting properties of three groups of PBMA-*b*-PDMAEMA brushes composed of a uniform PBMA inner block and a molecular weight gradient PDMAEMA outer block.<sup>10</sup> The block copolymer brushes were treated with hexane and water and characterized by water contact angle measurements, which revealed three different response regimes. When the PDMAEMA block was short, the PBMA segment dominated the surface after hexane treatment. In the partial response regime, the PDMAEMA and PBMA blocks coexisted at the air interface. Further increase in the PDMAEMA block length was found to suppress the rearrangement of the PBMA blocks after hexane treatment.

Gao *et al.* studied the solvent-induced formation of nanoscale patterns on PPEGMA-*b*-PMMA diblock copolymer brushes.<sup>11</sup> These brushes were produced by SI-ATRP from a silicon wafer and consisted of an inner PPEGMA block with a thickness of 23.4 nm and

an outer PMMA block with thicknesses ranging from 1.6 to 31.0 nm. The formation of nanoscale patterns in these brushes was studied by means of AFM, ellipsometry and water contact angle measurements. Depending on the PMMA block length different phase segregation regimes were observed. In the case of PMMA layer thicknesses  $< 4$  nm spherical PMMA domains were observed. The size of these spherical features increased with increasing PMMA block length until they started to come into contact and merge into “worm-like” structures at PMMA layer thicknesses of 10.5 nm. Further increase in the PMMA layer thickness resulted in the formation of striped patterns. The formation of these phase-separated structures was attributed to the fact that the PMMA chains tried to minimize the contact with the solvent but could not go inside the PPEGMA layer due to the relatively long ethylene glycol side chains in this block.<sup>12</sup> Similar observations were reported by Santer *et al.* who used the topographical switching properties of PMMA-*b*-PGMA brushes to drive the motion of silica nanoparticles deposited onto the brush.<sup>13,14</sup> Using AFM and contact angle measurements, Xu *et al.* studied PMMA/PHEMA gradient copolymer brushes.<sup>15</sup> They observed that upon treatment with  $\text{CH}_2\text{Cl}_2$  (a selective solvent for PMMA), the MMA-rich segments of the polymer chains swelled and migrated to the surface in order to maximize the contact between the solvent and the MMA-rich segments while at the same time the HEMA-rich segments collapsed and penetrated inside the polymer brush to reduce their interaction with the solvent. These solvent-induced rearrangements resulted in changes in surface roughness.

In addition to diblock copolymer brushes, several groups have also studied the solvent response of triblock copolymer brushes. Boyes *et al.* examined the swelling behavior of PS-*b*-PMMA-*b*-PS and PMMA-*b*-PS-*b*-PMMA triblock copolymer brushes.<sup>16</sup> These brushes were exposed to a solvent that was a good solvent for the middle block but a non-solvent for the tethered and outer blocks. For both systems, reversible and reproducible changes in the contact angle were observed, which indicated a conformational rearrangement and migration of the non-soluble blocks inside the brush and the soluble block to the surface. XPS measurements revealed changes in the surface atomic concentration and AFM showed an increase in roughness upon the solvent treatment, indicating the formation of micellar structures due to the migration of the outer blocks inside the layer. Similar observations were made by Huang *et al.* who investigated PMMA-*b*-PDMAEMA-*b*-PMMA and PMA-*b*-PMMA-*b*-PHEMA triblock copolymer brushes.<sup>17</sup>

The solvent responsiveness of mixed homopolymer brushes is different from that of block copolymer brushes. Exposure to a specific solvent triggers a selective swelling of one of the components of the brush and at the same time a collapse of the other polymer chains leading to a phase separation and the formation of nanoscale surface patterns (Figure 2).

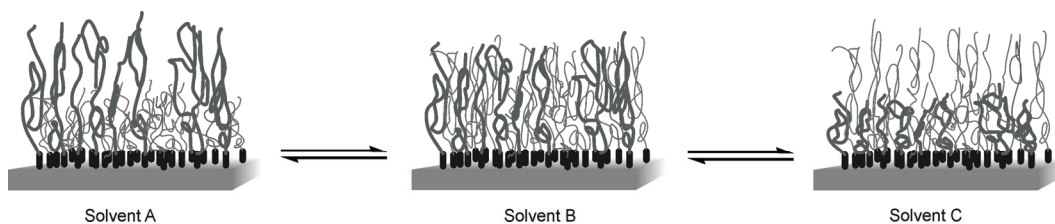


**Figure 2.** Solvent responsiveness of a binary mixed homopolymer brush; Solvent B is a non-selective solvent, whereas solvents A and C are selective for only one segments.

Zhao *et al.* studied mixed PMMA/PS brushes, which were grown from a flat silicon wafer using a difunctional “Y-shaped” initiator.<sup>18</sup> A series of mixed brushes with a constant PMMA molecular weight of 17500 g/mol and PS molecular weights ranging from 4300 to 26100 g/mol were investigated. Water contact angle measurements on films exposed to chloroform (a non-selective solvent) indicated a gradual transition from 74°, the value expected for pure PMMA, to 91°, the value for pure PS, with increasing PS molecular weight. Exposure to cyclohexane, which is a selective solvent for PS, did not lead to any changes in surface topography but did induce a reorganization that drives the PMMA chains to the interior of the brush to avoid unfavorable PMMA/cyclohexane contacts. Exposure of mixed brushes with PS segments slightly shorter or similar in length to the PMMA segments to acetic acid (a PMMA selective solvent), in contrast, resulted in the formation of micellar nanodomains with PMMA chains shielding a PS core. Zhao and coworkers also used their “Y-shaped” initiator to grow binary mixed PAA/PS brushes from silica nanoparticles.<sup>19</sup> Tyndall scattering and <sup>1</sup>H-NMR spectroscopy experiments demonstrated that the brush-coated particles could be dispersed both in chloroform, a PS selective solvent, as well as in methanol, a PAA selective solvent, which reflects the ability of the surface-tethered polymer chains to undergo structure changes in response to changes in solvent quality. Santer *et al.* have extensively studied solvent-induced topographical changes in PS/PMMA binary brushes.<sup>14,20</sup> These authors found that these mixed brushes can form microdomains upon exposure to

solvents that are selective to the PS (toluene) or PMMA (acetone) segments. Upon monitoring the resulting surface topographical changes with AFM over several switching cycles, it was observed that several microdomains recover their initial state after multiple acetone/toluene exposures. This memory effect has been proposed as a possible mechanism to direct movement of objects on these “smart” surfaces.

### 2.3. Thermoresponsive Polymer Brushes

Thermoresponsive polymer brushes prepared by SI-CRP have been explored for a wide variety of applications including chromatography,<sup>21-25</sup> controlled cell adhesion,<sup>26-28</sup> modulating membrane transport<sup>29</sup> as well as catalysis.<sup>30</sup> Most of the thermoresponsive brushes that have been reported show lower critical solution temperature (LCST) behavior. At temperatures below the LCST, these brushes are hydrophilic, while raising the temperature above the LCST leads to a collapse of the brushes when they are exposed to water and results in a hydrophobic surface. Table 1 provides an overview of different thermoresponsive polymer brushes that have been prepared using SI-CRP and also lists their transition temperatures as well as the nature of the transition. This section will highlight the thermoresponsive properties of various surface-attached polymer brushes and successively discusses homopolymer, random copolymer and block copolymer brushes.

PNIPAM is one of the most studied thermoresponsive polymers and surface-tethered PNIPAM brushes have attracted much attention in the past two decades.<sup>44</sup> Whereas in solution PNIPAM shows a sharp LCST at 32 °C,<sup>45</sup> the LCST transitions observed for PNIPAM brushes are broader, start at lower temperature and occur over a wider temperature range (from ~ 29 °C to ~ 40 °C).<sup>31-34</sup> Analogous to the free polymer in solution, the phase transition temperature of PNIPAM brushes also depends on the salt concentration.<sup>46</sup> However, in contrast to the linear decrease of the phase transition temperature with increasing salt concentration observed for the free polymer, surface-attached PNIPAM brushes display a non-linear behavior. Whereas changes in salt concentration markedly affect the LCST behavior of PNIPAM brushes, Rahane *et al.* found that varying pH between pH 3 and 8 has almost negligible impact on the swelling properties.<sup>47</sup>

**Table 1.** Overview of thermoresponsive polymer brushes prepared by SI-CRP.

Polymer brush	Transition temperature	Transition	Method <sup>a</sup>	Ref
PNIPAM	~ 29 °C to ~ 40 °C	LCST	WCA QELS WCA SPR	31-34
PPEGMEMA <sub>2</sub>	~ 21 to 25 °C	LCST	DLS <sup>1</sup> H-NMR	35
PPEGMEMA <sub>2</sub>	32.3 °C	LCST	WCA	36
PPEGMEMA <sub>3</sub>	~ 42 to 52 °C	LCST	DLS <sup>1</sup> H-NMR	35
PPEGMEMA <sub>3</sub>	~ 40 to 50 °C	LCST	DLS	30
PSBMA	~ 40 to 50 °C	UCST	WCA	37
PNIPAM- <i>co</i> -PAA (3 mol % AA) <sup>b</sup>	~ 21 °C (pH 2) ~ 24 °C (pH 4) ~ 32 °C (pH 7) ~ 36 °C (pH 9) ~ 45 °C (pH 11)	LCST	WCA	38
PPEGMEMA <sub>2</sub> - <i>co</i> -PPEGMEMA <sub>8.5</sub> (5 mol % PEGMEMA <sub>8.5</sub> ) <sup>b</sup>	~ 36 °C	LCST	WCA	36
PPEGMEMA <sub>2</sub> - <i>co</i> -PPEGMEMA <sub>8.5</sub> (10 mol % PEGMEMA <sub>8.5</sub> ) <sup>b</sup>	~ 40 °C			
PNIPAM- <i>co</i> -PDMAEMA (17 mol % DMAEMA) <sup>c</sup>	~ 40.7 °C	LCST	UV-vis	24
PNIPAM- <i>co</i> -PDMAEMA (20 mol % DMAEMA) <sup>c</sup>	~ 56.1 °C			
PNIPAM- <i>co</i> -PDMAEMA (37 mol % DMAEMA) <sup>c</sup>	~ 64.6 °C			
PNIPAM- <i>co</i> -PMBAM (0.74 mol % MBAM) <sup>b</sup>	31.26 °C	LCST	DSC AFM	39
PNIPAM- <i>co</i> -PMBAM (0.5 mol % MBAM) <sup>b</sup>	~ 32 °C	LCST	SPR	40
PNIPAM- <i>co</i> -PMBAM (1 mol % MBAM) <sup>b</sup>	~ 34 °C			
PNIPAM- <i>co</i> -PMBAM (2 mol % MBAM) <sup>b</sup>	~ 36 °C			
PDMAM- <i>b</i> -PNIPAM (61.3 mol % PDMAM) <sup>c</sup>	~ 25 to 32 °C	LCST	PCS	41
PSEMA- <i>b</i> -PNIPAM	No LCST observed	LCST	AFM	42
PNIPAM- <i>b</i> -PPEGMEMA	~ 33 °C (PNIPAM segment) ~ 55 °C (PPEGMEMA segment)	LCST	DSC, DLS SPR	43

<sup>a</sup>: Techniques used to determine the transition temperature; <sup>b</sup>: Molar percentage of the monomer in the polymerization mixture (*i.e.* feed composition); <sup>c</sup>: Molar percentage in the copolymer determined via <sup>1</sup>H-NMR. AFM: atomic force microscopy; DLS: dynamic light scattering; PCS: photon correlation spectroscopy; QELS: quasi-elastic light scattering; SPR: surface plasmon resonance; WCA: water contact angle.

This difference between the solution properties of PNIPAM and the properties of thin, surface-attached PNIPAM brushes has been attributed to the high chain density in the later case. The LCST transition of a PNIPAM brush is accompanied by an increase in the water contact angle of  $\sim 10$  to  $30^\circ$ <sup>33,48</sup> as well as a decrease of the polymer brush thickness<sup>32,33,49,50</sup> and stiffness.<sup>51</sup> Yim *et al.* used neutron reflectivity to investigate the collapse of PNIPAM brushes upon temperature increase. They observed that the brush contraction was not monotonic and that, upon heating or cooling, phase separation occurred in the temperature range of  $\sim 30$ - $33$  °C.<sup>52,53</sup> <sup>1</sup>H-NMR analysis (in D<sub>2</sub>O) of PNIPAM brush-coated gold nanorods<sup>32</sup> and carbon nanotubes<sup>54</sup> revealed that, upon temperature increase, the intensity of the proton signals of the PNIPAM units became weaker and could hardly be detected for temperatures  $> 40$  °C, which was attributed to the transition of the polymer brush from a hydrophilic to a hydrophobic state upon passing the LCST.

Several parameters have been found to influence the LCST behavior of PNIPAM brushes such as the brush thickness and grafting density. Yim *et al.* used neutron reflectivity to study the influence of the polymer molecular weight and brush density on the temperature-induced conformational changes of PNIPAM brushes.<sup>55,56</sup> For PNIPAM brushes with a high grafting density ( $0.0031$  chains/Å<sup>2</sup>), samples composed of lower molecular weight polymer chains were found to experience larger conformational changes upon varying the temperature across the LCST as compared to higher molecular weight PNIPAM brushes.<sup>55</sup> The authors, however, also noticed that low molecular weight brushes present a more complex behavior and exhibit phase separation.<sup>53</sup> Temperature-dependent neutron reflectivity experiments on low density ( $0.00063$  chains/Å<sup>2</sup>) PNIPAM brushes with different molecular weights revealed opposite behavior;<sup>56</sup> whereas the high molecular weight ( $152000$  g/mol) brush displayed conformational changes, the neutron reflectivity data did not reveal any conformational changes for the low molecular weight ( $33000$  g/mol) brush. Conformational changes were most prominent for brushes with intermediate grafting densities and high molecular weights. Plunkett *et al.* studied the PNIPAM chain collapse as a function of brush molecular weight and grafting density using water contact angle and surface force measurements, amongst others.<sup>57</sup> Surface force measurements showed that the chain collapse above the LCST decreased with decreasing grafting density and molecular weight. Above the LCST, the advancing water contact angle increases sharply on high molecular weight and dense PNIPAM brushes, whereas these changes are less pronounced on low molecular weight brushes at lower

densities. Similar observations have been reported by Idota *et al.*<sup>21</sup> The wettability of PNIPAM brushes further depends on the roughness of the substrate from which they are grafted.<sup>31</sup> For PNIPAM brush grown from flat surfaces, Sun *et al.* determined water contact angles of 63.5° and 93.2° at 25 °C, respectively, 40 °C. When these brushes were grown from structured surfaces patterned with microgrooves of 6 μm in width and 5 μm in depth, the water contact angles changed to 0° (25 °C), respectively, 149.3° (40 °C) and the brushes could be reversibly switched from a superhydrophilic to a superhydrophobic state.

The presence of crosslinking can also influence the LCST of PNIPAM brushes. Li *et al.* studied the behavior of a random copolymer brush made of *N*-isopropylacrylamide (NIPAM) and *N,N'*-methylenebisacrylamide (MBAM) with various amount of MBAM.<sup>40</sup> The influence of the amount of crosslinker on the LCST of the PNIPAM-*co*-PMBAM brushes was studied. It was found that 0.5 mol % (molar ratio in polymerization mixture) of MBAM did not affect the LCST value of the polymer brush, whereas the LCST increased to 34 °C and 36 °C when the amount of MBAM was increased to 1 or 2 mol %, respectively.

In addition to NIPAM, another monomer that has been widely used to prepare thermosensitive polymer brushes is poly(poly(ethylene glycol) methyl ether methacrylate) (PPEGMEMA). Li *et al.* studied the thermosensitivity of poly(di(ethylene glycol) methyl ether methacrylate) (PPEGMEMA<sub>2</sub>) and poly(tri(ethylene glycol) methyl ether methacrylate) (PPEGMEMA<sub>3</sub>) brush-coated silica particles and compared the phase transitions of the polymer brushes with those of the corresponding free polymers in water.<sup>35</sup> For both polymer brushes, as for PNIPAM brushes, no sharp transitions were observed compared to the free polymer in solution. The transition began at lower temperature compared to the free polymer and occurred over a broader temperature range (from ~ 21 °C to ~ 25 °C for PPEGMEMA<sub>2</sub> brushes and from ~ 42 °C to ~ 52 °C for PPEGMEMA<sub>3</sub> brushes). These differences were attributed to the close packing of the chains in the brush compared to the free chains in solution. In a subsequent publication, the same authors reported the preparation of Pd-loaded poly(acrylic acid) nanoparticles modified with a thermosensitive PPEGMEMA<sub>3</sub> brush, which were explored as recyclable catalysts for biphasic hydrogenation reactions.<sup>30</sup> Jonas *et al.* studied the effect of the nanoconfinement on the thermal behavior of PPEGMEMA<sub>2</sub> brushes.<sup>58</sup> They noticed that, compared to a non-structured polymer brush, patterned brushes showed an increased temperature-induced vertical swelling. The authors attributed this phenomenon to the



different packing of the chains, since in the patterned brushes the chains are initially less stretched than in an “infinite”, *i.e.* non-structured, brush and thus the chains are able to swell more.

Homopolymer brushes displaying upper critical solution temperature (UCST) behavior have been reported by Azzaroni *et al.*<sup>37</sup> These authors grafted poly(sulfobetaine methacrylate) (PSBMA) brushes via SI-ATRP from gold surfaces and followed the changes in the water contact angle with temperature. Due to the UCST behavior, PSBMA brushes are hydrophobic at room temperature (water contact angle  $\sim 79^\circ$ ) and more hydrophilic at high temperature (water contact angle  $\sim 58^\circ$ ). As for the LCST transition, the authors observed that the UCST of PSBMA brushes is different from the free PSBMA in solution (*i.e.*  $33^\circ\text{C}$ )<sup>59</sup> and occurs over a wider temperature range (from  $40$  to  $50^\circ\text{C}$ ).

Surface-initiated random copolymerization is an attractive strategy to tune the thermosensitive properties of polymer brushes. Jonas *et al.* demonstrated that thermosensitive polymer brushes with LCSTs between  $32$  and  $40^\circ\text{C}$  can be prepared by surface-initiated atom transfer radical copolymerization of 2-(2-methoxyethoxy)ethyl methacrylate and poly(ethylene glycol) methacrylate.<sup>36</sup> The LCST values of the copolymer brushes were found to depend linearly on the comonomer composition. When the second monomer that is used for the preparation of the copolymer brushes is sensitive to another stimulus than temperature, then dual responsive surfaces can be produced. This was shown by Xia *et al.* who grafted PNIPAM-based brushes containing 3 mol % acrylic acid from silicon substrates.<sup>38</sup> The copolymerization of acrylic acid introduced a pH-sensitive component and the authors demonstrated that the LCST of the brushes varied from  $21$  to  $45^\circ\text{C}$  depending on the pH.

In addition to homopolymer and random copolymer brushes, also thermosensitive block copolymer brushes have been prepared and investigated. Brooks and coworkers used SI-ATRP to prepare PDMAM-*b*-PNIPAM-modified PS latex particles.<sup>41</sup> Evaluation of the hydrodynamic thickness of the brush layer as a function of temperature revealed a gradual decrease in layer thickness over a broad temperature range ( $20$ - $38^\circ\text{C}$ ), in contrast to the sharp LCST that is observed for PNIPAM in solution. Li *et al.* have prepared double thermosensitive block copolymer brushes by consecutive SI-ATRP of NIPAM and PEGMEMA from initiator-modified gold nanoparticles. Temperature-dependent dynamic light scattering experiments revealed two thermal transitions, corresponding to the LCSTs of the different blocks.<sup>43</sup> Other double responsive diblock copolymers brushes that have



been prepared are composed of a pH-sensitive block and a thermosensitive block. Wang *et al.* used AFM to study the thermoresponsiveness of symmetric poly(2-succinyloxyethyl methacrylate)-*b*-poly(*N*-isopropylacrylamide) brushes.<sup>42</sup> Whereas at pH 9 an increase in temperature from 25 to 50 °C resulted in a decrease in film thickness, the brush seemed to be temperature-insensitive at pH 4. This loss of thermal responsiveness was attributed to hydrogen bonding between the constituent blocks. Dual (pH/temperature) responsive block copolymer brushes were also studied by Rahane *et al.*<sup>47</sup> In contrast to the example by Wang *et al.*, the PMAA-*b*-PNIPAM brushes prepared by these authors showed temperature-dependent swelling properties between pH 3 and 8. Rahane *et al.* noted that although hydrogen bonding interactions influence the pH-dependent actuation, it did not influence the LCST of the PNIPAM blocks, even if the transition was broad. LeMieux *et al.* prepared diblock copolymer brushes via successive photoiniferter-mediated polymerization of NIPAM and glycidyl methacrylate (GMA) followed by grafting of carboxylic acid-terminated poly(*n*-butyl acrylate).<sup>60</sup> Nanomechanical analysis of the film indicated that the elastic response can be tuned by external temperature.

## 2.4. pH and Ion Responsive Polymer brushes

Polyelectrolyte brushes are composed of polymer chains that contain charged repeating units. Depending on the nature of the charged groups, polyelectrolyte brushes are classified as strong or weak polyelectrolyte brushes.<sup>61</sup> In strong polyelectrolyte brushes, the number and position of charges along the chain is fixed. In this case, variation of pH or ionic strength will not influence the number of charges. In weak polyelectrolyte brushes, in contrast, the charge density is not fixed, but strongly depends on pH and ionic strength. The response of polyelectrolyte brushes to changes in pH and ionic strength has been subject of intense research efforts. The following two sections successively discuss the effects of changes in pH and ionic strength on the structure and properties of polyelectrolyte brushes prepared via SI-CRP.

### 2.4.1. pH Sensitive Polymer Brushes

A large number of reports has been published that describe the pH-sensitivity of polyelectrolyte brushes prepared via SI-CRP. This section will start with a basic discussion of the pH-induced conformational changes of two prototypical polyelectrolyte brushes, namely PAA as an example of a polyacid brush and PDMAEMA as an example of a polybase brush. After that, several other characteristics of homopolyelectrolyte brushes will be highlighted. Finally, the pH-sensitivity and properties of random and block copolymer brushes will be discussed.

In the case of PAA, the addition of base deprotonates the pendant acidic groups along the polymer brush backbone introducing charges within the layer. As a consequence, the polymer brush will swell due to Coulombic repulsions between the charged polymer chains. Brittain and coworkers observed a linear increase in PAA brush thickness from ~ 16 nm to ~ 26 nm upon increasing the pH from 2 to 8.<sup>62</sup> Further increasing the pH to ~ 10 was found to result in a small decrease in brush thickness. Two possible mechanisms were proposed to explain the observed decrease in brush thickness with increasing pH at pH > 8. A first possible explanation could be cleavage of the ester group of the surface-immobilized initiator. Secondly, the addition of additional ions (through the continued addition of base) to a fully deprotonated brush can lead to screening of the charges along the polymer backbone, which could also explain the observed decrease in brush thickness. Wu *et al.* have studied the effect of grafting density on the pH-induced conformational changes of PAA brushes.<sup>63</sup> In the osmotic brush regime, the degree of swelling of the PAA brushes was found to depend on brush density at pH 4 and 5.8, but was independent of grafting density at pH 10. These results indicate that at pH 4 and 5.8, the PAA brush behaves as a weak polyelectrolyte, whereas at pH 10 its behavior resembles that of a strong polyelectrolyte.

The pH-response of polybase brushes such as PDMAEMA is opposite to that of polyacid brushes; their wet thickness decreases with increasing pH due to deprotonation of the charged side groups. The pH-induced conformational changes of PDMAEMA brushes have been studied using various techniques. Sanjuan *et al.*, for example, used neutron reflectivity measurements to compare the swelling behavior of PDMAEMA at pH 2, 7 and 10.<sup>64</sup> The results indicated that the brushes adopted a less extended conformation as the pH of the solution becomes more basic. Neutron reflectivity has also been used by other groups to probe the pH-responsiveness of PDMAEMA brushes.<sup>65,66</sup>

The study by Geoghegan *et al.* revealed that the brushes swell by a factor of 2 at low pH, with the onset of swelling being dependent on grafting density.<sup>66</sup> More densely grafted brushes were found to swell at a lower pH, reflecting a shift in pKa as the grafting density changes. Furthermore, for swollen brushes, the composition-depth profile obtained from the reflectivity experiments pointed towards a region depleted in polymer between the substrate and the extended part of the brush. The pH-induced conformational changes of PDMAEMA brushes grafted from particles can be conveniently monitored with dynamic light scattering.<sup>67,68</sup> For PDMAEMA brushes grafted from polystyrene latex particles, Zhang *et al.* observed changes in particle size diameter of more than a factor of 2 by changing the pH from 3 to 10.<sup>67</sup> The pH-induced conformational changes of polyelectrolyte homopolymer brushes have been used for various applications. Several groups, for example, have described quartz crystal microbalance (QCM)-based pH-sensors, which were produced by modifying the resonator with a PAA brush coating.<sup>69,70</sup> Furthermore, the pH-induced swelling/collapse of polyelectrolyte brushes can be used to control the flocculation behavior of the corresponding polymer brush-coated particles. This has been reported for particles coated with PDMAEMA,<sup>68</sup> PSS(Na),<sup>68</sup> PVB(Na)<sup>68</sup> and P4VP brushes,<sup>71,72</sup> amongst others. The pH-induced conformational changes of polyelectrolyte brushes have also been used to actuate AFM cantilevers.<sup>73</sup> This was demonstrated by Huck and coworkers who modified AFM cantilevers with a poly(2-methacryloyloxyethyl phosphate) (PMEP) brush coating. At pH < 2, the polymer brush is water insoluble and collapses, while at very high pH values the surface-tethered polymer chains experience strong repulsive interactions. Both conditions lead to compressive stresses and a deflection of the cantilever. The protonation/deprotonation of the surface-tethered polyelectrolyte chains can also influence the wettability of the polymer brushes. Zhou and Huck, for example, found that PMEP brushes exhibited a three stage switching of wettability.<sup>74</sup> After exposure to pH < 1 solutions, the brushes were relatively hydrophobic (advancing contact angle > 65°). After immersion into a pH 4 solution, the brushes became more hydrophilic (contact angle ~ 49°). Treatment with basic aqueous solution (pH > 13) yielded almost completely wetting surfaces. Similar observations were also reported by Zhang *et al.*, who demonstrated that the pH-sensitivity of PDMAEMA brushes can be used to change the wettability of rough silicon surfaces from almost completely wetting at pH < 3 to very hydrophobic (water contact angle > 115°) at pH > 5.<sup>75</sup>

Surface-initiated copolymerization of oppositely charged monomers results in so-called polyampholyte brushes. Zauscher and coworkers modified microcantilevers with PNIPAM-*co*-PNVI brushes and demonstrated that the cantilever deflected linearly with a sensitivity of  $\sim 121$  nm/pH over the range from pH 4 to 6.<sup>76</sup> Sanjuan and Tran used neutron reflectivity to study the pH-response of PMAA-*co*-PDMAEMA copolymer brushes.<sup>77</sup> At low and high pH, these brushes acted as neutral polyelectrolyte brushes. For low net charge, however, *i.e.* at the isoelectric point, the polyampholyte effect results in a collapsed brush.

Ayres *et al.* studied the pH-responsiveness of poly(acrylic acid)-*b*-poly(vinylpyridine) block copolymer brushes.<sup>78</sup> Evaluation of the film thickness of brushes composed of blocks of similar lengths as a function of pH indicated that these films are swollen at extreme pH values but collapsed at intermediate pHs due to the polyampholyte effect. In asymmetric block copolymer brushes with a relatively long poly(vinylpyridine) segment, this behavior was also observed, though less pronounced. Quaternization of the vinylpyridine units significantly changed the pH-sensitivity and resulted in a system that showed a continuous decrease in film thickness with increasing pH.

#### 2.4.2. Ions Sensitive Polymer Brushes

In addition to pH, polyelectrolyte brushes are also sensitive to variation in ionic strength. Genzer, Szleifer and coworkers carried out theoretical and experimental studies to investigate the behavior of surface-attached polyelectrolytes.<sup>63,79</sup> Theoretical considerations predicted a different behavior for strong and weak polyelectrolyte brushes. For strong polyelectrolytes, the electrostatic interactions are largely screened at high salt concentrations, and the brush behaves as a neutral, *i.e.* collapsed, brush. Decreasing the salt concentration generates an unbalance between the ion concentration inside and outside the brush and results in electrostatic interactions that lead to swelling of the brush. This regime is referred to as the salted brush regime. Upon further decreasing the salt concentration, the brush enters the osmotic brush regime, where co-ions are expelled from the brush and the layer thickness reaches a limiting value. For weak polyelectrolyte brushes the scenario is different. In the neutral and salted brush regimes, the salt concentration inside and outside the brush is approximately equal and the internal degree of dissociation is the same as in bulk solution. In the osmotic brush regime, however, a significant electric potential difference is developed between the brush and the bulk

solution and in addition the salt concentration inside the brush is considerably higher. These unfavorable electrostatic conditions result in a discharge of the electrolyte groups and a collapse of the layer thickness. Experimental investigations of the wet thickness of PAA brushes at different pH values and a range of salt concentrations were in good agreement with the predicted behavior of weak polyelectrolyte brushes. In the salted brush regime, Szleifer, Genzer and coworkers found that above the mushroom-to-brush transition, which was observed at a brush density ( $\sigma$ ) of 0.08 chains/nm<sup>2</sup>, the wet PAA layer thickness (H) increased with increasing brush density.<sup>63</sup> The increase in wet PAA thickness followed a scaling law  $H \sim \sigma^n$  with  $n \approx 0.29 - 0.31$ , which was in good agreement with the theoretically predicted 1/3. The behavior of the PAA brushes in the osmotic brush regime was more complex. In contrast to theory, which predicted a decrease in wet thickness with increasing grafting density and an increase in wet thickness with increasing ionic strength, the experimental results revealed an increase in brush swelling with increasing brush density. Furthermore, the increase in wet layer thickness at high brush densities was found to increase with increasing ionic strength. Ayres *et al.* reported the effects of mono- and divalent salts on the behavior of PMAA brushes.<sup>62,80</sup> Upon decreasing the salt concentration, it was found that the threshold concentration that marks the onset of brush expansion was higher for the monovalent salt. Huck and coworkers have extensively studied the influence of the counterion on the structure and properties of PMETAC brushes.<sup>81-83</sup> In contrast to many other studies that use highly hydrated and mobile counterions, these authors investigated scarcely hydrated anions, which can undergo ion-pairing interactions with the quaternary ammonium groups in the brush.<sup>84-86</sup> The characteristics of the brush (*e.g.* wettability) were found to be very sensitive to the nature of the counterion. Upon exchanging the original chloride counterion with a variety of other counterions it was found that the wettability of the counterion-modified brushes increased from  $\text{ClO}_4^- > \text{SCN}^- > \text{I}^- > \text{Br}^- > \text{Cl}^- > \text{PO}_4^{3-}$ , which correlates with the Hofmeister classification of the hydrophobicity of these anions.<sup>87</sup>

## 2.5. References

1. Chen, J.-K.; Hsieh, C.-Y.; Huang, C.-F.; Li, P.-M.; Kuo, S.-W.; Chang, F.-C. *Macromolecules* **2008**, *41*, 8729-8736.
2. Bumbu, G. G.; Wolkenhauer, M.; Kircher, G.; Gutmann, J. S.; Berger, D. *Langmuir* **2007**, *23*, 2203-2207.
3. Wolkenhauer, M.; Bumbu, G. G.; Cheng, Y.; Roth, S. V.; Gutmann, J. S. *Applied Physics Letters* **2006**, *89*.
4. Bumbu, G. G.; Kircher, G.; Wolkenhauer, M.; Berger, R.; Gutmann, J. S. *Macromolecular Chemistry and Physics* **2004**, *205*, 1713-1720.
5. Aoki, H.; Kitamura, M.; Ito, S. *Macromolecules* **2008**, *41*, 285-287.
6. Li, L.; Li, J.; Lukehart, C. M. *Sensors and Actuators, B: Chemical Sensors and Materials* **2008**, *130*, 783-788.
7. Granville, A. M.; Boyes, S. G.; Akgun, B.; Foster, M. D.; Brittain, W. J. *Macromolecules* **2004**, *37*, 2790-2796.
8. Rowe, M. A.; Hammer, B. A. G.; Boyes, S. G. *Macromolecules* **2008**, *41*, 4147-4157.
9. Yu, K.; Wang, H. F.; Han, Y. C. *Langmuir* **2007**, *23*, 8957-8964.
10. Xu, C.; Wu, T.; Drain, C. M.; Batteas, J. D.; Fasolka, M. J.; Beers, K. L. *Macromolecules* **2006**, *39*, 3359-3364.
11. Gao, X.; Feng, W.; Zhu, S. P.; Sheardown, H.; Brash, J. L. *Langmuir* **2008**, *24*, 8303-8308.
12. Yin, Y. H.; Sun, P. C.; Li, B. H.; Chen, T. H.; Jin, Q. H.; Ding, D. T.; Shi, A. C. *Macromolecules* **2007**, *40*, 5161-5170.
13. Prokhorova, S. A.; Kopyshchev, A.; Ramakrishnan, A.; Zhang, H.; Ruhe, J. *Nanotechnology* **2003**, *14*, 1098-1108.
14. Santer, S.; Ruhe, J. *Polymer* **2004**, *45*, 8279-8297.
15. Xu, C.; Wu, T.; Mei, Y.; Drain, C. M.; Batteas, J. D.; Beers, K. L. *Langmuir* **2005**, *21*, 11136-11140.
16. Boyes, S. G.; Brittain, W. J.; Weng, X.; Cheng, S. Z. D. *Macromolecules* **2002**, *35*, 4960-4967.
17. Huang, W. X.; Kim, J. B.; Baker, G. L.; Bruening, M. L. *Nanotechnology* **2003**, *14*, 1075-1080.

18. Zhao, B.; Haasch, R. T.; MacLaren, S. *Journal of the American Chemical Society* **2004**, *126*, 6124-6134.
19. Li, D. J.; Sheng, X.; Zhao, B. *Journal of the American Chemical Society* **2005**, *127*, 6248-6256.
20. Santer, S.; Kopyshv, A.; Donges, J.; Yang, H. K.; Ruhe, J. *Advanced Materials* **2006**, *18*, 2359-2362.
21. Idota, N.; Kikuchi, A.; Kobayashi, J.; Akiyama, Y.; Okano, T. *Langmuir* **2006**, *22*, 425-430.
22. Seino, M.; Yokomachi, K.; Hayakawa, T.; Kikuchi, R.; Kakimoto, M.-A.; Horiuchi, S. *Polymer* **2006**, *47*, 1946-1952.
23. Nagase, K.; Kobayashi, J.; Kikuchi, A.; Akiyama, Y.; Kanazawa, H.; Okano, T. *Langmuir* **2007**, *23*, 9409-9415.
24. Nagase, K.; Kobayashi, J.; Kikuchi, A.; Akiyama, Y.; Kanazawa, H.; Okano, T. *Biomacromolecules* **2008**, *9*, 1340-1347.
25. Nagase, K.; Kobayashi, J.; Kikuchi, A. I.; Akiyama, Y.; Kanazawa, H.; Okano, T. *Langmuir* **2008**, *24*, 511-517.
26. Xu, F. J.; Zhong, S. P.; Yung, L. Y. L.; Tong, Y. W.; Kang, E. T.; Neoh, K. G. *Biomaterials* **2006**, *27*, 1236-1245.
27. Mizutani, A.; Kikuchi, A.; Yamato, M.; Kanazawa, H.; Okano, T. *Biomaterials* **2008**, *29*, 2073-2081.
28. Matsuda, T.; Ohya, S. *Langmuir* **2005**, *21*, 9660-9665.
29. Lokuge, I.; Wang, X.; Bohn, P. W. *Langmuir* **2007**, *23*, 305-311.
30. Li, D. J.; Dunlap, J. R.; Zhao, B. *Langmuir* **2008**, *24*, 5911-5918.
31. Sun, T. L.; Wang, G. J.; Feng, L.; Liu, B. Q.; Ma, Y. M.; Jiang, L.; Zhu, D. B. *Angewandte Chemie-International Edition* **2004**, *43*, 357-360.
32. Wei, Q. S.; Ji, J.; Shen, J. C. *Macromolecular Rapid Communications* **2008**, *29*, 645-650.
33. He, Q.; Kuller, A.; Grunze, M.; Li, J. B. *Langmuir* **2007**, *23*, 3981-3987.
34. Raula, J.; Shan, J.; Nuopponen, M.; Niskanen, A.; Jiang, H.; Kauppinen, E. I.; Tenhu, H. *Langmuir* **2003**, *19*, 3499-3504.
35. Li, D. J.; Jones, G. L.; Dunlap, J. R.; Hua, F. J.; Zhao, B. *Langmuir* **2006**, *22*, 3344-3351.
36. Jonas, A. M.; Glinel, K.; Oren, R.; Nysten, B.; Huck, W. T. S. *Macromolecules* **2007**, *40*, 4403-4405.

37. Azzaroni, O.; Brown, A. A.; Huck, W. T. S. *Angewandte Chemie-International Edition* **2006**, *45*, 1770-1774.
38. Xia, F.; Feng, L.; Wang, S. T.; Sun, T. L.; Song, W. L.; Jiang, W. H.; Jiang, L. *Advanced Materials* **2006**, *18*, 432-436.
39. Cui, Y.; Tao, C.; Zheng, S. P.; He, Q.; Ai, S. F.; Li, J. B. *Macromolecular Rapid Communications* **2005**, *26*, 1552-1556.
40. Li, D.; He, Q.; Cui, Y.; Wang, K.; Zhang, X.; Li, J. *Chemistry-a European journal* **2007**, *13*, 2224-2229.
41. Kizhakkedathu, J. N.; Kumar, K. R.; Goodman, D.; Brooks, D. E. *Polymer* **2004**, *45*, 7471-7489.
42. Wang, X.; Xiao, X.; Wang, X. H.; Zhou, J. J.; Li, L.; Xu, J. *Macromolecular Rapid Communications* **2007**, *28*, 828-833.
43. Li, D. X.; Cui, Y.; Wang, K. W.; He, Q.; Yan, X. H.; Li, J. B. *Advanced Functional Materials* **2007**, *17*, 3134-3140.
44. Schild, H. G. *Progress in Polymer Science* **1992**, *17*, 163-249.
45. Mark, J. E., *Polymer Data Handbook*. Oxford University Press Inc.: 1999.
46. Jhon, Y. K.; Bhat, R. R.; Jeong, C.; Rojas, O. J.; Szleifer, I.; Genzer, J. *Macromolecular Rapid Communications* **2006**, *27*, 697-701.
47. Rahane, S. B.; Floyd, J. A.; Metters, A. T.; Kilbey, S. M. *Advanced Functional Materials* **2008**, *18*, 1232-1240.
48. Balamurugan, S.; Mendez, S.; Balamurugan, S. S.; O'Brien, M. J.; Lopez, G. P. *Langmuir* **2003**, *19*, 2545-2549.
49. Li, J.; Chen, X. R.; Chang, Y. C. *Langmuir* **2005**, *21*, 9562-9567.
50. Wu, T.; Zhang, Y. F.; Wang, X. F.; Liu, S. Y. *Chemistry of Materials* **2008**, *20*, 101-109.
51. Benetti, E. M.; Zapotoczny, S.; Vancso, J. *Advanced Materials* **2007**, *19*, 268-271.
52. Yim, H.; Kent, M. S.; Mendez, S.; Balamurugan, S. S.; Balamurugan, S.; Lopez, G. P.; Satija, S. *Macromolecules* **2004**, *37*, 1994-1997.
53. Yim, H.; Kent, M. S.; Satija, S.; Mendez, S.; Balamurugan, S. S.; Balamurugan, S.; Lopez, G. P. *Physical Review E: Statistical, Nonlinear, and Soft Matter Physics* **2005**, *72*, -.
54. Kong, H.; Li, W. W.; Gao, C.; Yan, D. Y.; Jin, Y. Z.; Walton, D. R. M.; Kroto, H. W. *Macromolecules* **2004**, *37*, 6683-6686.



55. Yim, H.; Kent, M. S.; Satija, S.; Mendez, S.; Balamurugan, S. S.; Balamurugan, S.; Lopez, C. P. *Journal of Polymer Science, Part B-Polymer Physics* **2004**, *42*, 3302-3310.
56. Yim, H.; Kent, M. S.; Mendez, S.; Lopez, G. P.; Satija, S.; Seo, Y. *Macromolecules* **2006**, *39*, 3420-3426.
57. Plunkett, K. N.; Zhu, X.; Moore, J. S.; Leckband, D. E. *Langmuir* **2006**, *22*, 4259-4266.
58. Jonas, A. M.; Hu, Z.; Glinel, K.; Huck, W. T. S. *Nano Letters* **2008**, *8*, 3819-3824.
59. Schulz, D. N.; Peiffer, D. G.; Agarwal, P. K.; Larabee, J.; Kaladas, J. J.; Soni, L.; Handwerker, B.; Garner, R. T. *Polymer* **1986**, *27*, 1734-1742.
60. LeMieux, M. C.; Peleshanko, S.; Anderson, K. D.; Tsukruk, V. V. *Langmuir* **2007**, *23*, 265-273.
61. Rhe, J.; Ballauff, M.; Biesalski, M.; Dziezok, P.; Grohn, F.; Johannsmann, D.; Houbenov, N.; Hugenberg, N.; Konradi, R.; Minko, S.; Motorov, M.; Netz, R. R.; Schmidt, M.; Seidel, C.; Stamm, M.; Stephan, T.; Usov, D.; Zhang, H. N. *Polyelectrolytes with Defined Molecular Architecture I* **2004**, *165*, 79-150.
62. Treat, N. D.; Ayres, N.; Boyes, S. G.; Brittain, W. J. *Macromolecules* **2006**, *39*, 26-29.
63. Wu, T.; Gong, P.; Szleifer, I.; Vlcek, P.; Subr, V.; Genzer, J. *Macromolecules* **2007**, *40*, 8756-8764.
64. Sanjuan, S.; Perrin, P.; Pantoustier, N.; Tran, Y. *Langmuir* **2007**, *23*, 5769-5778.
65. Ryan, A. J.; Crook, C. J.; Howse, J. R.; Topham, P.; Jones, R. A. L.; Geoghegan, M.; Parnell, A. J.; Ruiz-Perez, L.; Martin, S. J.; Cadby, A.; Menelle, A.; Webster, J. R. P.; Gleeson, A. J.; Bras, W. *Faraday Discussions* **2005**, *128*, 55-74.
66. Geoghegan, M.; Ruiz-Perez, L.; Dang, C. C.; Parnell, A. J.; Martin, S. J.; Howse, J. R.; Jones, R. A. L.; Golestanian, R.; Topham, P. D.; Crook, C. J.; Ryan, A. J.; Sivia, D. S.; Webster, J. R. P.; Menelle, A. *Soft Matter* **2006**, *2*, 1076-1080.
67. Zhang, M. M.; Liu, L.; Zhao, H. Y.; Yang, Y.; Fu, G. Q.; He, B. L. *Journal of Colloid and Interface Science* **2006**, *301*, 85-91.
68. Chen, X. Y.; Randall, D. P.; Perruchot, C.; Watts, J. F.; Patten, T. E.; von Werne, T.; Armes, S. P. *Journal of Colloid and Interface Science* **2003**, *257*, 56-64.
69. Kurosawa, S.; Aizawa, H.; Talib, Z. A.; Athoff, B.; Hilborn, J. *Biosensors & Bioelectronics* **2004**, *20*, 1165-1176.

70. Liu, G. M.; Zhang, G. Z. *Journal of Physical Chemistry B* **2008**, *112*, 10137-10141.
71. Li, D. X.; He, Q.; Cui, Y.; Li, J. B. *Chemistry of Materials* **2007**, *19*, 412-417.
72. Li, D.; He, Q.; Yang, Y.; Möhwald, H.; Li, J. *Macromolecules* **2008**, *41*, 7254-7256.
73. Zhou, F.; Shu, W. M.; Welland, M. E.; Huck, W. T. S. *Journal of the American Chemical Society* **2006**, *128*, 5326-5327.
74. Zhou, F.; Huck, W. T. S. *Chemical Communications* **2005**, 5999-6001.
75. Zhang, Q. L.; Xia, F.; Sun, T. L.; Song, W. L.; Zhao, T. Y.; Liu, M. C.; Jiang, L. *Chemical Communications* **2008**, 1199-1201.
76. Abu-Lail, N. I.; Kaholek, M.; LaMattina, B.; Clark, R. L.; Zauscher, S. *Sensors and Actuators B-Chemical* **2006**, *114*, 371-378.
77. Sanjuan, S.; Tran, Y. *Macromolecules* **2008**, *41*, 8721-8728.
78. Ayres, N.; Cyrus, C. D.; Brittain, W. J. *Langmuir* **2007**, *23*, 3744-3749.
79. Gong, P.; Wu, T.; Genzer, J.; Szleifer, I. *Macromolecules* **2007**, *40*, 8765-8773.
80. Ayres, N.; Boyes, S. G.; Brittain, W. J. *Langmuir* **2007**, *23*, 182-189.
81. Choi, E. Y.; Azzaroni, O.; Cheng, N.; Zhou, F.; Kelby, T.; Huck, W. T. S. *Langmuir* **2007**, *23*, 10389-10394.
82. Zhou, F.; Biesheuvel, P. M.; Chol, E. Y.; Shu, W.; Poetes, R.; Steiner, U.; Huck, W. T. S. *Nano Letters* **2008**, *8*, 725-730.
83. Spruijt, E.; Choi, E. Y.; Huck, W. T. S. *Langmuir* **2008**, *24*, 11253-11260.
84. Azzaroni, O.; Moya, S.; Farhan, T.; Brown, A. A.; Huck, W. T. S. *Macromolecules* **2005**, *38*, 10192-10199.
85. Moya, S.; Azzaroni, O.; Farhan, T.; Osborne, V. L.; Huck, W. T. S. *Angewandte Chemie-International Edition* **2005**, *44*, 4578-4581.
86. Moya, S. E.; Azzaroni, O.; Kelby, T.; Donath, E.; Huck, W. T. S. *Journal of Physical Chemistry B* **2007**, *111*, 7034-7040.
87. Azzaroni, O.; Brown, A. A.; Huck, W. T. S. *Advanced Materials* **2007**, *19*, 151-154.

## 3. Tuning the pH Sensitivity of Poly(methacrylic acid) Brushes

### 3.1. Introduction

High density, surface-anchored weak polyelectrolytes, so-called "polymer brushes",<sup>1-5</sup> undergo conformational changes in response to variations in pH and/or ionic strength. These conformational changes are due to alterations in the charge density along the polymer chains, which occur when these brushes are exposed to aqueous media with different pH and/or ionic strength. Exposing *e.g.* a poly(methacrylic acid) (PMAA) brush to a basic aqueous solution results in deprotonation of the carboxylic acid side chain groups, which introduces charges along the polymer backbone and leads to swelling of the polymer brush. The pH responsiveness of weak polyelectrolyte brushes is not only of fundamental interest but is also relevant for various practical applications. Weak polyacid brushes, for example, have been proposed as nanometer-scale actuators<sup>6</sup> and have been used to allow pH-controlled water permeation through porous membranes<sup>7</sup> or enable charge-driven reversible polymer and protein adsorption.<sup>8,9</sup>

Among various other weak polyelectrolyte brushes that have been reported, poly(acrylic acid) (PAA) and poly(methacrylic acid) brushes have probably been the most extensively investigated.<sup>1</sup> Using, for example, atomic force microscopy (AFM) and ellipsometry it was demonstrated that the thickness of a PMAA brush can increase up to ~300% when switching from pH 3 to pH 10.<sup>10,11</sup> Protonation/deprotonation of the pendant carboxylic acid groups also influences the wetting properties of weak polyacid brushes, which are hydrophobic at low pH and hydrophilic at high pH.<sup>11-13</sup> Another very powerful technique to study the pH-dependent swelling properties of PAA and PMAA brushes is the quartz crystal microbalance (QCM).<sup>14,15</sup> Hilborn and coworkers investigated surface-tethered PAA brushes and found that the intensity of the resonance frequency shift upon switching between pH 4 and 5.4 depends on the brush thickness.<sup>16</sup>

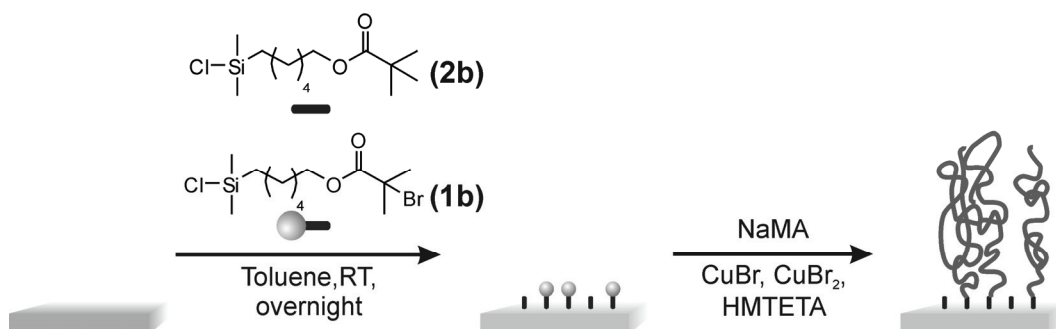
An accurate understanding of the influence of polymer chain length, grafting density and chemical composition on the pH and ionic strength induced conformational changes of weak polyelectrolyte brushes is essential to engineer the properties of these layers for practical applications. Although the pH- and ionic strength dependent swelling behavior of weak polyelectrolyte brushes has been the subject of a large number of studies and much insight has been obtained, there are still issues that have only received very little or no attention. In particular, studies that systematically investigate the effects of polymer chain length, grafting density and chemical composition are relatively scarce.<sup>12,16,17</sup> This chapter uses the QCM technique to systematically evaluate the influence of polymer chain length, grafting density and chemical composition on the pH responsiveness of weak polyacid brushes and consists of two parts. First, the pH responsiveness of a series of PMAA brushes with varying thickness and grafting densities was studied and the question addressed to which extent these parameters affect the overall apparent pKa and/or effective bulk pKa of the layer. While a PMAA brush usually responds in a relatively narrow pH window that is centered around the pKa of the brush, certain applications may call for a more gradual response to pH. The second part of this section explores the post-polymerization modification of PMAA brushes with various amine functionalized weak acids as an approach to tune the pH response and expand the dynamic response range of weak, PMAA based polymer brushes.

## 3.2. Results and discussion

### 3.2.1. Polymer brush synthesis

The poly(methacrylic acid) (PMAA) brushes were prepared following a two step process, which is outlined in Scheme 1. First, the substrate is modified with an ATRP initiator functionalized chlorosilane derivative **1b** (or a mixture of compound **1b** and the ATRP inactive chlorosilane derivative **2b**) followed by surface-initiated atom transfer radical polymerization (SI-ATRP) of sodium methacrylate (NaMA). As the substrate, both SiO<sub>2</sub> coated QCM crystals as well as silicon wafers were used. Whereas the SiO<sub>2</sub> coated QCM crystals were used to study the pH-dependent swelling properties of the

PMAA brushes, the kinetics of the SI-ATRP and the chemical characterization of the surface-grafted polymers were performed on samples grown from silicon wafers.



**Scheme 1.** Synthesis of PMAA brushes of varying grafting density via SI-ATRP.

Modification of a plasma cleaned silicon wafer with ATRP initiator **1b** results in a drastic increase in the water contact angle (from 0° to 84°) (Table 1). Further evidence for the successful grafting of the ATRP initiator **1b** was obtained from grazing angle FTIR experiments (Figure S1). The FTIR spectrum of the ATRP initiator modified substrate revealed three bands at  $\sim 2958\text{ cm}^{-1}$ ,  $\sim 2927\text{ cm}^{-1}$  and  $\sim 2854\text{ cm}^{-1}$ , which are due to the asymmetric and the symmetric CH<sub>2</sub> vibrations of the alkyl chain. At lower wavenumbers, a band due to the stretching vibrations of the C=O bond is observed at  $\sim 1735\text{ cm}^{-1}$ . In the fingerprint domain, the spectrum shows a very strong band at  $\sim 1236\text{ cm}^{-1}$ , which is assigned to the Si-O-Si asymmetric stretching. The aqueous based SI-ATRP protocol used in this chapter allowed for a rapid growth of PMAA brushes with thicknesses ranging from  $\sim 10\text{ nm}$  to  $\sim 80\text{ nm}$  within 15 min (Figure S2). The growth of the PMAA brushes from an ATRP initiator modified substrate resulted in a decrease in the water contact angle from 84° to 33° (Table 1). The reflectance-FTIR measurement of the PMAA brush coated silicon substrate reveals a broad band of strong intensity at  $\sim 3100 - 3500\text{ cm}^{-1}$  corresponding to the hydroxyl groups (Figure 5.A). The spectrum of the PMAA brush shows also two bands at  $\sim 2996\text{ cm}^{-1}$  and  $\sim 2936\text{ cm}^{-1}$  assigned to the asymmetric and the symmetric CH<sub>2</sub> vibrations. At to lower wavenumbers, two characteristic bands at  $\sim 1697\text{ cm}^{-1}$  and  $\sim 1180\text{ cm}^{-1}$  assign, respectively, to the C=O and the carboxylic acid C-OH stretching vibrations can be observed.

In order to evaluate the influence of grafting density on the pH responsiveness of the PMAA brushes, a series of samples was grown from substrates that were modified with

mixtures of the ATRP initiator modified chlorosilane **1b** and the ATRP inactive chlorosilane **2b**. Figure 1 shows the evolution of layer thickness as a function of the volume fraction of **1b** in the reaction solution that was used to modify the substrate. As the polymerization time was identical for all substrates, the increase in layer thickness with increasing volume fraction of **1b** reflects the gradual transition from a more collapsed to a more stretched chain conformation as the grafting density increases.

**Table 1.** Static water contact angles of the different surfaces.

Sample	Water contact angle
Silicon wafer <sup>a</sup>	0°
Silicon wafer + ATRP initiator	84°
PMAA brush	33°
PMAA brush + NHS	47°
PMAA brush + glutamic acid	30°
PMAA brush + 4-aminophenol	52°
PMAA brush + <i>O</i> -phosphorylethanolamine	16°

<sup>a</sup>: After plasma treatment.

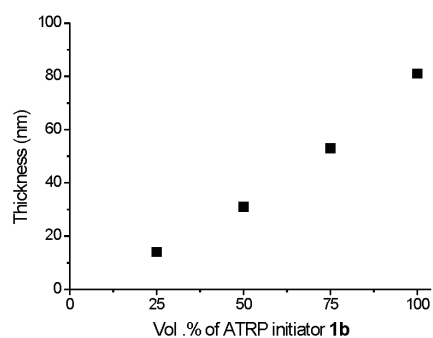


**Figure 1.** Evolution of the thickness of PMAA brushes grown by SI-ATRP of NaMA as a function of volume percentage of ATRP initiator **1b** used during the surface modification (Polymerization time 10 min).

### 3.2.2. Swelling properties of dense PMAA brushes

As a typical example, Figure 2 shows the response of a QCM chip modified with a 11 nm thick PMAA brush upon exposure to aqueous solutions with pH values increasing from pH 4 to pH 7.5. The PMAA brush used for the experiments shown in Figure 2 was grown from a surface that was modified only with ATRP initiator **1b** and is referred to as a dense brush in this study. Since the swelling properties of PMAA brushes are also sensitive to inorganic ions,<sup>10,18</sup> the experiments were carried out using low ionic strength (10 mM) Na<sub>2</sub>HPO<sub>4</sub>/citrate buffer solutions. At low pH, the PMAA chains are protonated and the brush is in the collapsed state. Under these conditions, the polymer brush acts as a rigid film, which leads to a low damping of the QCM resonator. At high pH values, the PMAA chains are deprotonated, which results in swelling of the polymer brush, an increase in viscoelasticity and an increased damping of the resonator.<sup>16</sup> From Figure 2, an apparent pKa of ~ 6.25 can be estimated. This value is not only different than the pKa of the corresponding free polymer in solution<sup>19</sup> or of a carboxylic acid functionalized self-assembled monolayer (SAM),<sup>20</sup> but the pKa transition of the surface tethered PMAA chains also occurs over a much broader pH range. These effects have been observed before using other techniques and have been attributed to the high grafting density of the surface anchored polymer chains.<sup>12</sup> Swelling and collapse of PMAA brushes in response to changes in pH from 10.5 to 3 has been reported to occur on a time scale of ~ 6 seconds.<sup>21</sup> In contrast, for the experiments shown in Figure 2, it took about 3 minutes with every 0.5 pH unit increase to reach equilibrium (Figure S3). This difference may be attributed to the relatively gradual increase in pH for the experiment shown in Figure 2 as compared to literature<sup>21</sup> (0.5 pH unit versus 7.5 pH units), as well as to the intrinsic properties of polymer brush modified QCM resonators.<sup>13,15,16,22,23</sup> The change in resonance frequency upon varying the pH between 4 and 4.5 was constant over up to 7 switching cycles underlining the reversibility of the pH-induced swelling/collapse (Figure S4).

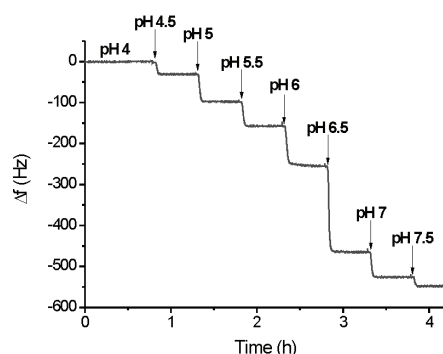


**Figure 2.** Typical response of a QCM chip modified with an 11 nm thick PMAA brush upon exposure to buffer solutions with increasing pH.

Figure 3 summarizes the pH-response of a series of 5 QCM chips modified with PMAA brushes with thicknesses ranging from 5 to 91 nm. Comparison of the normalized frequency shift reveals that the thinner PMAA brushes show similar behavior, whereas for the thicker PMAA brush (91 nm) a slightly higher pKa value was observed. Furthermore at any given pH value, the intensity of the observed frequency shift was found to increase linearly with brush thickness (Figure S5). The slight thickness dependence of the pKa of PMAA brushes as suggested by the data presented in Figure 3B is in contrast to findings by Santonicola *et al.* who found identical pKa values for PMAA brushes with thickness of  $\sim 30$ , respectively,  $\sim 90$  nm.<sup>13</sup>

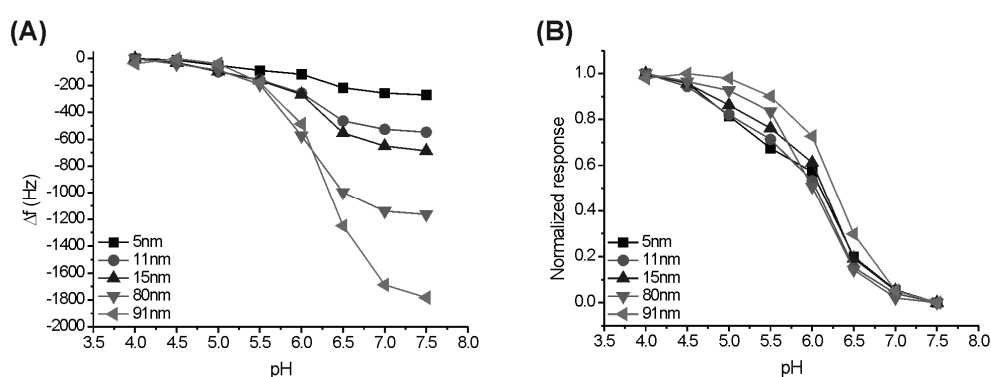


**Figure 3.** Shift (A) and normalized shift (B) of five PMAA brush coated QCM chips of different thicknesses as a function of pH.



### 3.2.3. Influence of the polymer brush density on the swelling behavior

Evaluation of the pH response of a series of QCM chips modified with PMAA brushes of different grafting densities revealed that the intensity of the frequency shift increases with increasing brush density (Figure 4A). This observation reflects the increased mass of polymer that is immobilized on the surface when increasing the grafting density.<sup>24</sup> Comparison of the normalized response of the different brushes indicates that grafting density influences the swelling properties (Figure 4B). The apparent pKa of the PMAA brushes seems to depend on grafting density; lower density brushes are responding, *i.e.* swelling, at a lower pH as compared to more dense brushes. It is important to note here that the results shown in Figure 4 were obtained with PMAA brushes that were all prepared using the same polymerization time. As a result, the samples do not only differ in grafting density, but also in terms of brush thickness. To decouple the effects of thickness and grafting density, Figure S6 in the Supporting Information compares the pH response of a 15 nm thick dense (100%) PMAA brush with that of a 14 nm thick low density (25%) brush. The results in Figure S6 (Supporting Information) also indicate and confirm that the apparent pKa of the brushes seems to depend on grafting density with lower density brushes responding at a lower pH as compared to more dense brushes. In the literature, contradictory results concerning the influence of grafting density on the apparent pKa of polyacid brushes have been reported. While Lego *et al.* concluded that low density poly(acrylic acid) (PAA) brushes started swelling at higher pH than the higher density analogues,<sup>25</sup> the observations of Currie and co-workers are in line with the data shown in Figure 4B and indicated the opposite behavior.<sup>26,27</sup> Currie *et al.* attributed the shift in apparent pKa with increasing graft density to the decrease in the degree of dissociation of polyacid brushes with increasing grafting density, which is also in line with theoretical predictions.<sup>28,29</sup>

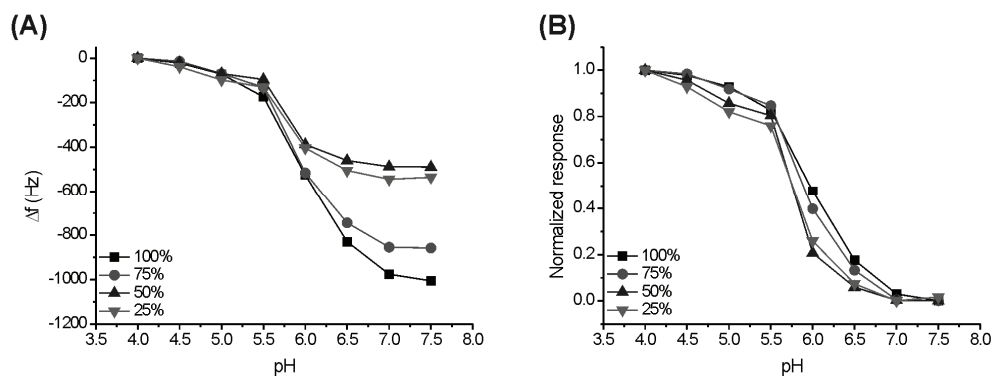
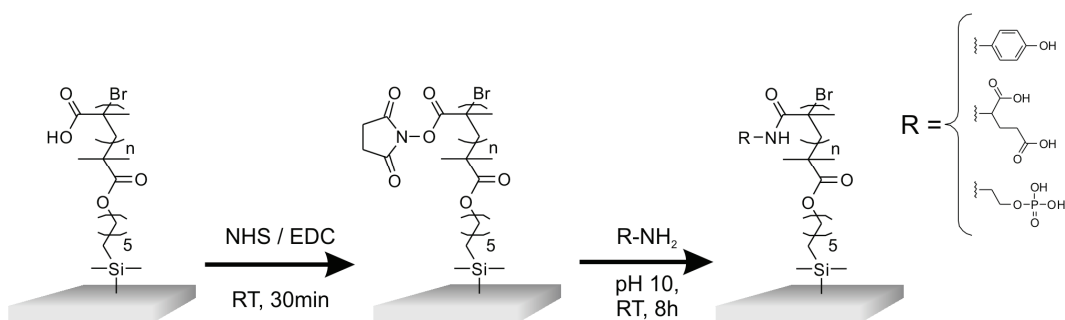


**Figure 4.** Shift (A) and normalized shift (B) of the resonance frequency for QCM chips coated with PMAA brushes of different densities as a function of pH. (Polymerization time 10 min. Percentages refer to the volume % of ATRP initiator **1b** that was used to modify the substrate from which the brushes were grown).

### 3.2.4. Post-polymerization modification and QCM study of the resulting brushes

As illustrated in Figures 3 and 4, a QCM chip modified with a PMAA brush shows a nonlinear pH response and the largest frequency shifts, *i.e.* the highest sensitivity, are observed around the pKa of the polymer ( $\sim 6$ ). For certain applications, however, an increased sensitivity at other pH values or an expanded dynamic response range may be desired. One strategy to engineer the pH response of QCM sensors modified with polyacid brushes would involve the surface-initiated polymerization of different weak acid functionalized monomers. An interesting alternative approach that would circumvent the need to synthesize a new polymer brush for every new pH sensitive monomer would be to use the PMAA brushes as a platform for the post-polymerization modification with different pH-sensitive functional groups. *N*-Hydroxysuccinimide (NHS) activation followed by reaction of the intermediate active ester with appropriate primary amines is a well-established strategy for the post-polymerization modification of polyacid brushes (Scheme 2).<sup>30-32</sup> In this chapter, post-polymerization modification was carried out with three different primary amines containing acidic functional groups with pKa values covering a wide pH range *viz.* 4-aminophenol (pKa  $\sim 10.3$ ), *O*-phosphorylethanolamine (pKa<sub>1</sub>  $\sim 1.6$ , pKa<sub>2</sub>  $\sim 6.0$ ) and glutamic acid (pKa<sub>1</sub>  $\sim 2.2$ , pKa<sub>2</sub>  $\sim 4.3$ ).



**Scheme 2.** NHS mediated post-polymerization modification of PMAA brushes with various functional amines.

The activation and post-polymerization modification of the PMAA brushes can be conveniently monitored using FTIR spectroscopy and via water contact angle measurements. Upon reaction of the PMAA brushes with NHS, the broad band at  $\sim 3100 - 3500 \text{ cm}^{-1}$ , as well as the bands at  $\sim 1697 \text{ cm}^{-1}$  and  $\sim 1180 \text{ cm}^{-1}$  in the FTIR spectrum of the unmodified PMAA brush, which correspond, respectively, to the O-H $\cdots$ O stretching, the C=O vibration and the C-OH stretching, vanish (Figure 5). At the same time, two characteristic bands at  $\sim 1806 \text{ cm}^{-1}$  and at  $\sim 1756 \text{ cm}^{-1}$  appear, which can be assigned, respectively, to the ester carbonyl stretching and the vibration of succinimidyl carbonyls.<sup>33</sup> The NHS activation also results in an increase the water contact angle from  $33^\circ$  to  $47^\circ$  (Table 1). In the XPS survey scan, a new peak at  $\sim 399 \text{ eV}$ , corresponding to the  $\text{N}_{1s}$  signal, appears after activation of the PMAA brush with NHS (Figure S7). After reacting the NHS activated PMAA brushes with the different amines for a period of 8 hrs, the broad FTIR band above  $\sim 3300 \text{ cm}^{-1}$  corresponding to the O-H $\cdots$ O stretch appears again and the two characteristic bands of the NHS groups (at  $\sim 1806 \text{ cm}^{-1}$  and at  $\sim 1756 \text{ cm}^{-1}$ ) vanish. Various new bands between  $\sim 1650 - 1750 \text{ cm}^{-1}$ , which are due to the mono-substituted amide groups, appear. In case of the glutamic acid modified PMAA brush, two overlapping bands at  $\sim 1661 \text{ cm}^{-1}$  and  $\sim 1567 \text{ cm}^{-1}$  can be seen in the FTIR spectrum, which are due to carboxylate groups. Post-polymerization modification of the NHS activated PMAA brushes with the different amines also results in changes in the water contact angle, which decreases from  $47^\circ$  (for the PMAA-NHS brush) to  $16^\circ$  and  $30^\circ$  for brushes post-modified with O-phosphorylethanolamine and glutamic acid, respectively (Table 1). In case of the 4-aminophenol modified brushes, however, a slight increase in the water contact angle from  $47^\circ$  to  $52^\circ$  was observed.

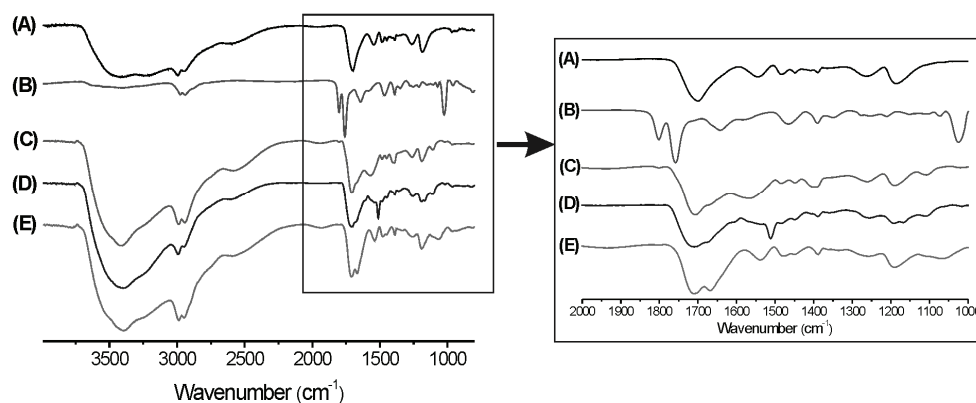


**Figure 5.** Reflectance FTIR spectra of (A) a PMAA brush ( $\sim 80$  nm); (B) an NHS activated PMAA brush; (C) a PMAA brush post-modified with glutamic acid; (D) a PMAA brush post-modified with 4-aminophenol and (E) a PMAA brush post-modified with *O*-phosphorylethanolamine. The spectra in Figures B-E are from post-modified brushes that were prepared from a PMAA brush with a thickness of  $\sim 80$  nm.

The FTIR spectra shown in Figure 5 were recorded on post-modified PMAA brushes obtained after a reaction time of 8 hrs. These relatively long reaction times were necessary since FTIR spectroscopy still revealed the presence of unreacted active ester groups after 1 hr (Figure S8, S9 and S10). The reaction between the active ester brushes and the different amines was performed at pH 10 in order to ensure full deprotonation of the primary amines. At lower pH very little incorporation of the amines was observed, while at higher pH (pH 12) complete cleavage of the polymer brush chains occurred within 30 min (data not shown). Since the post-polymerization modification of the NHS-activated PMAA brushes was carried out at pH 10, an additional experiment was performed to assess the stability of the active ester groups under these conditions (Figure S11). Monitoring the intensity of the FTIR bands at  $\sim 3300 - 3500$  cm<sup>-1</sup> (carbonyl C-O-H $\cdot$ O stretch) and  $\sim 1570$  cm<sup>-1</sup> (carboxylate groups) indicates that hydrolysis of the active ester groups becomes significant only after 2 - 4 hrs. As a consequence, because most of the amines used in this study react with the NHS activated brushes within 4 hrs (see Figure S8, S9 and S10), concurrent hydrolysis of the active ester groups does not seem to be very significant. FTIR analysis also revealed that the rates of incorporation of the different amines in the active ester brush depends on the chemical structures of the amine (Figure S8, Figure S9 and Figure S10). *O*-phosphorylethanolamine and 4-aminophenol reacted relatively fast and after about two, respectively, four hours the two characteristic

bands of the NHS-ester groups (at  $\sim 1806\text{ cm}^{-1}$  and at  $\sim 1756\text{ cm}^{-1}$ ) could not be seen anymore. In case of the post-polymerization modification with glutamic acid, however, even after 16 hrs of incubation, the FTIR spectrum still reveals the presence of residual, unreacted active ester groups (Figure S10).

Further information about the post-polymerization modification of the NHS activated PMAA brushes was obtained from XPS analysis (Figure 6 and S7). The high resolution  $\text{C}_{1s}$  and  $\text{O}_{1s}$  scans of the PMAA brush could be fitted with the expected contributions of the different carbon, respectively oxygen, atoms. NHS activation results in a slight broadening of the signal  $\sim 285\text{ eV}$  in the  $\text{C}_{1s}$  high resolution scan new signal, which is due to the increased number of different aliphatic carbon atoms, as well as the appearance of a  $\text{N}_{1s}$  signal at  $\sim 393\text{ eV}$ . Upon post-polymerization modification, the position of the  $\text{N}_{1s}$  signal does not appreciably change. In the case of the post-polymerization modification with *O*-phosphorylethanolamine two additional signals at  $\sim 192\text{ eV}$  and  $\sim 134\text{ eV}$ , corresponding respectively to the  $\text{P}_{2s}$  and the  $\text{P}_{2p}$  phosphorus signal, appear. The large number of different carbon and heteroatoms in the post-modified polymer brushes does not allow an accurate deconvolution of the high resolution scans, which would enable to determine the conversion of the post-polymerization modification reactions. For the brushes post-modified with *O*-phosphorylethanolamine, however, the difference in atomic percentage between N (3.98%) and P (2.84%) indicates a conversion of  $\sim 72\%$  for this amine. In case of the post-polymerization modification with 4-aminophenol, the conversion can be estimated by deconvolution of the  $\text{O}_{1s}$  signal. From the relative areas of the peak assigned to the amide carboxyl oxygen and the phenolic oxygen the conversion can be estimated to  $\sim 84\%$ . In addition to steric reasons and diffusion limitations, the none-quantitative conversion of the NHS active ester groups may also be partially attributed to the fact that NHS esters are known to undergo side reactions such as ring-opening.<sup>34-37</sup>

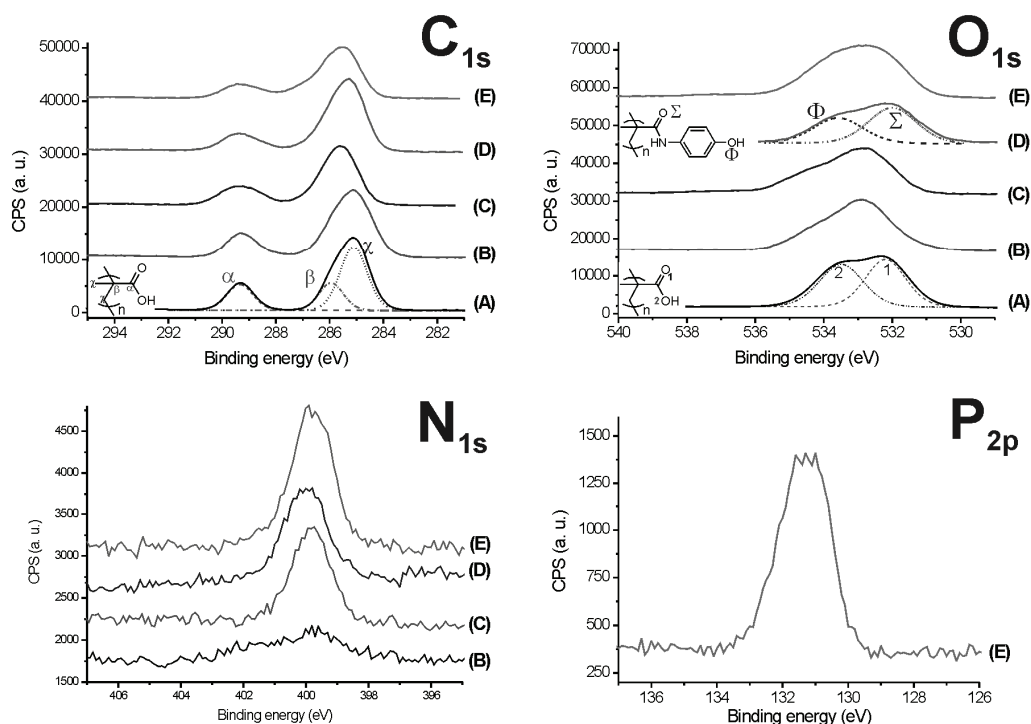


**Figure 6.** XPS high resolution  $C_{1s}$ ,  $O_{1s}$ ,  $N_{1s}$  and  $P_{2p}$  scans of (A) a PMAA brush ( $\sim 80$  nm); (B) an NHS activated PMAA brush; (C) a PMAA brush post-modified with glutamic acid; (D) a PMAA brush post-modified with 4-aminophenol and (E) a PMAA brush post-modified with *O*-phosphorylethanolamine. The spectra in Figures B-E were recorded on post-modified brushes that were prepared from a PMAA brush with a thickness of  $\sim 80$  nm.

Figure 7 compares the normalized pH response of a QCM chip functionalized with an unmodified PMAA brush with that of PMAA functionalized QCM chips that have been post-modified with 4-aminophenol, *O*-phosphorylethanolamine and glutamic acid. A Figure, which shows the changes in the absolute frequency shift with pH for the different coatings is included in the Supporting Information (Figure S12). This Figure indicates that there are no significant differences in the absolute frequency shift for the different samples at pH 4 and pH 7.5. The normalized data in Figure 7, however, clearly indicate that post-polymerization modification is a versatile strategy to tune both the responsiveness, *i.e.* the pH of maximum response, as well as the response range of PMAA based brushes. While the glutamic acid modified PMAA brush displays a pH response that is essentially identical to that of the unmodified PMAA brush, the response curve of the 4-aminophenol modified brush is shifted to slightly higher pH, which is attributed to the higher pKa of the phenolic side chain functional groups ( $\sim 10.3$ ) as

compared to the methacrylic acid carboxylic groups. Post-polymerization modification with *O*-phosphorylethanolamine is interesting as it allows to engineer the response range of the polymer brush coated QCM crystal. Compared to a QCM chip coated with an unmodified PMAA brush, a chip covered with an *O*-phosphorylethanolamine modified PMAA brush shows a more gradual and linear response over a much broader pH range. The different pH response of the *O*-phosphorylethanolamine post-modified brush is attributed to the fact that the phosphoric acid groups possess two pKa values that are relatively far apart ( $pK_{a1} \sim 1.6$ ,  $pK_{a2} \sim 6.0$ ).

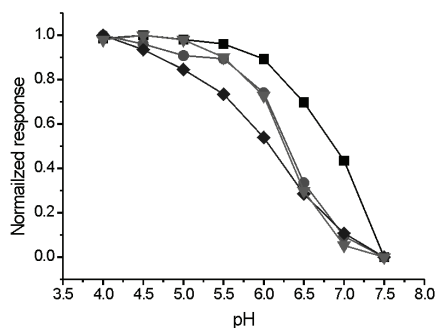


**Figure 7.** Normalized pH response of QCM chips coated with an unmodified PMAA brush ( $\sim 80$  nm) ( $\blacktriangledown$ ); a PMAA brush post-modified with 4-aminophenol ( $\blacksquare$ ); a PMAA brush post-modified with *O*-phosphorylethanolamine ( $\blacklozenge$ ) and a PMAA brush post-modified with glutamic acid ( $\bullet$ ).

### 3.3. Conclusions

This chapter has presented the results from a systematic series of QCM experiments that were aimed at further understanding and, ultimately, engineering of the pH-induced swelling properties of poly(methacrylic acid) brushes. As a result of the high grafting density and strong interpolymer interactions, the pKa value of the surface-tethered PMAA was found to occur at a pH that was different from that of the equivalent free polymer in solution. A systematic investigation of the influence of the polymer brush thickness and grafting density on the overall layer swelling properties revealed that the denser and the thicker the polymer film, the greater the absolute pH-induced QCM response. Furthermore, the apparent pKa of the overall polymer film was found to

decrease with decreasing grafting density of the PMAA brush. The second part of this report has investigated the feasibility of the NHS-mediated post-polymerization modification of PMAA brushes to engineer the pH-responsiveness of these polymer films. By using appropriate amino functionalized acids, it was possible to tune both the pH of maximum response as well as to expand the dynamic response range of the PMAA brushes. As weak polyelectrolyte brushes are attractive as actuators or to allow pH controlled transport or adsorption, the results of this study may facilitate to engineer the properties of these thin polymer films and further expand their possible range of applications.



## 3.4. Experimental

### 3.4.1. Materials

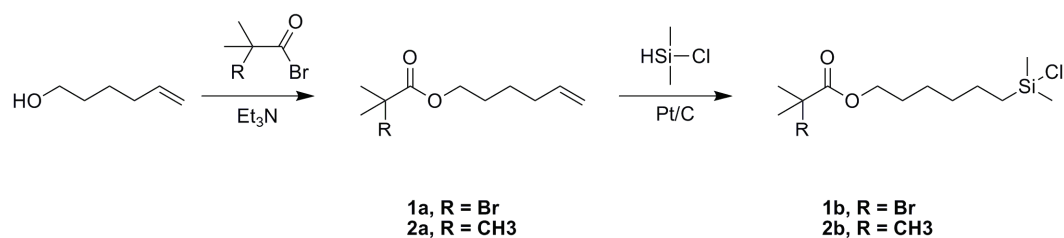
All chemicals were purchased from Aldrich and used as received. Toluene was dried by passage through two columns of molecular sieves using a Pure Solv 400 solvent purification system. Ultrahigh quality Milli-Q water with a resistance of 18.2 M $\Omega$ .cm (at 25 °C) was obtained from a Millipore Milli-Q gradient machine fitted with a 0.22  $\mu$ m filter.

### 3.4.2. Methods

Polymer brushes were grown from silicon wafers and QCM chips, which were cleaned using a microwave induced oxygen plasma system (Diener electronic GmbH, Germany). Reflectance Fourier transform infrared (FTIR) spectroscopy was carried out on a nitrogen purged Nicolet Magna-IR 560 spectrometer equipped with a Micro Specular Reflectance accessory (Specac Ltd., UK). Grazing angle Attenuated Total Reflectance Fourier transform infrared spectroscopy was performed on a nitrogen purged Nicolet 6700 FT-IR spectrometer equipped with a VariGATR™ grazing angle ATR accessory (Harrick Scientific Products Inc, NY) fixing the incident angle at 65°. X-ray photoelectron spectroscopy (XPS) was carried out using an Axis Ultra instrument from Kratos Analytical equipped with a conventional hemispheric analyzer. The X-ray source employed was a monochromatic Al K $\alpha$  (1486.6 eV) source operated at 100 W and 10<sup>-9</sup> mbar; XPS spectra were calibrated using the carbonyl carbon signal at 289.3 eV.<sup>38</sup> Water contact angle measurements were performed using a DataPhysics OCA 35 contact angle measuring instrument. Polymer brush thicknesses were measured by Atomic Force Microscopy (AFM), which was performed in Tapping mode on a Veeco Multimode Nanoscope IIIa SPM controller (Digital instruments, Santa Barbara, CA) using NSC14/no Al Mikromasch (Tallinn, Estonia) cantilevers. Quartz Crystal Microbalance (QCM) measurements were performed at 25 °C with a Q-Sense E4 system (Q-Sense, Sweden) using SiO<sub>2</sub> coated quartz crystals purchased from ICM (Oklahoma City, USA) and recording the fundamental resonance frequency. For the pH sensitivity measurements, the

polymer coated QCM chips were exposed to various 10 mM Na<sub>2</sub>HPO<sub>4</sub>/citrate buffer solutions of different pH values.

### 3.4.3. Procedures



**Scheme 3.** Synthesis of the SI-ATRP initiator (**1b**) and the ATRP inactive equivalent (**2b**).

#### 3.4.3.1. Synthesis of SI-ATRP initiator (**1b**)

##### *Synthesis of 5-hexen-1-yl 2-bromo-2-methylpropionate (**1a**)*

5-Hexen-1-ol (6.00 mL, 50 mmol) and freshly distilled triethylamine (7.00 mL, 50 mmol) were dissolved in dichloromethane (30 mL). The solution was stirred under nitrogen and cooled with an ice bath. Next,  $\alpha$ -bromoisobutyryl bromide (6.15 mL, 50 mmol) was added dropwise and the resulting mixture stirred under nitrogen at 0 °C for one hour and additional 3 hours at room temperature. The precipitated triethylammonium bromide was removed by filtration and the product washed with a saturated ammonium chloride solution. The organic phase was dried over MgSO<sub>4</sub> and the solvent removed under reduced pressure. 5-Hexen-1-yl 2-bromo-2-methylpropionate was obtained as a colorless oil after by vacuum distillation (120 °C, 10 mbar). Yield: 81 %. <sup>1</sup>H NMR (400 MHz, CDCl<sub>3</sub>,  $\delta$ ): 1.47 (m, 2H, -CH<sub>2</sub>-), 1.66 (m, 2H, -CH<sub>2</sub>-), 1.91 (s, 6H, C-CH<sub>3</sub>), 2.07 (m, 2H, -CH<sub>2</sub>-), 4.15 (t, 2H, O=C-O-CH<sub>2</sub>), 4.98 (m, 2H, C=CH<sub>2</sub>), 5.78 (s, 1H, -CH=CH<sub>2</sub>). <sup>13</sup>C NMR (400 MHz, CDCl<sub>3</sub>,  $\delta$ ): 25.75, 28.32 (-CH<sub>2</sub>-), 30.77 (C-CH<sub>3</sub>), 33.76 (-CH<sub>2</sub>-), 55.96 (C-CH<sub>3</sub>), 66.13 (O=C-O-CH<sub>2</sub>), 114.11 (C=CH<sub>2</sub>), 139.14 (C=CH<sub>2</sub>), 171.69 (C=O).

##### *Synthesis of (6-(2-(2-Bromo-2-methyl)propionyloxy)hexyldimethylchlorosilane (**1b**)*

2.23 g (9 mmol) 5-Hexen-1-yl-2-bromo-2-methylpropionate was refluxed overnight under nitrogen at 50 °C with 10 mL (90 mmol) dimethylchlorosilane in presence of 20 mg Pt/C (10% Pt). After the reaction, the solution was filtered over anhydrous sodium sulfate

in order to remove the catalyst. The solvent was evaporated under reduced pressure and **1b** was obtained as colorless oil after vacuum distillation (150 °C, 0.4 mbar). Yield: 90 %. <sup>1</sup>H NMR (400 MHz, CDCl<sub>3</sub>, δ): 0.37 (m, 6H, Si-CH<sub>3</sub>), 0.79 (m, 2H, -CH<sub>2</sub>-), 1.37 (m, 6H, -CH<sub>2</sub>-), 1.65 (m, 2H, -CH<sub>2</sub>-), 1.90 (s, 6H, C-CH<sub>3</sub>), 4.14 (t, 2H, O=C-O-CH<sub>2</sub>). <sup>13</sup>C NMR (400 MHz, CDCl<sub>3</sub>, δ): 1.61 (Si-CH<sub>3</sub>), 18.81, 22.80, 25.35, 28.16 (-CH<sub>2</sub>-), 30.73 (C-CH<sub>3</sub>), 32.36 (-CH<sub>2</sub>-), 55.91 (C-CH<sub>3</sub>), 65.97 (O=C-O-CH<sub>2</sub>), 171.63 (C=O).

#### 3.4.3.2. Synthesis of SI-ATRP inactive chlorosilane (**2b**)

The ATRP inactive 6-(chloro(dimethyl)silyl)hexyl pivalate **2b** was synthesized via the same protocol than the SI-ATRP initiator **1b** using pivaloyl chloride instead of α-bromoisobutyryl bromide.

##### *Hexen-5-enyl pivalate (2a)*

<sup>1</sup>H NMR (400 MHz, CDCl<sub>3</sub>, δ): 1.16 (s, 9H, C-CH<sub>3</sub>), 1.43 (m, 2H, -CH<sub>2</sub>-), 1.61 (m, 2H, -CH<sub>2</sub>-), 2.66 (m, 2H, -CH<sub>2</sub>-), 4.03 (t, 2H, O=C-O-CH<sub>2</sub>), 4.96 (m, 2H, C=CH<sub>2</sub>), 5.76 (s, 1H, -CH=CH<sub>2</sub>). <sup>13</sup>C NMR (400 MHz, CDCl<sub>3</sub>, δ): 25.75, 28.32 (-CH<sub>2</sub>-), 30.77 (C-CH<sub>3</sub>), 33.76 (-CH<sub>2</sub>-), 55.96 (C-CH<sub>3</sub>), 66.13 (O=C-O-CH<sub>2</sub>), 114.11 (C=CH<sub>2</sub>), 139.14 (C=CH<sub>2</sub>), 171.69 (C=O).

##### *6-(chloro(dimethyl)silyl)hexyl pivalate (2b)*

<sup>1</sup>H NMR (400 MHz, CDCl<sub>3</sub>, δ): 0.39 (m, 6H, Si-CH<sub>3</sub>), 0.82 (m, 2H, -CH<sub>2</sub>-), 1.18 (s, 9H, C-CH<sub>3</sub>), 1.37 (m, 6H, -CH<sub>2</sub>-), 1.61 (m, 2H, -CH<sub>2</sub>-), 4.03 (t, 2H, O=C-O-CH<sub>2</sub>). <sup>13</sup>C NMR (400 MHz, CDCl<sub>3</sub>, δ): 1.60 (Si-CH<sub>3</sub>), 18.84, 22.84, 25.49 (-CH<sub>2</sub>-), 27.16 (C-CH<sub>3</sub>), 28.45, 32.47 (-CH<sub>2</sub>-), 38.68 (C-CH<sub>3</sub>), 64.31 (O=C-O-CH<sub>2</sub>), 178.54 (C=O).

#### 3.4.3.3. Immobilization of the ATRP initiator

First, the silicon wafers were sonicated for 5 min in acetone and dried. The silicon surfaces were then exposed to an oxygen plasma (180 W, 10 min) and subsequently the clean wafers were kept overnight and in the dark in a 10 mM solution of **1b**, or in a 10 mM mixture of **1b** and **2b**, in anhydrous toluene. Afterwards, the slides were extensively rinsed with chloroform, dried under nitrogen and transferred to the appropriate reactors for the polymerizations. Silicon oxide coated QCM chips were modified in a similar way, but were not sonicated.

#### 3.4.3.4. Surface-initiated atom transfer radical polymerization

In a Schlenck tube, 0.293 mL (1.00 mmol) 1,1,4,7,10,10-hexamethyltriethylene tetramine (HMTETA) and 40.5 mg (0.18 mmol) CuBr<sub>2</sub> were dissolved in 5.4 mL Milli-Q water and the mixture was subsequently subjected to three freeze-pump-thaw cycles. Once the solution was degassed, 45 mg (0.31 mmol) CuBr was added under nitrogen and allowed to dissolve. In a separate Schlenck tube, 9.3 g (86.11 mmol) sodium methacrylate (NaMA) was dissolved in 10 mL Milli-Q water. The resulting solution was degassed by three freeze-pump-thaw cycles and then added to the solution containing the catalyst system. Then, the polymerization mixture was transferred, using a cannula, into a polymerization reactor containing the ATRP initiator modified silicon wafers or QCM chips and the reaction was allowed to proceed for the desired time at room temperature under nitrogen atmosphere. After polymerization, the slides were thoroughly rinsed with deionized water and left overnight in water in order to extract all the sodium ions. Patterned polymer brushes for Atomic Force Microscopy (AFM) studies were prepared from patterned ATRP initiator modified substrates, which were obtained as previously described.<sup>39</sup>

#### 3.4.3.5. Post-polymerization modification reactions

The activation of the poly(methacrylic acid) (PMAA) brushes with *N*-hydroxysuccinimide (NHS) in presence of *N*-(3-dimethylaminopropyl)-*N'*-ethylcarbodiimide hydrochloride (EDC), was performed as previously described.<sup>31</sup> The NHS activated polymer brushes were directly used for the post-polymerization modification, which was carried out by incubating the substrates in a 0.1 M aqueous solution of the appropriate amine (0.05 M in case of 4-aminophenol) at pH 10. After 8 hrs, the substrates were thoroughly rinsed with water and dried under nitrogen.

### 3.5. References

1. Barbey, R.; Lavanant, L.; Paripovic, D.; Schüwer, N.; Sugnaux, C.; Tugulu, S.; Klok, H.-A. *Chemical Reviews* **2009**, *109*, 5437-5527.
2. Brittain, W. J.; Minko, S. *Journal of Polymer Science Part a-Polymer Chemistry* **2007**, *45*, 3505-3512.
3. Edmondson, S.; Osborne, V. L.; Huck, W. T. S. *Chemical Society Reviews* **2004**, *33*, 14-22.
4. Pyun, J.; Kowalewski, T.; Matyjaszewski, K. *Macromolecular Rapid Communications* **2003**, *24*, 1043-1059.
5. Zhao, B.; Brittain, W. J. *Progress in Polymer Science* **2000**, *25*, 677-710.
6. Comrie, J. E.; Huck, W. T. S. *Macromolecular Rapid Communications* **2008**, *29*, 539-546.
7. Ito, Y.; Inaba, M.; Chung, D.-J.; Imanishi, Y. *Macromolecules* **1992**, *25*, 7313-7316.
8. de Vos, W. M.; Meijer, G.; de Keizer, A.; Cohen Stuart, M. A.; Kleijn, J. M. *Soft Matter* **2010**, *6*, 2499-2507.
9. Evers, F.; Reichhart, C.; Steitz, R.; Tolan, M.; Czeslik, C. *Physical Chemistry Chemical Physics* **2010**, *12*, 4375-4382.
10. Biesalski, M.; Johannsmann, D.; Rühle, J. *Journal of Chemical Physics* **2002**, *117*, 4988-4994.
11. Parnell, A. J.; Martin, S. J.; Dang, C. C.; Geoghegan, M.; Jones, R. A. L.; Crook, C. J.; Howse, J. R.; Ryan, A. J. *Polymer* **2009**, *50*, 1005-1014.
12. Dong, R.; Lindau, M.; Ober, C. K. *Langmuir* **2009**, *25*, 4774-4779.
13. Santonicola, G. M.; de Groot, W. G.; Memesa, M.; Meszyńska, A.; Vancso, J. G. *Langmuir* **2010**, *26*, 17513-17519.
14. Laloyaux, X.; Mathy, B.; Nysten, B.; Jonas, A. M. *Macromolecules* **2010**, *43*, 7744-7751.
15. Liu, G.; Zhang, G. *Journal of Physical Chemistry B* **2008**, *112*, 10137-10141.
16. Kurosawa, S.; Aizawa, H.; Talib, Z. A.; Atthoff, B.; Hilborn, J. *Biosensors & Bioelectronics* **2004**, *20*, 1165-1176.
17. Wu, T.; Gong, P.; Szleifer, I.; Vlček, P.; Šubr, V.; Genzer, J. *Macromolecules* **2007**, *40*, 8756-8764.
18. Zhang, H. N.; Rühle, J. *Macromolecules* **2005**, *38*, 4855-4860.

19. Ruiz-Pérez, L.; Pryke, A.; Sommer, M.; Battaglia, G.; Soutar, I.; Swanson, L.; Geoghegan, M. *Macromolecules* **2008**, *41*, 2203-2211.
20. Wang, J.; Frostman, L. M.; Ward, M. D. *Journal of Physical Chemistry* **1992**, *96*, 5224-5228.
21. Parnell, A. J.; Martin, S. J.; Jones, R. A. L.; Vasilev, C.; Crook, C. J.; Ryan, A. J. *Soft Matter* **2009**, *5*, 296-299.
22. Buttry, D. A.; Ward, M. D. *Chemical Reviews* **1992**, *92*, 1355-1379.
23. Schüwer, N.; Klok, H.-A. *Advanced Materials* **2010**, *22*, 3251-3255.
24. Sauerbrey, G. *Zeitschrift Fur Physik* **1959**, *155*, 206-222.
25. Lego, B.; Sken, W. G.; Giasson, S. *Macromolecules* **2010**, *43*, 4384-4394.
26. Currie, E. P. K.; Sieval, A. B.; Avena, M.; Zuilhof, H.; Sudhölter, E. J. R.; Cohen Stuart, M. A. *Langmuir* **1999**, *15*, 7116-7118.
27. Currie, E. P. K.; Sieval, A. B.; Fleer, G. J.; Cohen Stuart, M. A. *Langmuir* **2000**, *16*, 8324-8333.
28. Israëls, R.; Leermakers, F. A. M.; Fleer, G. J. *Macromolecules* **1994**, *27*, 3087-3093.
29. Zhulina, E. B.; Birshtein, T. M.; Borisov, O. V. *Macromolecules* **1995**, *28*, 1491-1499.
30. Cullen, S. P.; Liu, X.; Mandel, I. C.; Himpfel, F. J.; Gopalan, P. *Langmuir* **2008**, *24*, 913-920.
31. Dai, J.; Bao, Z.; Sun, L.; Hong, S. U.; Baker, G. L.; Bruening, M. L. *Langmuir* **2006**, *22*, 4274-4281.
32. Navarro, M.; Benetti, E. M.; Zapotoczny, S.; Planell, J. A.; Vancso, G. J. *Langmuir* **2008**, *24*, 10996-11002.
33. Dordi, B.; Schonherr, H.; Vancso, G. J. *Langmuir* **2003**, *19*, 5780-5786.
34. Degrand, C.; Limoges, B.; Blankespoor, R. L. *Journal of Organic Chemistry* **1993**, *58*, 2573-2577.
35. Devenish, S. R. A.; Hill, J. B.; Blunt, J. W.; Morris, J. C.; Munro, M. H. G. *Tetrahedron Letters* **2006**, *47*, 2875-2878.
36. Šavrda, J. *Journal of Organic Chemistry* **1977**, *42*, 3199-3200.
37. Wong, S. Y.; Putnam, D. *Bioconjugate Chemistry* **2007**, *18*, 970-982.
38. Barbey, R.; Klok, H.-A. *Langmuir* **2010**, *26*, 18219-18230.
39. Tugulu, S.; Harms, M.; Fricke, M.; Volkmer, D.; Klok, H.-A. *Angewandte Chemie International Edition* **2006**, *45*, 7458-7461.

### 3.6. Supporting Information

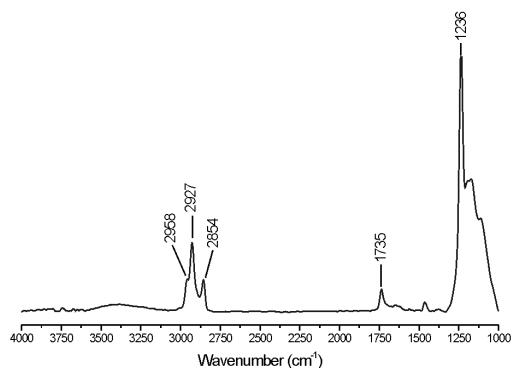


**Figure S1.** Grazing-Angle Attenuated Total Reflectance FTIR spectrum of an ATRP initiator **1b** functionalized silicon wafer.

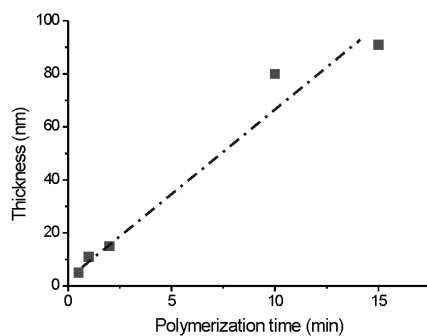


**Figure S2.** Evolution of film thickness with polymerization time for PMAA brushes grown from a silicon wafer modified with ATRP initiator **1b**.

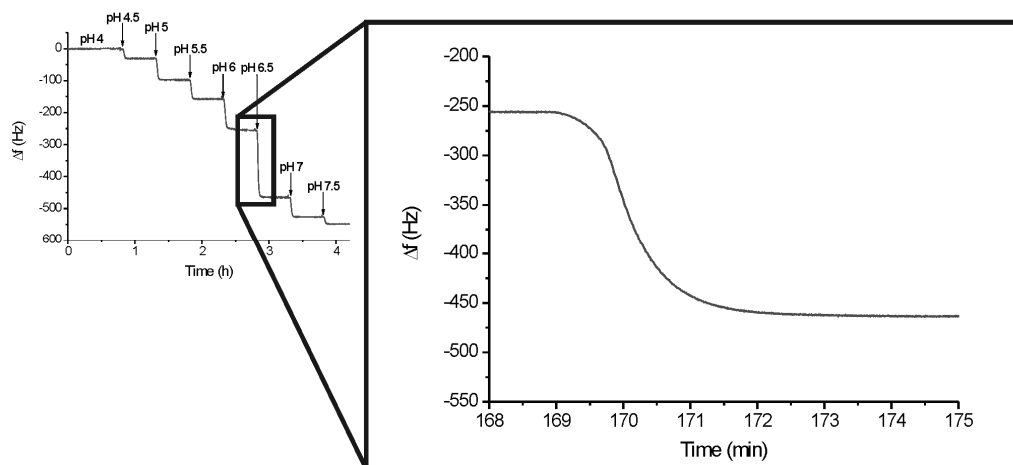


**Figure S3.** Expansion of the response of a QCM chip modified with a 11 nm thick PMAA brush to a change in pH from 6 to 6.5.

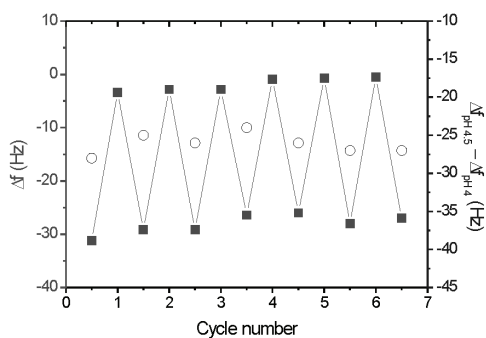


**Figure S4.** Frequency shift (■) and frequency shift difference (○) observed upon exposing a QCM chip modified with a 11 nm thick PMAA brush alternately to pH 4 and pH 4.5 buffer solutions over 6 switching cycles.



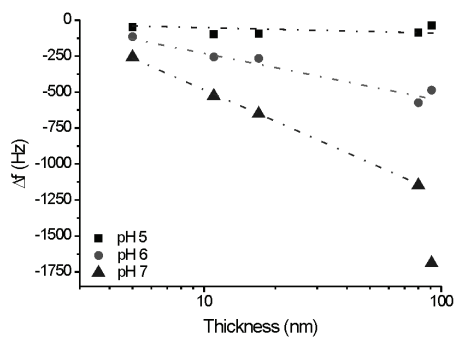


**Figure S5.** Shift in the resonance frequency of PMAA brush coated QCM chips as a function of the brush thickness at different pH values.

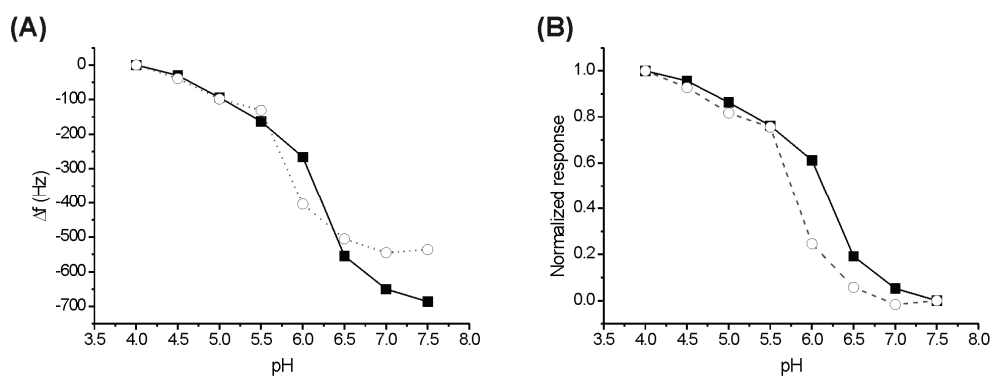


**Figure S6.** pH response (A) and normalized pH response (B) of QCM chips coated with a  $\sim 15$  nm thick dense PMAA brush (■) and a  $\sim 14$  nm thick low density (25 %) PMAA brush (○).

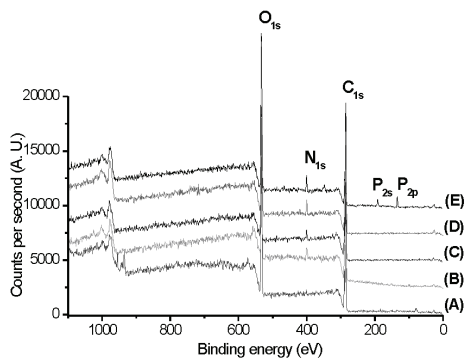


**Figure S7.** XPS survey scan of (A) a PMAA brush (~ 80 nm); (B) an NHS activated PMAA brush; (C) a PMAA brush post-modified with glutamic acid; (D) a PMAA brush post-modified with 4-aminophenol and (E) a PMAA brush post-modified with *O*-phosphorylethanolamine. The spectra in Figures B-E were recorded on post-modified brushes that were prepared from a PMAA brush with a thickness of ~ 80 nm.

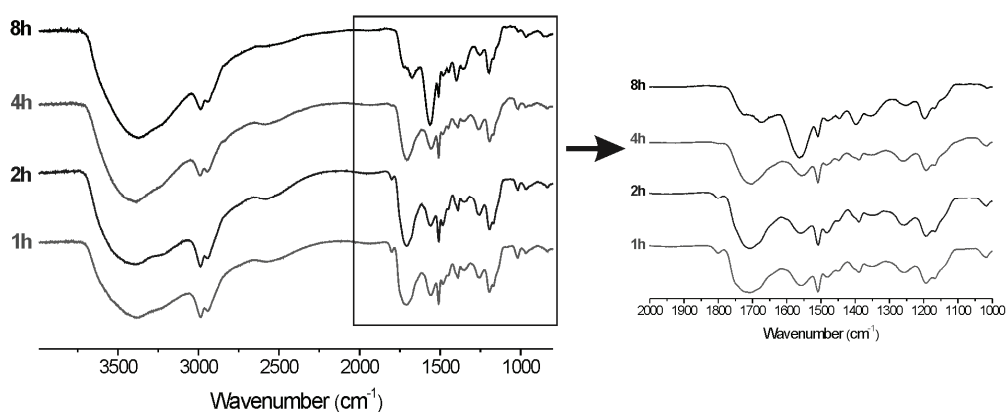


**Figure S8.** FTIR spectra of an NHS activated PMAA brush (~ 200 nm) after incubation in 0.05 M 4-aminophenol solution at pH 10 for 1, 2, 4 and 8 hrs.

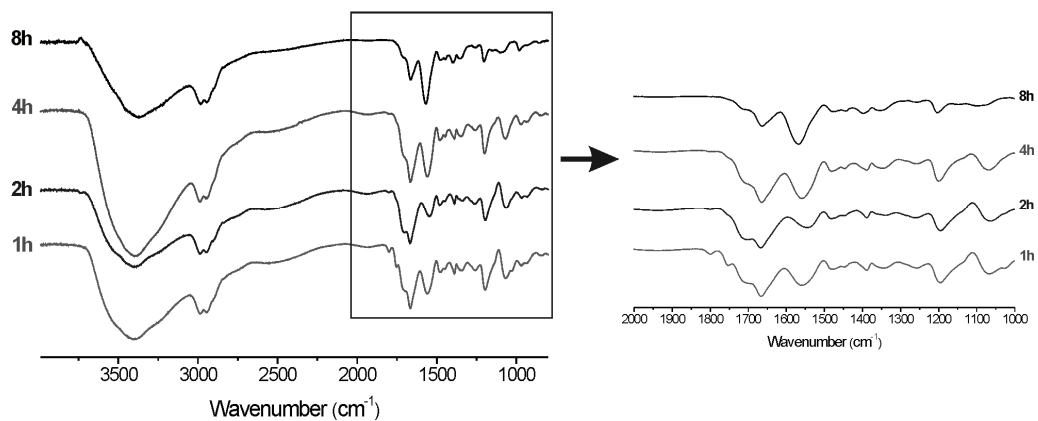


**Figure S9.** FTIR spectra of an NHS activated PMAA brush (~ 200 nm) after incubation in 0.1 M *O*-phosphorylethanolamine solution at pH 10 for 1, 2, 4 and 8 hrs.

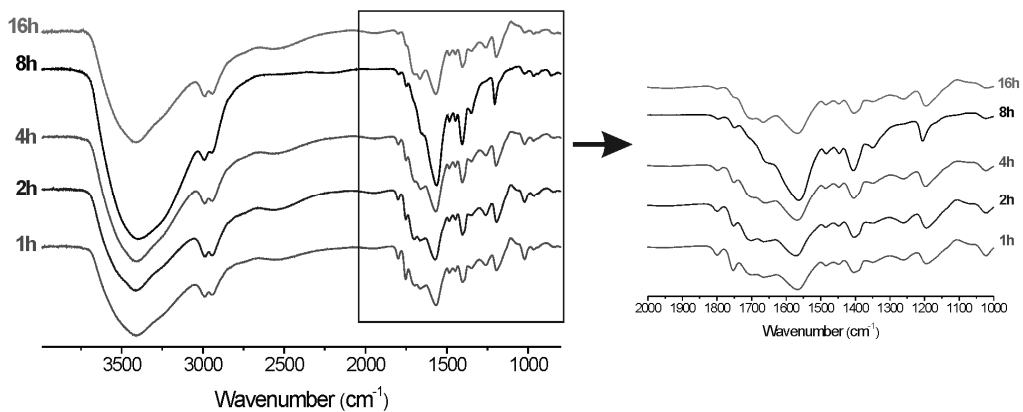


**Figure S10.** FTIR spectra of an NHS activated PMAA brush (~ 200 nm) after incubation in 0.1 M glutamic acid solution at pH 10 for 1, 2, 4, 8 and 16 hrs.

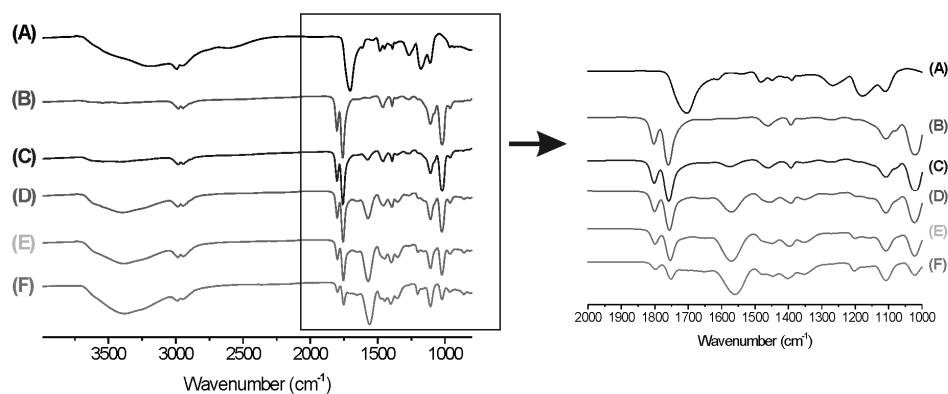


**Figure S11.** FTIR spectra of (A) a PMAA brush ( $\sim 200$  nm), (B) an NHS-activated PMAA brush and of NHS-activated PMAA brushes incubated in pH 10 aqueous solution for 1 h (C), 2 hrs (D), 4 hrs (E) and 8 hrs (F).

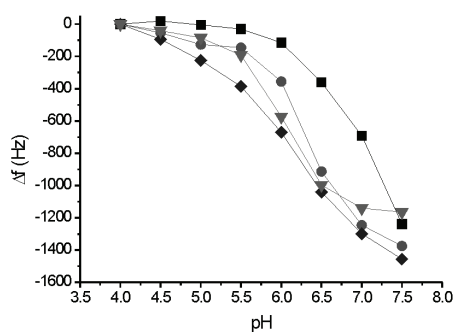


**Figure S12.** pH response of QCM chips coated with an unmodified PMAA brush ( $\sim 80$  nm) ( $\blacktriangledown$ ); a PMAA brush post-modified with 4-aminophenol ( $\blacksquare$ ); a PMAA brush post-modified with *O*-phosphorylethanolamine ( $\blacklozenge$ ) and a PMAA brush post-modified with glutamic acid ( $\bullet$ ).

## 4. A Potassium-Selective Quartz Crystal Microbalance Sensor Based on Crown-Ether Functionalized Polymer Brushes

### 4.1. Introduction

Thin organic films are frequently used as the active layer in a variety of ion sensors. One approach involves coating the surface of an electrode,<sup>1</sup> a quartz crystal microbalance (QCM),<sup>2</sup> surface plasmon resonance<sup>3</sup> or microcantilever<sup>4</sup> chip with a self-assembled monolayer (SAM) of an appropriate functionalized thiol or disulfide. Although their successful use has been described in a number of reports, the surface concentration of ion-selective functional groups is restricted to a single monolayer, which potentially limits the sensitivity and detection limit of these devices. Alternatively, the electrode or sensor chip surface can be modified using *e.g.* drop- or spincoating or photopolymerization with a polymer coating, which either physically entraps the ionophore or to which the ionophore is covalently bound.<sup>5-11</sup> As they are much thicker than a self-assembled monolayer, these polymer coatings can provide much higher ionophore surface concentrations. A drawback of drop- or spincoating or photopolymerization, however, is that these techniques provide limited control over the thickness, architecture and composition of the resulting polymer coatings, which may restrict the possibility to engineer the properties of these sensory layers at the molecular level.

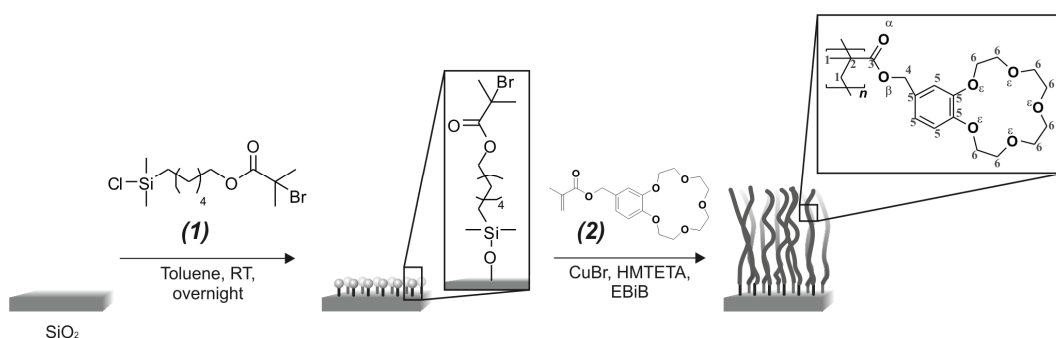
Surface-initiated controlled radical polymerization (SI-CRP) represents an interesting alternative strategy to produce thin polymer coatings. This approach results in polymer films, which are referred to as polymer brushes since all polymer chains are tethered with one chain end to the substrate. In contrast to the more conventional techniques mentioned above, SI-CRP allows precise control over the thickness, composition and architecture of the resulting polymer brushes.<sup>12-16</sup> While the temperature and pH-induced conformational changes of thermo- and/or pH responsive polymer brushes have been extensively studied

using *e.g.* QCM and SPR experiments,<sup>12</sup> which potentially provides the basis for the development of polymer brush based temperature and pH sensors, only very few reports have been published that use SI-CRP to fabricate ion-selective polymer coatings. Two examples that have been reported include the work by Kang *et al.*<sup>17</sup> and Locklin and coworkers<sup>18</sup> who described the use of dye modified polymer brushes as fluorescent or colorimetric ion-sensors.

This report describes the fabrication of a potassium selective Quartz Crystal Microbalance with Dissipation Monitoring (QCM-D) sensor obtained via direct surface-initiated atom transfer radical polymerization (SI-ATRP) of a methacrylated benzo-15-crown-5 derivative. The results of a systematic study of the influence of brush thickness on the properties of the QCM-D based ion sensor are presented and it will be demonstrated that the sensitivity of the sensor increases linearly with brush thickness. Finally, it will be shown that the benzo-15-crown-5 functionalized polymer brushes are able to selectively detect potassium ions, even in the presence of a large excess of a lower affinity competing ion such as sodium.

## 4.2. Results and discussion

The preparation of the benzo-15-crown-5 functionalized polymer brush active layers involves two steps and is illustrated in Scheme 1. First, the SiO<sub>2</sub> substrate is modified with an ATRP initiator functionalized chlorosilane derivative (**1**), followed by direct surface-initiated polymerization of methacryloyl-4'-oxymethylbenzo-15-crown-5 (**2**). As the substrate, both SiO<sub>2</sub> coated QCM-D crystals as well as silicon wafers were used. The later substrates were used to study the kinetics of the polymerization reaction and for the chemical characterization of the resulting brushes. Monomer **2** was selected for the studies presented here since it is readily synthesized via published protocols and benzo-15-crown-5 is a well-know potassium selective ionophore.<sup>19</sup>



**Scheme 1.** Synthesis of benzo-15-crown-5 functionalized polymer brushes via SI-ATRP.

Polymer brushes containing complex side chain functional groups can be prepared either via direct polymerization of the corresponding monomer or via post-polymerization modification of an appropriate reactive precursor polymer brush. The post-polymerization modification approach is attractive to overcome problems with the direct polymerization of complex side chain functional monomers, which can sometimes be difficult to polymerize. A drawback of this strategy, however, is that a quantitative modification of the reactive precursor polymer is very challenging. Therefore, instead of using post-polymerization modification,<sup>20</sup> this study explored the direct SI-ATRP of monomer **2** to prepare benzo-15-crown-5 functionalized polymer brushes. With a catalyst system consisting of CuBr and HMTETA and using EBiB as sacrificial initiator polymer brushes with thicknesses up to 275 nm can be obtained within 75 min (Figure 1A). After a short induction period of ~ 15 min, brush thickness increases linearly with polymerization time, which reflects the controlled nature of the ATRP process. The resulting polymer brushes were characterized with XPS and FTIR spectroscopy. The high resolution C<sub>1s</sub> and O<sub>1s</sub> XPS spectra can be deconvoluted to afford the contributions of the different C- and O-atoms in the expected ratios.

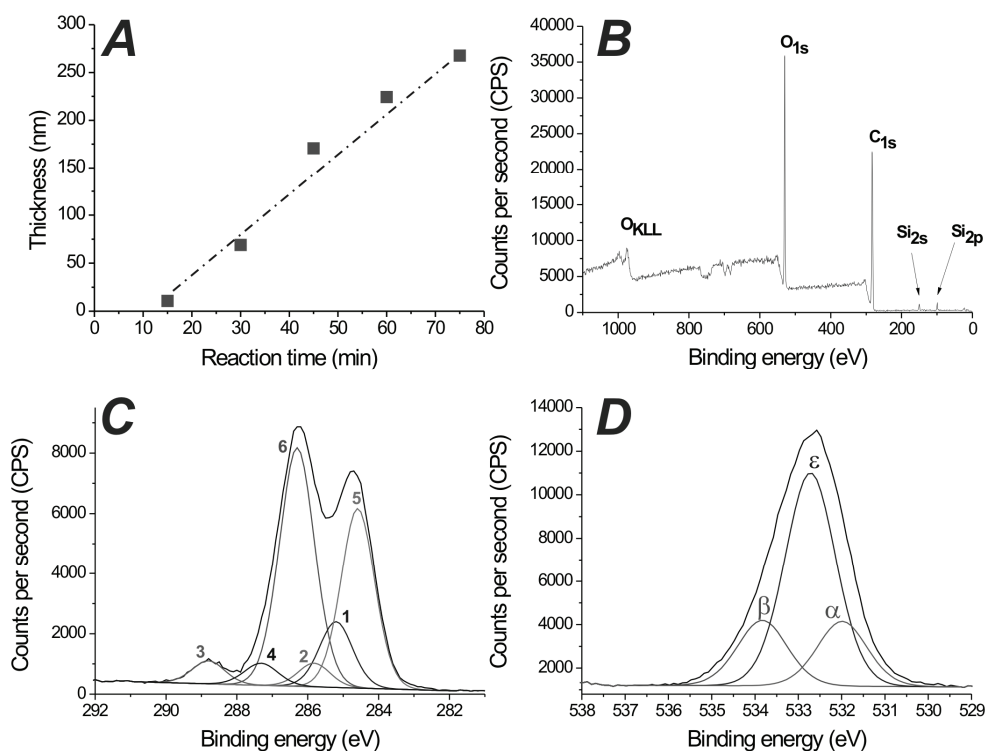


**Figure 1.** (A) Evolution of brush thickness with polymerization time. (B) XPS survey and high-resolution XPS spectra of the C<sub>1s</sub> (C) and O<sub>1s</sub> (D) signals of a 240 nm thick polymer brush (the numbers and Greek letters indicate the different C- and O-atoms as depicted in Scheme 1).

The FTIR spectrum of a crown ether functionalized brush (Figure 2) reveals two bands at  $\sim 2929\text{ cm}^{-1}$  and  $\sim 2867\text{ cm}^{-1}$  corresponding, respectively, to the asymmetric and the symmetric CH<sub>2</sub> stretching vibrations as well as a strong C=O stretch vibration band at  $\sim 1720\text{ cm}^{-1}$ . At lower wavenumbers, three bands at  $\sim 1608\text{ cm}^{-1}$ ,  $\sim 1587\text{ cm}^{-1}$  and  $\sim 1517\text{ cm}^{-1}$  are observed, which are due to the stretching of the aromatic C=C bond. In the fingerprint domain, the spectrum shows two weak bands at  $\sim 1052\text{ cm}^{-1}$ ,  $\sim 1257\text{ cm}^{-1}$  and a low intensity band at  $\sim 1130\text{ cm}^{-1}$ , which correspond to the asymmetric C-O-C stretching of the aromatic and aliphatic ether bonds, respectively.



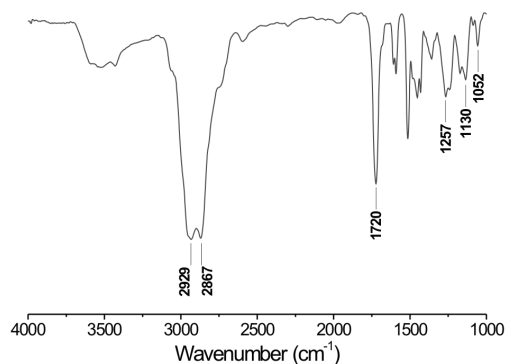


**Figure 2.** Reflectance FTIR spectrum of a 169 nm thick benzo-15-crown-5 functionalized polymer brush.

Next, the feasibility of a QCM crystal coated with a benzo-15-crown-5 functionalized polymer brush to monitor changes in potassium ion concentration was evaluated. Figure 3A, as a typical example, illustrates the changes in resonance frequency and dissipation, which can be observed with a 96 nm thick brush coating as the concentration of KCl increases from  $2.5 \times 10^{-4}$  M to  $10^{-2}$  M. With increasing potassium chloride concentration, the resonance frequency decreases and the dissipation increases. Since the changes in resonance frequency are much larger than the variation in the dissipation, the observed response is primarily a mass loading effect. This is supported by AFM measurements, which revealed that almost no swelling or collapse of the polymer layer could be observed upon exposure to a KCl solution (Supporting Information, Figure S1). The small increase in the dissipation, however, indicates that binding and uptake of KCl by the polymer brush coating is not necessarily exclusively a mass loading effect, but may also influence the viscoelastic properties of the coating. As illustrated in Figure 3A, binding of potassium chloride was not completely reversible. The sensor response, however, to multiple alternating exposures to aqueous potassium chloride and deionized water was constant over multiple switching cycles (Figure S2). Figure 3B plots the shift in the resonance frequency as a function of potassium concentration for four polymer brush coatings with thicknesses ranging from 96 - 185 nm. For all four investigated brush thicknesses, a linear decrease in resonance frequency with increasing potassium concentration was observed. The absolute response ( $\Delta f$ ), however, depends on brush thickness and increases with increasing thickness of the benzo-15-crown-5 functionalized polymer layer. The slope of the plots in Figure 3B is a measure for the sensitivity (in Hz.L/mol) of the polymer brush layer and increases linearly with brush thickness (Figure

3C). Figure 3C clearly demonstrates the potential of surface-initiated controlled radical polymerization to generate sensory layers with high sensitivities, which can be accurately controlled by variation in brush thickness.

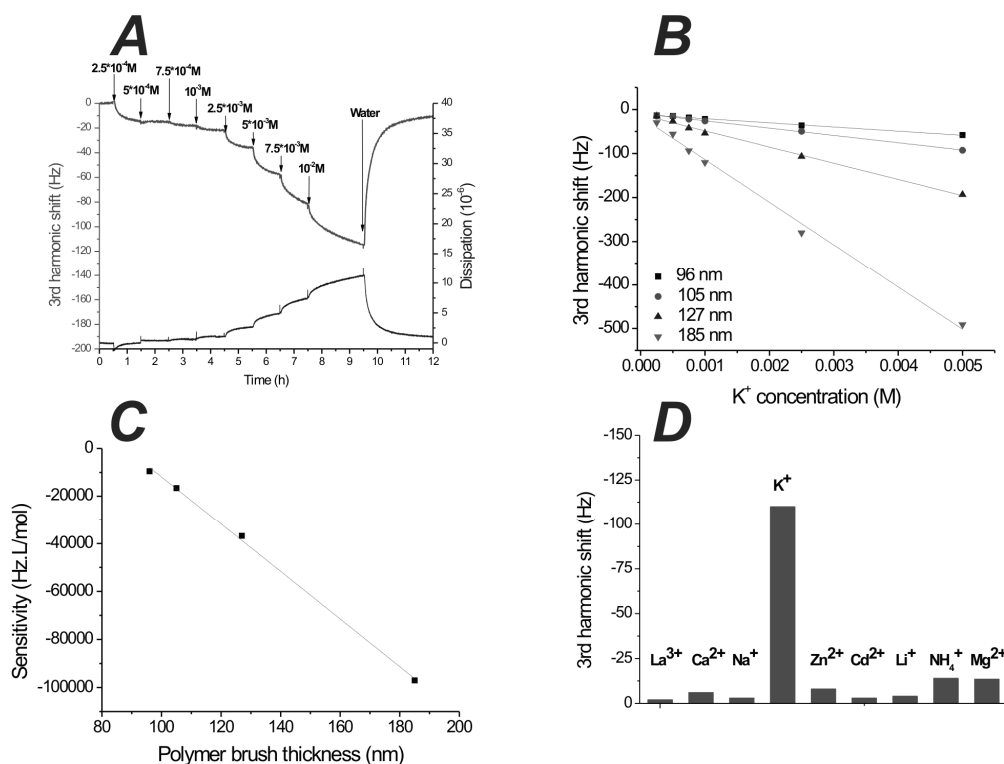


**Figure 3.** (A) Typical response of a 96 nm thick polymer brush coated QCM chip to various KCl concentrations; (B) Shift in the 3<sup>rd</sup> harmonic resonance frequency for four benzo-15-crown-5 polymer brushes of different thicknesses as a function of  $[KCl]$ ; (C) Sensitivity of the benzo-15-crown-5 functionalized polymer brush sensor as a function of brush thickness; (D) Comparison of the shift of the 3<sup>rd</sup> harmonic resonance frequency of a 96 nm thick benzo-15-crown-5 functionalized polymer brush upon exposure to  $1.0 \times 10^{-2} M$  solutions of different chloride salts.

Figure 3D compares the response of a 96 nm thick benzo-15-crown-5 functionalized brush to 0.01 M solutions of various salts, all with the same anion. The response of the QCM-D based sensor to  $K^{+}$  is 8 to 55 times larger than to the other cations, which is in agreement with the reported cation binding properties and selectivity of benzo-15-crown-5<sup>19,21</sup> and polymer-bound benzo-15-crown-5 derivatives.<sup>22,23</sup> A comparison of the selectivity of a 96 nm thick sensor coating with that of a 127 nm thick coating did not reveal a significant influence of the brush thickness (Supporting Information, Figure S3).

To further investigate the selectivity of the benzo-15-crown-5 based QCM-D sensor, additional experiments were carried out in which the potassium concentration was varied in aqueous solutions containing a high concentration of an interfering lower affinity cation, *i.e.* 0.1 M NaCl. As illustrated in Figure 4A, the frequency shifts that are measured upon gradually increasing the potassium concentration in a 0.1 M NaCl solution are similar to those observed in absence of NaCl (see Figure 3A). In contrast, and in agreement with the potassium-selectivity of the polymer brush coating, the addition of gradually increasing concentrations of NaCl to a 0.1M KCl solution only resulted in minor frequency shifts (Figure 4B).

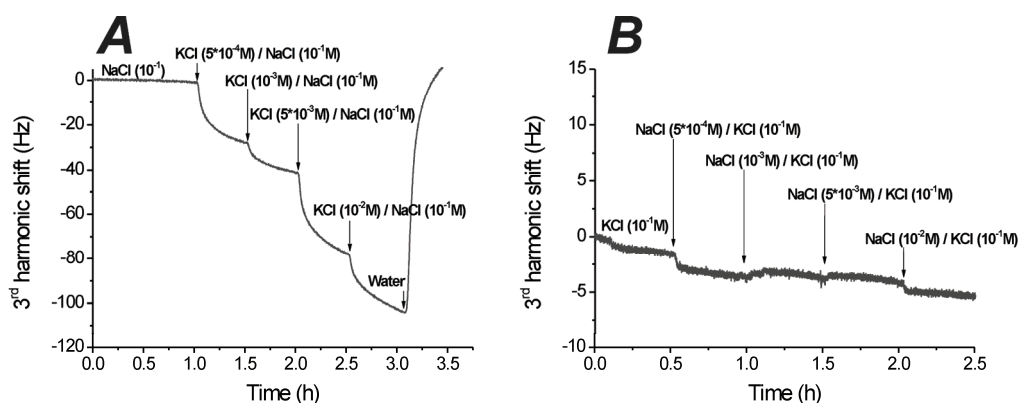


**Figure 4.** (A) Typical response of a 96 nm thick benzo-15-crown-5 functionalized polymer brush coated QCM-D chip to increasing concentrations of KCl in the presence of 0.1 M NaCl; (B) Response of a 96 nm thick benzo-15-crown-5 functionalized polymer brush coated QCM-D chip to increasing concentrations of NaCl in the presence of 0.1 M KCl.

### 4.3. Conclusions

In conclusion, this report has demonstrated the feasibility of crown-ether containing polymer brushes prepared via surface-initiated atom transfer radical polymerization to act as the active layer in QCM-D based ion sensors. The use of SI-ATRP allows access to potassium selective sensing layers that are covalently attached to the QCM-D chip and with receptor surface concentrations that are much higher than *e.g.* SAMs. The QCM-D based sensor presented here allows the selective detection of potassium, even in aqueous solutions that contain a high excess of a lower affinity, interfering ion such as sodium.

Furthermore, SI-ATRP allows to precisely control the thickness of the polymer brushes, which, as has been demonstrated, can be used to tune and enhance the sensitivity of the QCM-D sensor. Whereas the sensitivity can be optimized by adjusting the thickness of the polymer brush, the selectivity of the sensor was not found to be significantly influenced by changes in brush thickness. While this report only represents a first proof-of-concept study, it clearly highlights some of the unique features offered by surface-initiated polymerization techniques for the fabrication of active, sensory layers.

## 4.4. Experimental

### 4.4.1. Materials

All chemicals were purchased from Aldrich and used as received unless noted otherwise. Methacryloyl chloride was passed over a short column of basic alumina prior to use. The ATRP initiator (**1**), (6-(2-bromo-2-methyl)propionyloxy)hexyldimethylchlorosilane, was synthesized as previously described.<sup>24</sup>

### 4.4.2. Methods

The substrates were cleaned using a Tepla 300 microwave induced plasma system (PVA TePla AG, Germany). Brush thicknesses were determined using a computer-controlled null-ellipsometer (Philips Plasmos SD 2300) operating with a He-Ne laser at  $\lambda = 632.8$  nm and an angle of incidence of  $70^\circ$ . Film thicknesses were calculated using a double layer silicon / polymer brush model. The refractive indices used for the calculations were  $n = 3.7$  for the silicon substrate and  $n = 1.45$  for the polymer. X-ray photoelectron spectroscopy (XPS) was carried out using an Axis Ultra instrument from Kratos Analytical equipped with a conventional hemispheric analyzer. The X-ray source employed was a monochromatic Al  $K\alpha$  (1486.6 eV) source operated at 100 W and  $10^{-9}$  mbar. Quartz Crystal Microbalance with Dissipation (QCM-D) measurements were performed with a Q-Sense E4 system (Q-Sense, Sweden) using  $\text{SiO}_2$  coated quartz crystals purchased from Q-Sense and recording the third harmonic of the resonant frequency. Reflectance Fourier transform infrared (FTIR) spectroscopy was carried out on a Nicolet Magna-IR 560 spectrometer. Patterned polymer brushes for atomic force microscopy (AFM) studies were prepared from patterned ATRP initiator modified substrates, which were obtained as previously described.<sup>25</sup> AFM was performed in liquid in Tapping-mode on a Veeco Multimode Nanoscope IIIa SPM controller (Digital instruments, Santa Barbara, CA) using MPP-31100-10 Veeco cantilever.

### 4.4.3. Procedures

#### 4.4.3.1. Synthesis of methacryloyl-4'-oxymethylbenzo-15-crown-5

4'-Hydroxymethylbenzo-15-crown-5 was prepared following the procedure reported by Percec *et al.*<sup>26</sup> Monomer (**2**) was obtained by esterification of 4'-hydroxymethylbenzo-15-crown-5 with methacryloyl chloride as described by Kimura *et al.*<sup>27</sup> To this end, 4'-hydroxymethylbenzo-15-crown-5 (4 g, 18.12 mmol) and freshly distilled triethylamine (3 mL, 18.12 mmol) were dissolved in dichloromethane (30 mL). The mixture was stirred under nitrogen and cooled with an ice bath. After that, methacryloyl chloride (2.2 mL, 18.12 mmol) was added dropwise and the resulting solution stirred under nitrogen at 0 °C for one hour and an additional three hours at room temperature. The triethylammonium bromide was removed by filtration and the product washed with a saturated ammonium chloride solution. The organic phase was dried over MgSO<sub>4</sub> and the solvent removed under reduced. The monomer **2** was obtained as a white powder after reprecipitation in methanol at -30 °C. Yield: 96 %. <sup>1</sup>H NMR (400 MHz, CDCl<sub>3</sub>, δ): 1.94 (s, 3H, CH<sub>3</sub>), 3.75 (s, 8H, O-CH<sub>2</sub>-CH<sub>2</sub>-O), 3.91 (m, 4H, Ar-O-CH<sub>2</sub>-CH<sub>2</sub>-Or), 4.12 (m, 4H, Ar-O-CH<sub>2</sub>-CH<sub>2</sub>-O), 5.09 (s, 2H, Ar-CH<sub>2</sub>-O-), 5.56 (s, 1H, C=CH<sub>2</sub>), 6.11 (s, 1H, C=CH<sub>2</sub>), 6.84-6.86 (m, 3H, Ar H). <sup>13</sup>C NMR (400 MHz, CDCl<sub>3</sub>, δ): 18.16 (CH<sub>3</sub>), 66.17 (Ar-CH<sub>2</sub>-O-), 68.91, 69.38, 70.5, 70.92 (crown ether), 113.61, 114.22, 121.39, 136.97 (Ar), 125.5 (C=CH<sub>2</sub>), 128.97 (C=CH<sub>2</sub>), 148.98 (C=O). HRMS (ESI, m/z): [M + Na]<sup>+</sup> calcd for C<sub>19</sub>H<sub>26</sub>O<sub>7</sub>Na, 389.1576; found, 389.1559.

#### 4.4.3.2. Immobilization of the ATRP initiator

First, the silicon wafers were sonicated for 5 min in acetone and dried. The silicon surfaces were then exposed to an oxygen plasma (500 W, 4 min) and subsequently the clean wafers were kept overnight and in the dark in a 10 mM solution of **1** in anhydrous toluene. Afterwards, the slides were extensively rinsed with chloroform, dried under nitrogen and transferred to the appropriate reactors for the polymerizations. Silicon oxide coated QCM chips were modified in a similar way, but were not sonicated.

#### **4.4.3.3. Surface-initiated atom transfer radical polymerization**

In a Schlenck tube, 1,1,4,7,10,10-hexamethyltriethylene tetramine (HMTETA) (1.2 mL, 4.41 mmol) was dissolved in anhydrous 1-propanol (2 mL) and the mixture was subsequently subjected to three freeze-pump-thaw cycles. Once the solution was degassed, CuBr (160 mg, 1.12 mmol) was added under nitrogen and allowed to dissolve. In a separate Schlenck tube, **2** (1 g, 2.79 mmol) and ethyl  $\alpha$ -bromoisobutyrate (EBiB) (10  $\mu$ L, 0.068 mmol) were dissolved in anhydrous 1-propanol (18 mL). The resulting solution was degassed by three freeze-pump-thaw cycles and then added to the solution containing the catalyst system. Then, the polymerization mixture was cannula transferred into a polymerization reactor containing the ATRP-initiator modified silicon wafer or QCM chip. The polymerization was allowed to proceed at room temperature for the desired time. After that, the substrates were thoroughly rinsed with methanol and dried under nitrogen.

## 4.5. References

1. Flink, S.; Boukamp, B. A.; van den Berg, A.; van Veggel, F. C. J. M.; Reinhoudt, D. N. *Journal of the American Chemical Society* **1998**, *120*, 4652-4657.
2. Cygan, M. T.; Collins, G. E.; Dunbar, T. D.; Allara, D. L.; Gibbs, C. G.; Gutsche, C. D. *Analytical Chemistry* **1999**, *71*, 142-148.
3. Hong, S.; Kang, T.; Moon, J.; Oh, S.; Yi, J. *Colloids and Surfaces a-Physicochemical and Engineering Aspects* **2007**, *292*, 264-270.
4. Ji, H.-F.; Finot, E.; Dabestani, R.; Thundat, T.; Brown, G. M.; Britt, P. F. *Chemical Communications* **2000**, 457-458.
5. Drake, P. L.; Price, G. J. *Polymer International* **2000**, *49*, 926-930.
6. Gomes, M. T. S. R.; Costa, J. R. M. L.; Oliveira, J. A. B. P. *Talanta* **2003**, *59*, 247-252.
7. Haak, J. R.; Vanderwal, P. D.; Reinhoudt, D. N. *Sensors and Actuators B-Chemical* **1992**, *8*, 211-219.
8. Price, G. J.; Drake, P. L. *Reactive & Functional Polymers* **2006**, *66*, 109-121.
9. Price, G. J.; Drake, P. L. *Sensors and Actuators B-Chemical* **2006**, *114*, 466-472.
10. Bakker, E.; Pretsch, E. *Angewandte Chemie-International Edition* **2007**, *46*, 5660-5668.
11. Privett, B. J.; Shin, J. H.; Schoenfisch, M. H. *Analytical Chemistry* **2008**, *80*, 4499-4517.
12. Barbey, R.; Lavanant, L.; Paripovic, D.; Schüwer, N.; Sugnaux, C.; Tugulu, S.; Klok, H.-A. *Chemical Reviews* **2009**, *109*, 5437-5527.
13. Brittain, W. J.; Minko, S. *Journal of Polymer Science Part a-Polymer Chemistry* **2007**, *45*, 3505-3512.
14. Edmondson, S.; Osborne, V. L.; Huck, W. T. S. *Chemical Society Reviews* **2004**, *33*, 14-22.
15. Pyun, J.; Kowalewski, T.; Matyjaszewski, K. *Macromolecular Rapid Communications* **2003**, *24*, 1043-1059.
16. Zhao, B.; Brittain, W. J. *Progress in Polymer Science* **2000**, *25*, 677-710.
17. Peng, Q.; Xie, M.-G.; Neoh, K.-G.; Kang, E.-T. *Chemistry Letters* **2005**, *34*, 1628-1629.
18. Fries, K.; Samanta, S.; Orski, S.; Locklin, J. *Chemical Communications* **2008**, 6288-6290.



19. Gokel, G., *Crown Ethers and Cryptands*. Royal Society of Chemistry, Cambridge, U.K. ed.; Cambridge : The Royal Society of Chemistry, cop.: 1991.
20. Murata, H.; Prucker, O.; Rühle, J. *Macromolecules* **2007**, *40*, 5497-5503.
21. Luboch, E.; Cygan, A.; Biernat, J. F. *Tetrahedron* **1991**, *47*, 4101-4112.
22. Kimura, K.; Maeda, T.; Shono, T. *Die Makromolekulare Chemie* **1981**, *182*, 1579-1586.
23. Nakajima, M.; Kimura, K.; Shono, T. *Analytical Chemistry* **1983**, *55*, 463-467.
24. See Chapter 3: Tuning the pH Sensitivity of Poly(Methacrylic Acid) Brushes.
25. Tugulu, S.; Harms, M.; Fricke, M.; Volkmer, D.; Klok, H.-A. *Angewandte Chemie International Edition* **2006**, *45*, 7458-7461.
26. Percec, V.; Johansson, G.; Heck, J.; Ungar, G.; Batty, S. V. *Journal of the Chemical Society-Perkin Transactions I* **1993**, 1411-1420.
27. Kimura, K.; Tamura, H.; Maeda, T.; Shono, T. *Polymer Bulletin* **1979**, *1*, 403-407.

## 4.6. Supporting Information

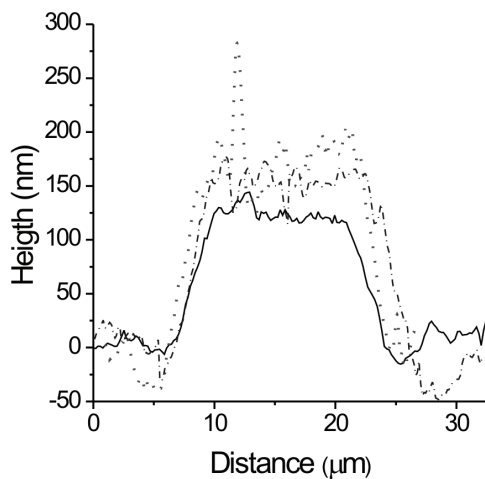


**Figure S1.** 2D cross-sectional AFM profiles of a benzo-15-crown-5 functionalized polymer brush in different environments: solid line, “dry” brush; dot, deionized water; dash dot, saturated KCl solution.

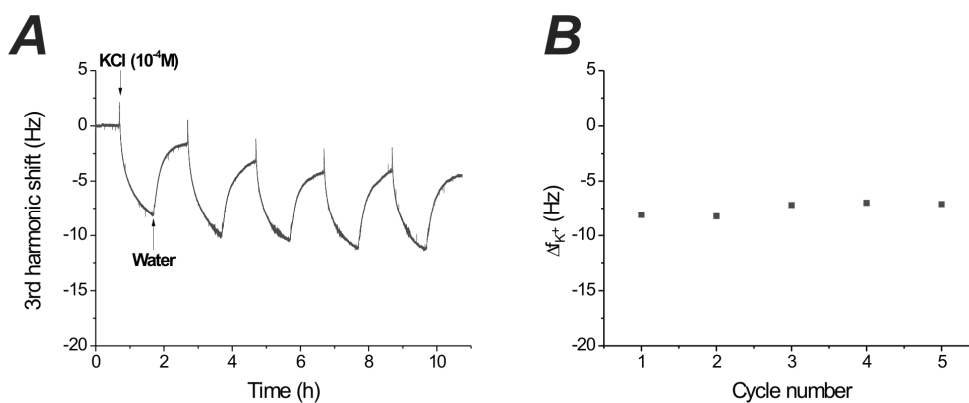


**Figure S2.** (A) Response of a 96 nm thick polymer brush coated QCM chip upon cycling between deionized water and a  $10^{-4}$  M KCl solution; (B) Evolution of the frequency shift difference ( $\Delta f_{K^+}$ ), which is the difference between the 3<sup>rd</sup> harmonic shift measured upon exposure of a benzo-15-crown-5 functionalized polymer brush to  $10^{-4}$  M KCl and deionized water, respectively, as a function of the number of switching cycles.

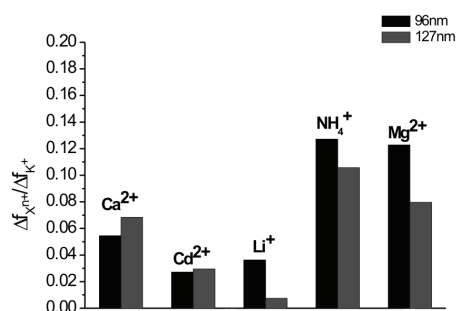


**Figure S3.** Comparison of the response of a 96 nm thick benzo-15-crown-5 functionalized polymer brush to  $10^{-2}$  M solutions of different cations;  $\Delta f_{X^{n+}}$  represents the shift due to ion  $X^{n+}$  at a concentration of  $10^{-2}$  M and  $\Delta f_{K^+}$  is the shift induced by a  $10^{-2}$  M solution of potassium chloride.



## **5. Peptide Functionalized Polymer Brushes for Voltammetric Based Mercury (II) Detection**

### **5.1. Introduction**

Mercury is a highly toxic heavy metal that can be found in many polluted rivers and lakes of industrial countries.<sup>1-4</sup> Mercury is a poison for wildlife<sup>3,5-7</sup> and is also the cause of several serious medical diseases.<sup>8,9</sup> Therefore mercury monitoring has attracted many attentions during the past decades.<sup>10,11</sup> Electrochemical sensors that have already been reported to probe mercury (II) ions in aqueous media involve the selective surface modification of electrodes. Examples include DNA or oligonucleotide based coatings,<sup>10,12,13</sup> functional self-assembled monolayers (SAM),<sup>14</sup> drop-casted polymer<sup>15</sup> or electropolymerized thin films.<sup>16-18</sup>

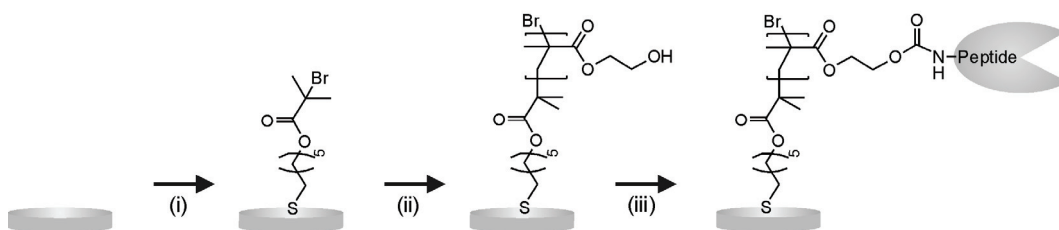
Dense assembly of surface grafted polymer chains, so-called polymer brushes,<sup>19</sup> have been successfully used as the active layer in QCM,<sup>20</sup> SPR,<sup>21</sup> fluorescence or cantilever based devices.<sup>22,23</sup> The use of polymer brushes as the active coating for electrochemical sensing has, however, received little attention.<sup>24</sup> As compared to the surface modification techniques mentioned above, polymer brushes offer an enhanced stability and a higher functional group surface concentration.

This section describes the use peptide functionalized polymer brushes as the active layer for voltammetric based mercury sensing. The peptide used in this study is a metallothionein like sequence, which is a member of a family of proteins known for their ability to bind heavy metal ions.<sup>25,26</sup> The results of both cyclic voltammetry experiments, that aimed at exploring in detail the Hg<sup>2+</sup> sensing properties of the peptide functionalized polymer brush coating will be presented, as well as square-wave voltammetry experiments that were carried out to investigate the limit of detection.

## 5.2. Results and discussion

### 5.2.1. Synthesis of the Hg<sup>2+</sup> sensitive polymer brush

The synthesis of peptide functionalized polymer brushes from a gold surface is a three step process which is illustrated in Scheme 1. In the first step, the clean gold substrate is covered with a self-assembled monolayer (SAM) of an atom transfer radical polymerization (ATRP) initiator from which the polymerization will take place in a second step. Finally the Hg<sup>2+</sup> sensitive peptide is incorporated within the PHEMA brushes via a *p*-nitrophenyl chloroformate (NPC) mediated post-polymerization modification following a previously reported protocol.<sup>27</sup> The Hg<sup>2+</sup> sensitive peptide sequence (Ala-Ala-Ala-Cys-Ala-Ala-His-Cys-Trp-Ala-Glu-NH<sub>2</sub>), which structure is displayed in Figure S1, was inspired by cystein rich proteins, called Metallothionein, that are well known for their ability to bind heavy metal ions.<sup>25</sup> Furthermore, the peptide sequence used in this study has already proven to exhibit a good sensitivity and selectivity toward mercury (II) ions.<sup>26</sup> In this chemical structure, the metal ions recognition takes place via chelation by the cysteine residues.<sup>28</sup>



**Scheme 1.** Schematic representation of the synthesis and post-polymerization modification of PHEMA brushes onto gold surface, (i) 6-mercaptohexyl 2-bromo-2-methylpropanoate (**1**) - 4 hrs; (ii); H<sub>2</sub>O/HEMA/CuBr/CuBr<sub>2</sub>/bipy (ii) NPC/Et<sub>3</sub>N/THF - 1 hr; Peptide (1 mM)/DMAP (2.5 mM)/DMF - 16 hrs followed by quenching with ethanolamine.

The formation of the SAM of ATRP initiator on the clean gold surface can be evidenced by a drastic increase in the water contact angle of the substrate from 28° to 79° (Table 1). Compared to the typical procedure from the literature in which the formation a SAM requires a incubation of the substrate overnight,<sup>19</sup> in this study we used lower reaction time since it was demonstrated that the completion of SAM of thiol terminated molecules onto gold substrate occurs in shorter time.<sup>29</sup>

The FTIR spectra of the PHEMA brush coated gold surface shows a characteristic broad band of strong intensity around  $3500\text{ cm}^{-1}$  corresponding to the hydroxyl groups and various bands below  $3000\text{ cm}^{-1}$  assigned to the  $\text{CH}_2$  vibrations; a strong carbonyl peak can as well as be seen at  $\sim 1727\text{ cm}^{-1}$  (Figure 1). The PHEMA brushes were further characterized using XPS analysis. The high resolution  $\text{C}_{1s}$  and  $\text{O}_{1s}$  spectra could be fitted to afford the expected contributions of the different atoms (Figure S2). The growth of the PHEMA brush from the surface also results in a decrease in the water contact and the resulting polymer film presents a hydrophilic surface (Table 1).

The introduction of the peptide in the polymer layer by post-polymerization modification using NPC mediated chemistry can be efficiently monitored by FTIR spectroscopy. As compared to the PHEMA brush coated gold electrode, the NPC activated PHEMA brush reveals three new characteristic FTIR peaks at  $\sim 3120\text{ cm}^{-1}$ ,  $3082\text{ cm}^{-1}$  and  $\sim 1769\text{ cm}^{-1}$ , which are assigned, respectively, to the aromatic  $\text{CH}_2$  vibrations (two peaks) and the carbonate chemical groups. In the FTIR spectrum of the peptide functionalized PHEMA brush these three characteristic peaks cannot longer be observed, but instead an extra carbonyl band at  $\sim 1664\text{ cm}^{-1}$ , which is due to the peptide amide bond (Figure 1), appears. The peptide decorated brushes were further investigated by XPS, which revealed in the survey scan four news peaks at  $\sim 398\text{ eV}$ ,  $\sim 226\text{ eV}$ ,  $\sim 161\text{ eV}$  and  $\sim 151\text{ eV}$  corresponding, respectively to  $\text{N}_{1s}$ ,  $\text{S}_{2s}$  and  $\text{S}_{2p}$  (two peaks) (Figure S2). The atomic concentration of sulfur in the PHEMA brush loaded with the peptide (0.89%) indicates a conversion, at the rim of the brush, of  $\sim 40\%$ . This low conversion is due principally to steric hindrance in the polymer assembly which restricts the peptide to penetrate in depth within the polymer layer. The introduction of the mercury-binding peptide does not lead to drastic changes the water contact angle and substrate remains hydrophilic (Table 1).

**Table 1.** Summary of the water contact angle of the different surfaces.

Sample	WCA*
Gold surface	$28^\circ$
Gold surface + ATRP initiator	$79^\circ$
Gold surface + PHEMA brush	$45^\circ$
Gold surface + peptide functionalized PHEMA brush	$50^\circ$

\*WCA: Water contact angle.

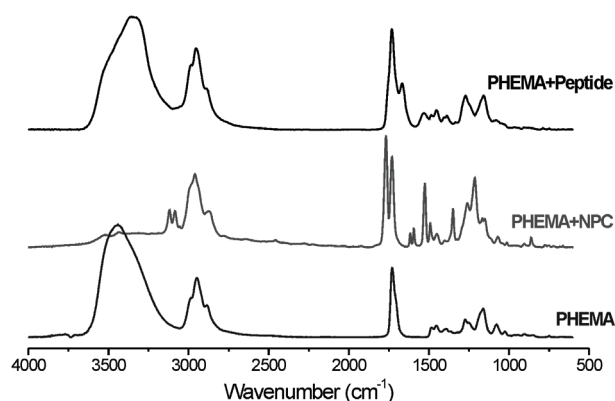


**Figure 1.** FTIR spectra of a PHEMA brush, a PHEMA brush activated with NPC and PHEMA brush post-modified with the mercury binding peptide (brushes thickness ~ 180 nm).

### 5.2.2. Cyclic voltammetry experiments

In this study, all the voltammetric experiments were performed in acetate buffer solutions, since the chelation of  $\text{Hg}^{2+}$  by thiol groups is known to be pH sensitive.<sup>28,30,31</sup> The sensing properties of the peptide functionalized polymer brush were firstly investigated by cyclic voltammetry. Figure 2 compares the cyclic voltammograms of a native gold coated, a PHEMA brush coated and a peptide functionalized polymer brush coated microelectrode in presence of  $\text{Hg}^{2+}$  at a concentration of 10  $\mu\text{M}$ . The native gold coated electrode displays only a limited response during the reoxidation process with a current peak at 0.3 V, but not clear peak assigned to the reduction of the  $\text{Hg}^{2+}$  ions could be observed at this concentration. While the PHEMA brush coated electrode exhibits a broad redox peak of weak intensity, the peptide functionalized PHEMA brush shows two clear redox peaks of strong intensity at around -0.6 V, for the reduction of the chelated mercury ion, and at around -0.5 V, for the reoxidation the heavy metal. The difference in the re-oxidation peak position between gold coated electrode (0.3 V) and the peptide functionalized PHEMA brush (-0.5 V) is due to the chelation of mercury by the cysteine residues of the peptide. Interestingly, the none-functionalized PHEMA brush coated microelectrode shows much lower intensity response than the peptide decorated PHEMA brush and no sharp redox peaks could be observed highlighting the sensitivity gain offered by the peptide post-polymerization modification.



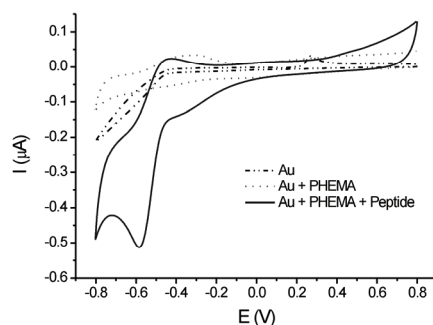


**Figure 2.** Cyclic voltammograms of a native gold, a PHEMA brush coated (52 nm) and peptide functionalized polymer coated (131 nm) microelectrode in presence of at a concentration of  $\text{Hg}^{2+}$  10  $\mu\text{M}$  (scan rate 50 mV/s).

For a given mercury (II) ion concentration, the current intensity of the re-oxidation peak increases with the thickness of peptide functionalized PHEMA brush (Figure S3). The position of the reduction and oxidation peak, however, did not vary with the film thickness (data not shown).

Next, the influence of the  $\text{Hg}^{2+}$  concentration on the response intensity was studied (Figure 3). A linear increase in the reduction and oxidation current intensity with the mercury (II) ions concentration was observed in the concentration range investigated (Figure 3B). The reduction and oxidation potential, however, slightly drifted with increasing the  $\text{Hg}^{2+}$  concentration. This may be ascribed to a decrease in the electron transfer kinetics with increasing mercury (II) ion concentration originating from the properties of the poorly conductive PHEMA based coating. Additionally previous electrochemical study on cysteine rich metal ion binding peptide reported a dependence of the peak potentials on the concentration of metal ions.<sup>32,33</sup>

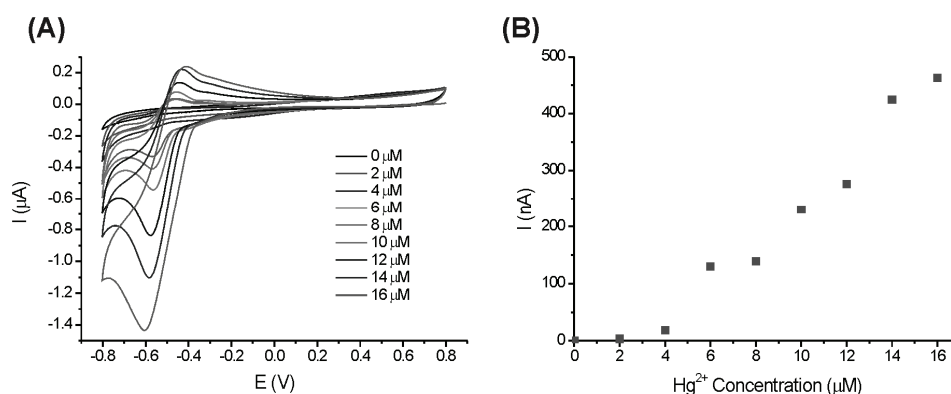


**Figure 3.** (A) Cyclic voltammograms and (B) corresponding re-oxidation peak intensity of a 186 nm thick peptide functionalized polymer brush coated electrode in presence of various Hg<sup>2+</sup> concentration (scan rate 50 mV/s).

At a given concentration, the intensity of the re-oxidation peak was constant over up to 10 cycles illustrating the reversibility of the redox process and demonstrating as well that the functional polymer coating is able to withstand charge transfer processes without damage or aging (Figure S4). The reversibility of the redox process was further demonstrated by investigating, at given mercury (II) ions concentration, the influence of the scan rate used during the cyclic voltammetry measurements on the peak current intensity. A linear relation was found between the oxidation peak currents and the square root of the scan rates, which is in agreement with the Randles-Sevcik equation that predicts, for a reversible electrochemical process, that the current scales proportionally to square root of the scan rate (Figure S5).<sup>34</sup> The presence of one single current peak for the reduction and the oxidation of the Hg<sup>2+</sup> chelated in the peptide modified polymer brush, regardless the scan rate or the mercury (II) ions concentration, suggests that oxidation and reduction are both single step reaction. The selectivity of the functional polymer layer toward various heavy metal ions was investigated by cyclic voltammetry experiments. In the potential range studied (0.8 V to -0.8 V) the system was not able to detect Pb<sup>2+</sup>, Cd<sup>2+</sup>, Cu<sup>2+</sup> or Zn<sup>2+</sup> in the μM range (Figure S6). Nevertheless in presence of a twofold excess of these interfering ions, the response to Hg<sup>2+</sup> was significantly reduced (Figure 4 and S6). The data presented in Figure 4 suggest a competitive heavy metal ions binding.

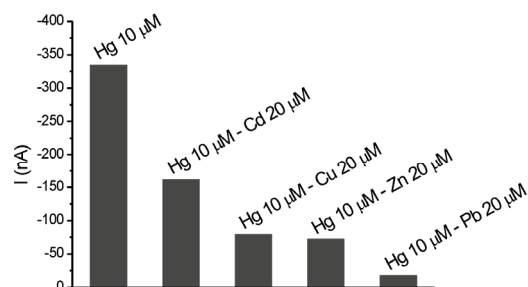


**Figure 4.** Functionalized polymer brush coated microelectrode reduction peak intensity in presence of various solution containing different interfering ions (data calculated from Figure S6).

### 5.2.3. Square wave voltammetry experiments

In a second step we investigated the sensitivity of our peptide decorated polymer brush using square wave voltammetry. This technique allows the detection of  $\text{Hg}^{2+}$  in the sub-nanomolar range (Figure 5), which makes the polymer brush coated microelectrodes amongst the most sensitive polymer-based system for mercury detection.<sup>11,14</sup> The reoxidation peak potential, in square wave voltammetry, was slightly shifted toward the positive potential as compared to the cyclic voltammetry results.

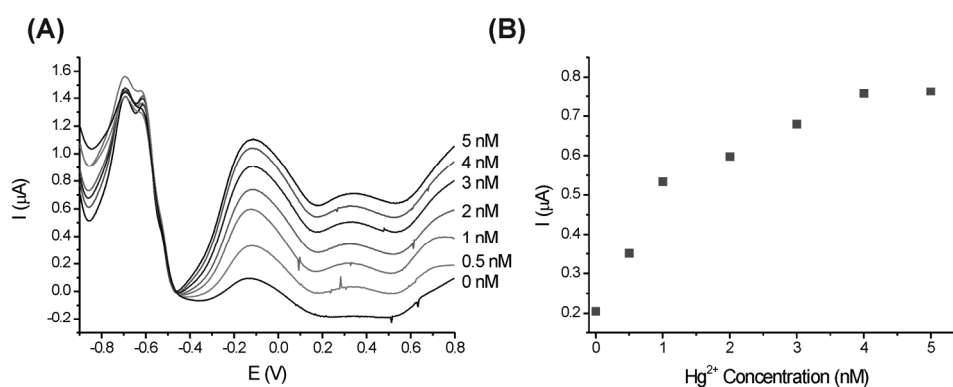


**Figure 5.** (A) Square-wave voltammograms and (B) corresponding re-oxidation peak current intensity of a 52 nm thick peptide functionalized polymer brush coated electrode in presence of various  $\text{Hg}^{2+}$  concentration.

### **5.3. Conclusions**

Peptide functionalized polymer brushes prepared via SI-ATRP can be successfully used to probe heavy metal ions. The polymer coated gold electrode exhibits a higher mercury sensitivity than the bar gold electrode, and allows a detection down to the nanomolar range. The recognition of mercury (II) ions by the functional polymer brush is a reversibility and reproducible process and a linear current peak response to the  $\text{Hg}^{2+}$  concentration was observed in the range investigated.

## 5.4. Experimental

### 5.4.1. Materials

Fmoc protected amino acids, O-Benzotriazole-*N,N,N',N'*-tetramethyl-uronium-hexafluoro-phosphate (HBTU) and 1-Hydroxybenzotriazole (HOBT.H<sub>2</sub>O) were obtained from IRIS Biotech GmbH (Marktredwitz, Germany). *N,N'*-Dimethylformamide (DMF) and HPLC gradient grade methanol were purchased from VWR. *N*-methylpyrrolidone (NMP) and diethyl ether (Et<sub>2</sub>O) was obtained from Schweizerhall. All other chemicals were obtained from Sigma-Aldrich, except the CertiPUR<sup>®</sup> metal ions standard solutions which were purchased from Merck (Hg(NO<sub>3</sub>)<sub>2</sub>, Cd(NO<sub>3</sub>)<sub>2</sub>, Cu(NO<sub>3</sub>)<sub>2</sub>, Zn(NO<sub>3</sub>)<sub>2</sub>, and Pb(NO<sub>3</sub>)<sub>2</sub>). The polymerization inhibitor in 2-hydroxyethyl methacrylate (HEMA) was removed by passing the monomer through a column of activated basic aluminum oxide. Organic solvents were dried by passage through two columns of molecular sieves using a Pure Solv<sup>™</sup> 400 solvent purification system. Ultrahigh quality Milli-Q water with aresistance of 18.2 MΩ.cm (at 25°C) was obtained from a Millipore Milli-Q gradient machine fitted with a 0.22 μm filter. The gold coated microelectrode were obtained as previously reported.<sup>35</sup>

### 5.4.2. Methods

Reflectance Fourier transform infrared (FTIR) spectroscopy of the polymer brushes was carried out on a Nicolet Magna-IR 560 spectrometer equipped with a Micro Specular Reflectance accessory (Specac Ltd., UK). The substrates were cleaned using a microwave induced oxygen plasma system (Diener electronic GmbH, Germany). X-ray photoelectron spectroscopy (XPS) was carried out using an Axis Ultra instrument from Kratos Analytical equipped with a hemispheric analyzer. The X-ray source employed was a monochromatic Al Kα (1486.6 eV) source operated at 100 W and 10<sup>-9</sup> mbar. Water contact angle measurements were performed using a DataPhysics OCA 35 contact angle measuring instrument. Polymer brushes thicknesses were measured using atomic force microscopy (AFM) which was performed in Tapping mode on a Veeco Multimode Nanoscope IIIa SPM controller (Digital instruments, Santa Barbara, CA) using NSC14/no Al Mikromasch (Tallinn, Estonia) cantilever. Cyclic and square-wave voltammetry

experiments were performed on a  $\mu$ Autolab potentiostat Type II (Metrohm) using an Ag/AgCl reference electrode and a platinum counter electrode. The voltammetry experiments were conducted in presence of sodium acetate 5 mM (buffering salt) and sodium chloride 0.1 M (supporting electrolyte). For the cyclic voltammetry measurements, the data were acquired by scanning potential from 800 mV to -800 mV and then back to 800 mV. Prior to the measurement, the electrode was maintained at a potential of 800 mV for 30 s as a cleaning pretreatment. For the square-wave voltammetry experiments scanning potential from -900mV to 800mV at a frequency of 50Hz and a step potential of 4 mV applying, prior to the measurement, a deposition potential of - 900 mV for 120 s.

### **5.4.3. Procedure**

#### **5.4.3.1. Peptide synthesis and purification**

The peptide sequence (Ala-Ala-Ala-Cys-Ala-Ala-His-Cys-Try-Ala-Glu-NH<sub>2</sub>) was synthesized using a CEM Liberty<sup>®</sup> automated microwave peptide synthesizer by Fmoc chemistry from a Rink amide AM resin (0.71 mmol/g loading). The deprotection of Fmoc group was achieved in two subsequent steps using 20 % piperidine with 0.1 M HOBT in DMF for 1 minute and subsequently 6 minutes using 58 W of microwave energy at 75  $\pm$  5  $^{\circ}$ C. With 5-fold 10 mL DMF, the resin was washed and cooled to 25  $^{\circ}$ C. A single 0.2 M (10 mL) amino acid coupling for each residue of the peptide sequence was performed with stock solutions of activator (0.5 M HOBT and 0.5 M HBTU in DMF, 4 mL) as the activator mixture and 2 M DIPEA in NMP (2 mL) as the base. The final molar ratio of the amino acid : activator : base during the reaction was 1 : 1 : 2 and the coupling reaction proceeded for 7 minutes using 25 W of microwave energy at 70  $\pm$  5  $^{\circ}$ C. After completion of the synthesis, the peptide was cleaved from the resin and deprotected using 15 mL of a mixture of trifluoroacetic acid (TFA), triisopropylsilane (TIS), ethan-1,2-dithiol and MilliQ water in the volume ratio 92.5 : 2.5 : 2.5 : 2.5 % for 3.5 - 4 hours at room temperature. After peptide cleavage, the TFA containing filtrate was added to 30 mL of cold Et<sub>2</sub>O. The crude peptide precipitate was washed with cold Et<sub>2</sub>O 4-fold and subsequently lyophilized prior to purification.

The peptide was purified by preparative high pressure liquid chromatography (HPLC) using a Waters 600 automated gradient controller pump module connected to a Waters

prep degasser system. The elution of the peptides was monitored by using a Waters 2487 dual  $\lambda$  absorbance detector and collected using a Waters fraction collector III. Purification of the peptide was achieved using an Atlantis<sup>®</sup> OBD<sup>™</sup> C-18 reverse phase column (Waters) equilibrated with a water/TFA (0.1 % TFA in water, Solvent A) and acetonitrile/TFA (0.1 % TFA in methanol, Solvent B). Elution was achieved at 20 mL/min by typically running gradients of 40 to 70 % solvent B over 20 minutes. The peptide eluted at ~ 55% solvent A / ~ 45 % Solvent B, was rotary evaporated to remove the methanol and was lyophilized to yield a white fluffy powder (~ 100 mg).

#### 5.4.3.2. Synthesis of 6-mercaptohexyl 2-bromo-2-methylpropanoate (1)

1.82 mL (13.36 mmol) 6-Mercapto-1-hexanol and 1.08 mL (13.36 mmol) free distilled pyridine were dissolved in 40 mL of dichloromethane. The solution was stirred under nitrogen and cooled with an ice bath. Next, 1.64 mL (13.36 mmol)  $\alpha$ -bromoisobutyryl bromide was added dropwise and the resulting mixture stirred under nitrogen at 0 °C for one hour and let stirred overnight at room temperature. Then the mixture was washed two times with a saturated ammonium chloride solution, the organic phase was extracted and dried over MgSO<sub>4</sub> and the solvent removed under reduced pressure. 6-mercaptohexyl 2-bromo-2-methylpropanoate **1** was obtained as a colorless oil after by vacuum distillation (130 °C, vacuum line). <sup>1</sup>H NMR (400 MHz, CDCl<sub>3</sub>,  $\delta$ ): 1.28 (t, 1H, -SH), 1.38 (m, 4H, -CH<sub>2</sub>-), 1.58 (m, 2H, -CH<sub>2</sub>-), 1.64 (m, 2H, -CH<sub>2</sub>-), 1.88 (s, 6H, C-CH<sub>3</sub>), 2.49 (q, 2H, CH<sub>2</sub>-S-), 4.12 (t, 2H, O=C-O-CH<sub>2</sub>). <sup>13</sup>C NMR (400 MHz, CDCl<sub>3</sub>,  $\delta$ ): 24.16 (-CH<sub>2</sub>-S-), 24.98, 27.55, 27.93 (-CH<sub>2</sub>-), 30.46 (-C(CH<sub>3</sub>)<sub>2</sub>), 33.50 (-CH<sub>2</sub>-), 55.69 (-C(CH<sub>3</sub>)<sub>2</sub>), 65.55 (O=C-O-CH<sub>2</sub>), 171.22 (O-C=O).

#### 5.4.3.3. Formation of the SAM of SI-ATRP initiator

The substrate were washed with acetone and dried and subsequently exposed to an oxygen plasma (18 W, 10 min). Directly after the substrate were immersed for 4h00 in a 10 mM ethanol solution of 6-mercaptohexyl 2-bromo-2-methylpropanoate **1**. Afterwards, the substrates were extensively rinsed with ethanol, methanol and dried under nitrogen. Both microelectrodes and gold coated silicon wafers were used as substrate, the chemical characterization were performed on the polymer brush functionalized gold coated silicon wafers.

#### **5.4.3.4. Surface-initiated atom transfer radical polymerization of 2-hydroxyethyl methacrylate**

SI-ATRP of HEMA was performed as previously described by Huang *et al.*,<sup>37</sup> using a system composed of H<sub>2</sub>O/HEMA/CuBr/CuBr<sub>2</sub>/bipy (1645/244/1/0.3/2.9, molar ratio). Patterned polymer brushes for Atomic Force Microscopy (AFM) studies were obtained as previously described.<sup>38</sup>

#### **5.4.3.5. Post-polymerization modification**

The post-polymerization modification (Scheme 1) was carried out following the procedure reported earlier by Tugulu *et al.*<sup>39</sup>



## 5.5. References

1. Lin, Y.; Larssen, T.; Vogt, R. D.; Feng, X. B. *Applied Geochemistry* **2010**, *25*, 60-68.
2. Larssen, T. *Environmental Pollution* **2010**, *158*, 24-25.
3. Hylander, L. D.; Goodsite, M. E. *Science of the Total Environment* **2006**, *368*, 352-370.
4. Li, P.; Feng, X. B.; Qiu, G. L.; Shang, L. H.; Li, Z. G. *Journal of Hazardous Materials* **2009**, *168*, 591-601.
5. Scheuhammer, A. M. *Environmental Pollution* **1987**, *46*, 263-295.
6. Wolfe, M. F.; Schwarzbach, S.; Sulaiman, R. A. *Environmental Toxicology and Chemistry* **1998**, *17*, 146-160.
7. Tan, S. W.; Meiller, J. C.; Mahaffey, K. R. *Critical Reviews in Toxicology* **2009**, *39*, 228-269.
8. Kempuraj, D.; Asadi, S.; Zhang, B. D.; Manola, A.; Hogan, J.; Peterson, E.; Theoharides, T. C. *Journal of Neuroinflammation* **2010**, *7*, 1-7.
9. Crespo-López, M. E.; Macedo, G. L.; Pereira, S. I. D.; Arrifano, G. P. F.; Picanco-Diniz, D. L. W.; do Nascimento, J. L. M.; Herculano, A. M. *Pharmacological Research* **2009**, *60*, 212-220.
10. Selid, P. D.; Xu, H. Y.; Collins, E. M.; Face-Collins, M. S.; Zhao, J. X. *Sensors* **2009**, *9*, 5446-5459.
11. Namour, P.; Lepot, M.; Jaffrezic-Renault, N. *Sensors* **2010**, *10*, 7947-7978.
12. Han, D.; Kim, Y. R.; Oh, J. W.; Kim, T. H.; Mahajan, R. K.; Kim, J. S.; Kim, H. *Analyst* **2009**, *134*, 1857-1862.
13. Wu, D. H.; Zhang, Q.; Chu, X.; Wang, H. B.; Shen, G. L.; Yu, R. Q. *Biosensors & Bioelectronics* **2010**, *25*, 1025-1031.
14. Zhu, Z. Q.; Su, Y. Y.; Li, J.; Li, D.; Zhang, J.; Song, S. P.; Zhao, Y.; Li, G. X.; Fan, C. H. *Analytical Chemistry* **2009**, *81*, 7660-7666.
15. Sanchez, A.; Walcarius, A. *Electrochimica Acta* **2010**, *55*, 4201-4207.
16. Doménech, A.; Doménech-Carbó, M. T.; García-España, E.; Soriano, M. D. *Analyst* **1999**, *124*, 1661-1667.
17. Somers, V.; Leaner, J.; Mason, R.; Iwuoha, E.; Morrin, A. *Electrochimica Acta* **2010**, *55*, 4240-4246.
18. Bakhtiarzadeh, F.; Ab Ghani, S. *Electroanalysis* **2010**, *22*, 549-555.

19. Barbey, R.; Lavanant, L.; Paripovic, D.; Schüwer, N.; Sugnaux, C.; Tugulu, S.; Klok, H.-A. *Chemical Reviews* **2009**, *109*, 5437-5527.
20. Schüwer, N.; Klok, H.-A. *Advanced Materials* **2010**, *22*, 3251-3255.
21. Kusumo, A.; Bombalski, L.; Lin, Q.; Matyjaszewski, K.; Schneider, J. W.; Tilton, R. D. *Langmuir* **2007**, *23*, 4448-4454.
22. Peng, Q.; Xie, M. G.; Neoh, K. G.; Kang, E. T. *Chemistry Letters* **2005**, *34*, 1628-1629.
23. Zhou, F.; Shu, W. M.; Welland, M. E.; Huck, W. T. S. *Journal of the American Chemical Society* **2006**, *128*, 5326-5327.
24. Welch, M.; Rastogi, A.; Ober, C. *Soft Matter* **2011**, *7*, 297-302.
25. Kojima, Y.; Kagi, J. H. R. *Trends in Biochemical Sciences* **1978**, *3*, 90-93.
26. Joshi, B. P.; Park, J.; Lee, W. I.; Lee, K. H. *Talanta* **2009**, *78*, 903-909.
27. Tugulu, S.; Arnold, A.; Sielaff, I.; Johnsson, K.; Klok, H.-A. *Biomacromolecules* **2005**, *6*, 1602-1607.
28. Lenz, G. R.; Martell, A. E. *Biochemistry* **1964**, *3*, 745-750.
29. Moya, S. E.; Brown, A. A.; Azzaroni, O.; Huck, W. T. S. *Macromolecular Rapid Communications* **2005**, *26*, 1117-1121.
30. Nieto, O.; Rodriguez, A. R. *Bioelectrochemistry and Bioenergetics* **1996**, *40*, 215-222.
31. Mendieta, J.; Chivot, J.; Muñoz, A.; Rodriguez, A. R. *Electroanalysis* **1995**, *7*, 663-669.
32. Nieto, O.; Rodriguez, A. R. *Electroanalysis* **1999**, *11*, 175-182.
33. Harlyk, C.; Bordin, G.; Nieto, O.; Rodriguez, A. R. *Journal of Electroanalytical Chemistry* **1998**, *446*, 139-150.
34. Bard, A. J.; Faulkner, L. R., *Electrochemical methods: fundamentals and applications - 2nd ed.* New York : Wiley, 2001.
35. Belmont, C.; Tercier, M. L.; Buffle, J.; Fiaccabrino, G. C.; KoudelkaHep, M. *Analytica Chimica Acta* **1996**, *329*, 203-214.
36. Huang, W. X.; Kim, J. B.; Bruening, M. L.; Baker, G. L. *Macromolecules* **2002**, *35*, 1175-1179.
37. Tugulu, S.; Harms, M.; Fricke, M.; Volkmer, D.; Klok, H.-A. *Angewandte Chemie International Edition* **2006**, *45*, 7458-7461.

## 5.6. Supporting Information

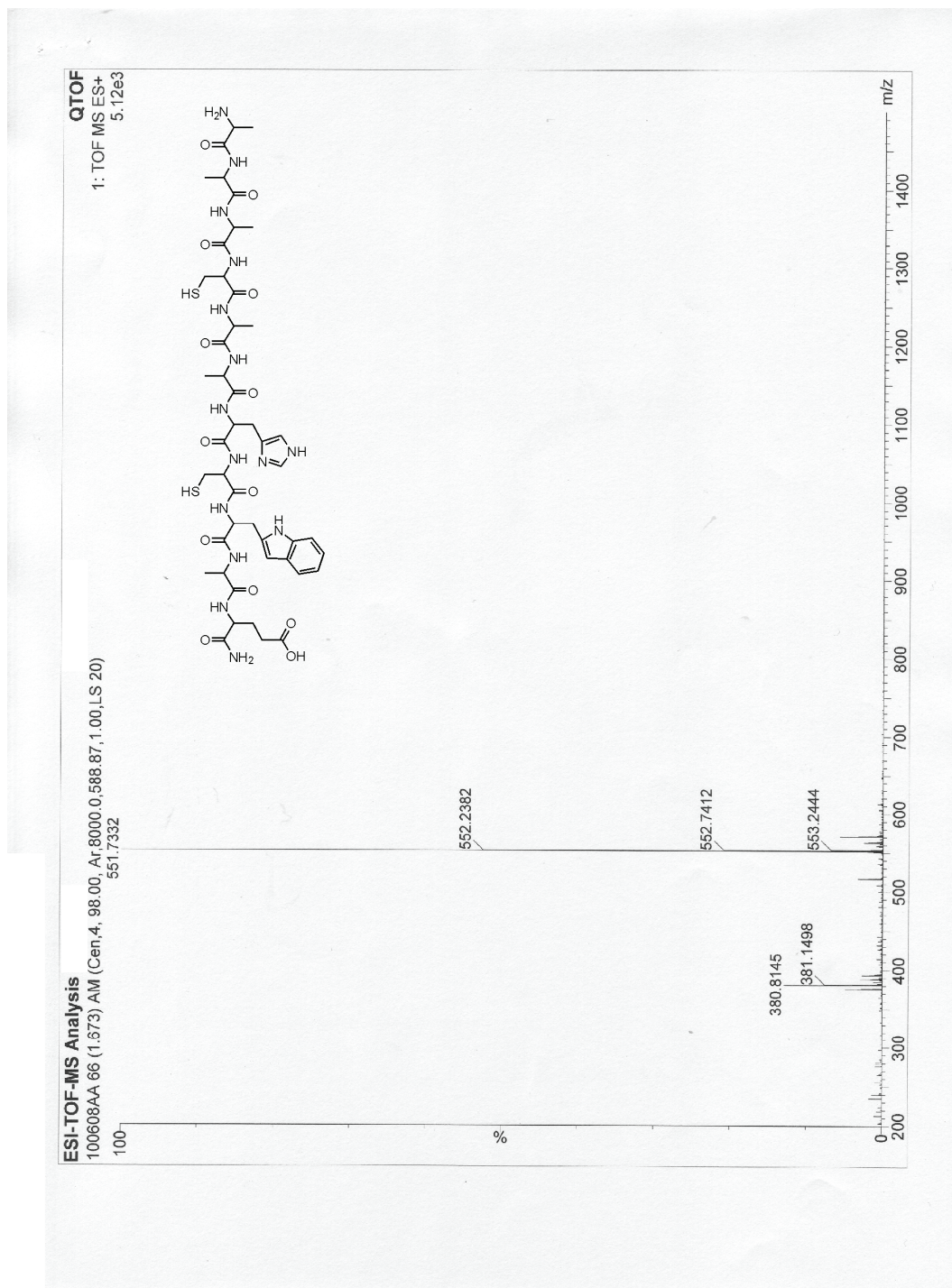


**Figure S1.** ESI-TOF-MS of the Hg<sup>2+</sup> binding peptide used in this study.

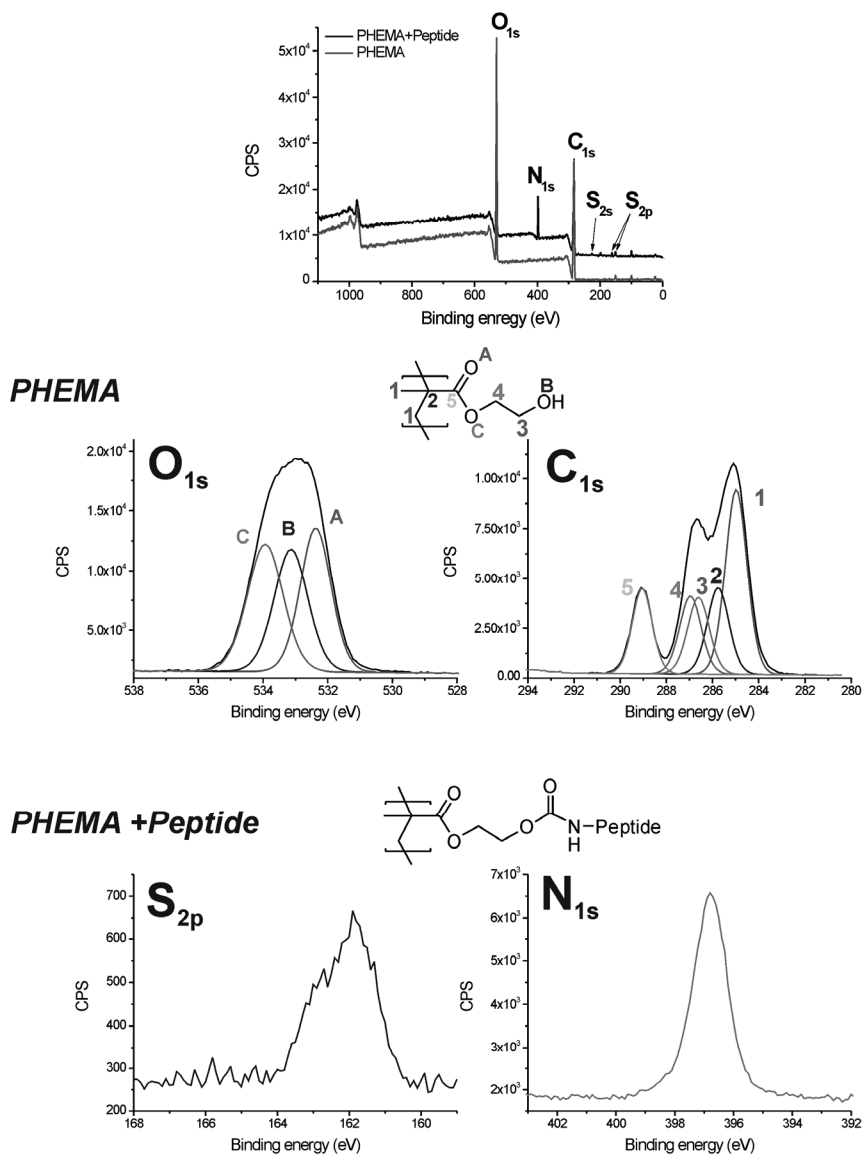


**Figure S2.** XPS survey and high-resolution XPS spectra of a PHEMA brush and a peptide functionalized PHEMA brush (brush thickness ~ 180 nm).

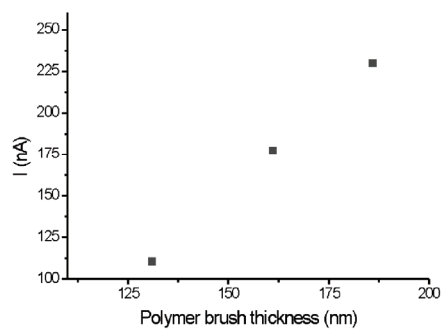


**Figure S3.** Intensity of the cyclic voltammetry re-oxidation peak as a function of the film thickness. ( $[\text{Hg}^{2+}]$  10  $\mu\text{M}$  / scan rate 50mV/s).

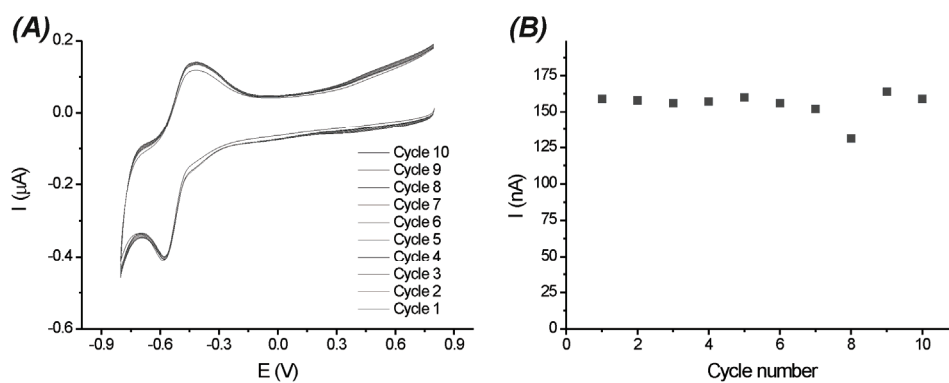


**Figure S4.** Cyclic voltammograms (A) and corresponding re-oxidation peak intensity versus cycle number of a peptide functionalized polymer brush coated microelectrode in presence of  $\text{Hg}^{2+}$  at a concentration of 8  $\mu\text{M}$  (scan rate 50mV/s - brush thickness  $\sim$  131 nm).

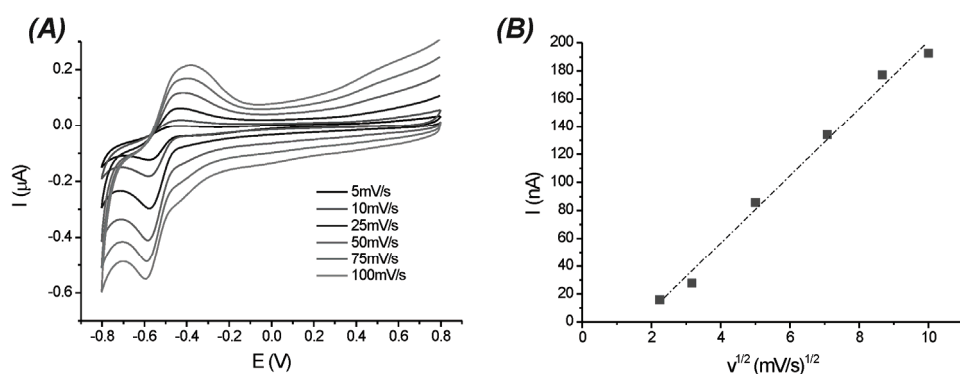


**Figure S5.** Cyclic voltammograms (A) and corresponding plot of the re-oxidation peak intensity versus square root of the scan rate (B) of a peptide functionalized polymer coated microelectrode in presence of  $\text{Hg}^{2+}$  at a concentration of  $8 \mu\text{M}$  (scan rate  $50\text{mV/s}$  - brush thickness  $\sim 131 \text{ nm}$ ).

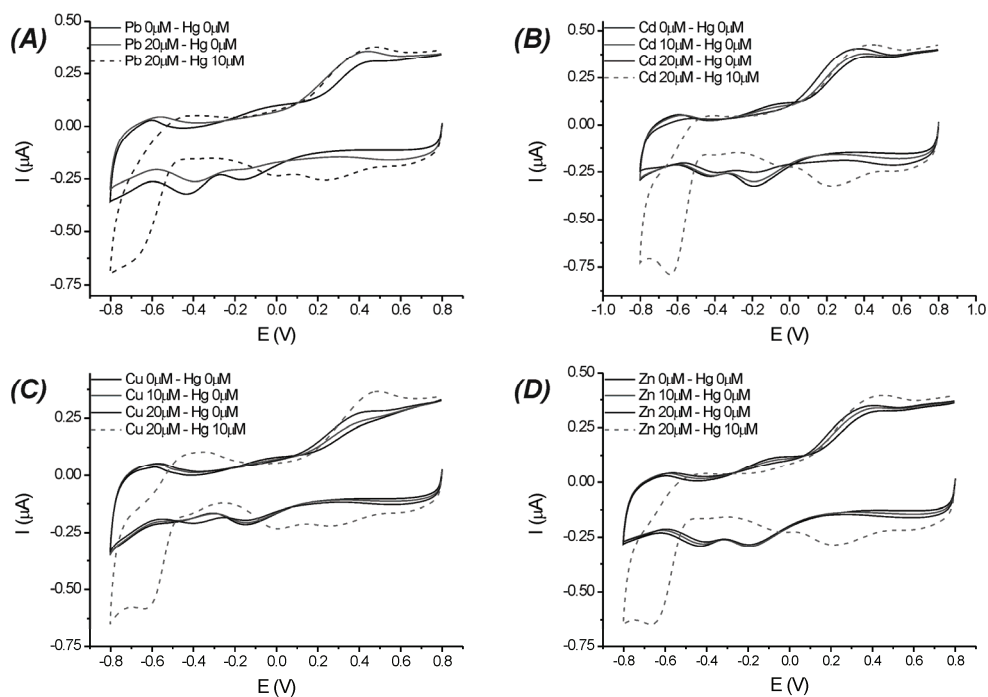


**Figure S6.** Cyclic voltammograms of a 186 nm thick peptide functionalized polymer brush in presence of various solutions containing different mixture of heavy metals ions.



## **6. Neutron Reflectivity Study on the Post-Polymerization Modification of Poly(2-hydroxyethyl methacrylate) Brushes**

### **6.1. Introduction**

Polymer brushes are ultrathin, surface grafted polymer layers in which all polymer chains are tethered with one of their chain ends to a substrate.<sup>1-5</sup> At sufficiently high grafting densities, steric repulsions force the chains to stretch out resulting in a densely packed arrangement of surface grafted polymer chains. The use of controlled/"living" surface-initiated radical polymerization techniques allows to precisely control the thickness, composition and architecture of polymer brushes, which makes them very attractive coatings to control the surface properties of a broad range of materials.

For many applications, polymer brushes are required that contain specific functional groups. Functionalized polymer brushes can be prepared either via direct surface-initiated polymerization of the appropriate side-chain functional monomer or via post-polymerization modification of a suitable, reactive polymer brush. Although the relatively high functional group tolerance of "living"/controlled radical polymerization techniques allows the direct surface-initiated polymerization of a wide variety of side chain functional monomers, there is still a large number of complex side chain functional monomers that cannot be directly polymerized. Post-polymerization modification is an attractive alternative to overcome these problems and to enable the preparation of polymer brushes with complex functional groups. In spite of the fact that post-polymerization modification is a well-established strategy to synthesize functional polymer brushes,<sup>1</sup> only very little is known about the distribution of the resulting functional groups throughout the polymer brush layer. Steric constraints during the post-polymerization modification reaction, however, may result in a non-homogeneous distribution of functional groups and concentration gradients throughout the polymer brush, which, in turn may influence the final properties of the polymer brush.

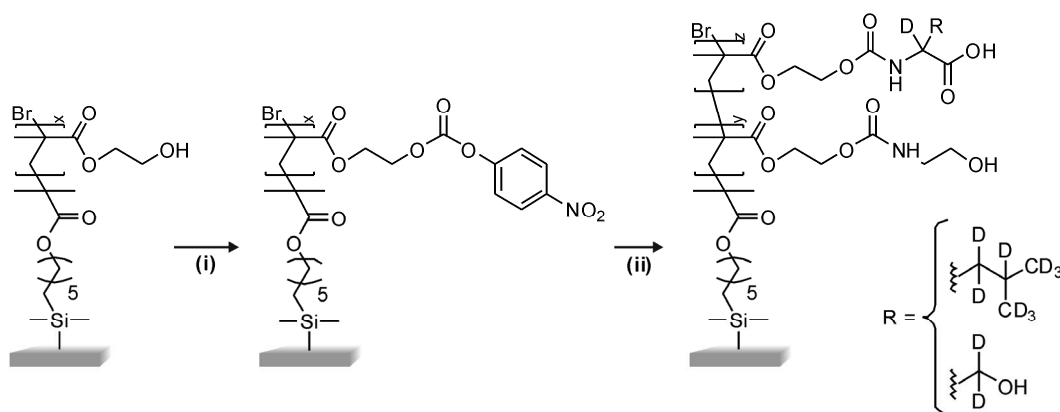
This section describes the results of a study that was aimed at investigating the influence of film thickness and grafting density on the distribution of functional groups in a polymer brush prepared via post-polymerization modification. To investigate the position and distribution of functional groups in the polymer brush films, neutron reflectivity was used. This technique has already been used to determine the structure of neutral and polyelectrolyte brushes,<sup>6,7</sup> to monitor swelling behaviour of weak polyelectrolyte or thermosensitive brushes<sup>8,9</sup> or to study the chain-end distribution in polymer brushes.<sup>10</sup> The experiments discussed in this section were performed with poly(2-hydroxyethyl methacrylate) brushes, which were post-modified with deuterated leucine (D-10 leucine) and deuterated serine (D-3 serine) after activation of the side chain hydroxyl groups with *p*-nitrophenyl chloroformate (NPC). The NPC activation strategy is commonly used for the post-polymerization modification of hydroxyl side chain functional polymer brushes.<sup>11-15</sup> The distribution of the leucine and serine residues in the final polymer brush films was determined by neutron reflectivity taking advantage of the neutron scattering contrast between hydrogen and deuterium.<sup>16</sup> The ability to understand and measure the distribution of functional groups in polymer brushes prepared via surface-initiated atom transfer radical polymerization is important not only as it may provide guidelines for the synthesis of homogeneous functional brushes, but also since it may indicate opportunities to, via judicious choice of the reaction conditions, produce non-homogeneous, but precisely controlled, polymer brushes. The latter may lead to polymer brush with new and interesting properties.

## 6.2. Results and discussion

The post-polymerization modification of the PHEMA brushes that is investigated in this study is illustrated in Scheme 1. To evaluate the effect of brush thickness and density, a library of PHEMA brushes was prepared with thicknesses of  $\sim 100$  up to  $\sim 880$  Å and grafting densities, expressed as the volume percentage of the ATRP initiator in the mixture of chlorosilanes that was used to modify the substrates of 25, 50, 75 and 100 %. Since the post-polymerization modification may depend on the nature of the amine that is used, PHEMA brushes were modified both with a polar and uncharged amino acid



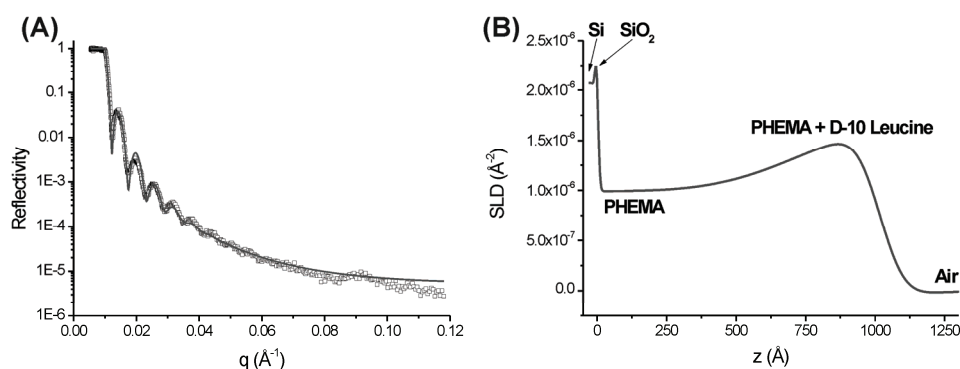
(serine) as well as with an amino acid that bears a hydrophobic and bulky side chain (leucine).



**Scheme 1.** Post-polymerization modification of PHEMA brushes with D-10 leucine and D-3 serine, (i) NPC/Et<sub>3</sub>N/THF, 1 hr; (ii) Amino acid/DMAP/DMF, 16 hrs followed by quenching with ethanolamine.

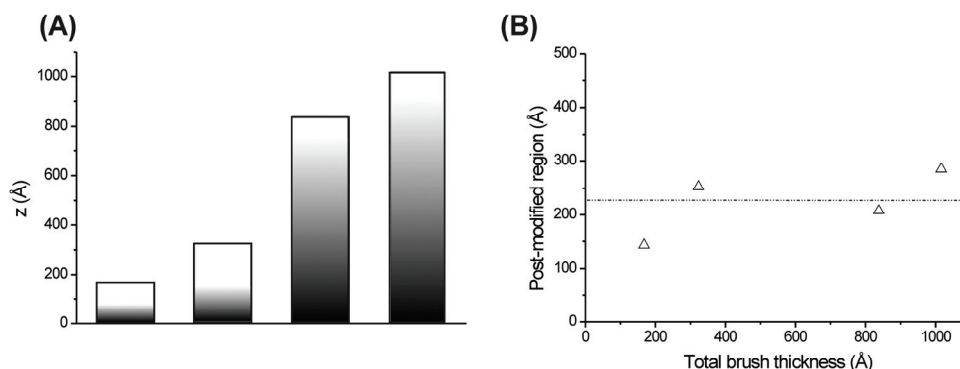
The post-modified brushes were studied with neutron reflectivity experiments. As a representative example, Figure 1 shows the experimental reflectivity profile and the corresponding scattering length density profile for a 1016 Å thick PHEMA brush after post-modification with D-10 leucine. After an abrupt transition at the silicon oxide-brush interface, the SLD increases gradually and reaches a maximum at the top of the polymer brush layer. The increase in the SLD with increasing distance from the silicon substrate reflects the leucine concentration gradient in the brush, going from a pure PHEMA brush near the silicon-brush interface to a leucine rich PHEMA brush at the top layer. The data in Figure 1 indicate that the NPC mediated post-polymerization modification of a 1016 Å thick PHEMA brush with D-10 leucine does not result in quantitative conversion of the hydroxyl side chain functional groups. The fit of the reflectivity data indicated that a high concentration of D-10 leucine is only found in the top ~ 285 Å of the brush. In between these extremes, the concentration of D-10 leucine increases gradually with increasing distance from the silicon substrate. Comparison of the experimentally determined SLD of the post-modified PHEMA and the theoretical value for D-10 leucine modified PHEMA suggests a maximum conversion at the top of the layer of ~ 73 %. The reflectivity data in Figure 1 were fitted with a 5 layer model: Si-bulk / SiO<sub>2</sub> / PHEMA / post-modified PHEMA / air model. A 10 layer model that takes into account a concentration gradient of

deuterated molecules within the polymer brush was also evaluated, however, the final distribution profiles were found to be similar to those obtained with the 5 layer model. Furthermore, the  $\chi^2$  parameter was smaller, *i.e.* the quality of the fit better, for the 5 layer model as compared to the 10 layer model. For the remains of this chapter, the 5 layer model has been used to describe the distribution of deuterated amino acids within the PHEMA brushes. The roughness of PHEMA block - post-modified PHEMA block interface, obtained experimentally from the fitting, provides a direct information about the interpenetration of these two model blocks, and corresponds to the concentration gradient of incorporated deuterated molecules between the two extreme values of the model.



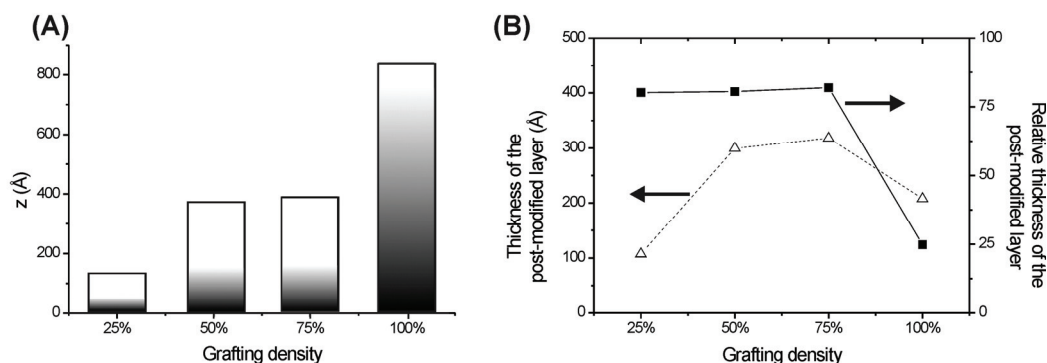
**Figure 1.** (A) Experimental reflectivity data (open squares) and the corresponding fit (solid line) of a 1016 Å PHEMA brush after post-polymerization modification with D-10 leucine. (B) Corresponding SLD profile.

Figure 2 summarizes the results of neutron reflectivity experiments that were carried out on PHEMA brushes of 4 different initial thicknesses after post-polymerization modification with D-10 leucine. Independently of the brush thickness, it was found that the post-polymerization modification conditions applied here only resulted in functionalization of the top ~ 200 Å layer (Figure 2B). The gray shading in Figure 2A (black: unmodified PHEMA; white: maximum conversion of hydroxyl groups) is a visual representation of the concentration gradient of deuterated groups in the brush as obtained from the experimental SLD profile (see *e.g.* Figure 1B).



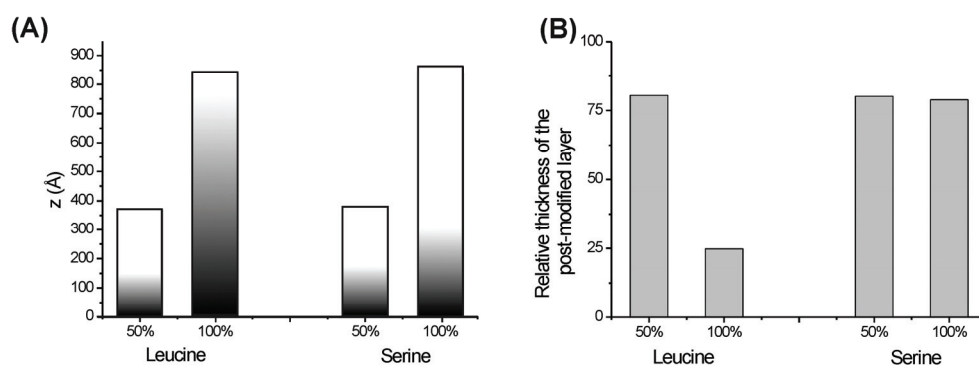
**Figure 2.** Influence of film thickness on the post-polymerization modification of poly(2-hydroxyethyl methacrylate) brushes with D-10 leucine. (A) Total thickness (bars) and thickness of the post-modified layer (top white area) for brushes of different thicknesses; (B) thickness of the D-10 leucine post-modified region as a function of the total PHEMA brush thickness.

Figure 3 illustrates the influence of grafting density on the post-polymerization modification of poly(2-hydroxyethyl methacrylate) brushes with D-10 leucine. Brushes of different grafting density (25 %, 50 %, 75 % and 100 % of active initiator) and with initial thicknesses of 70 Å, 200 Å, 250 Å and 880 Å, respectively, were activated with NPC and further reacted with D-10 leucine. Whereas for the densest brushes the thickness of the post-modified layer, *i.e.* the conversion of PHEMA side chain hydroxyl groups, accounts for ~ 25 % of the total brush thickness, ~ 82 % of the total film thickness is post-modified when the brush density is decreased to 75 %. The increase in overall conversion with decreasing graft density is probably due to the enhanced accessibility of the polymer brush layer with decreasing grafting density. Decreasing the grafting density from 75 % to 50 % or 25 % did not further improve the relative conversion, *i.e.* the relative thickness of the post-modified layer as compared to the total brush thickness.



**Figure 3.** Influence of grafting density on the post-polymerization modification of poly(2-hydroxyethyl methacrylate) brushes with D-10 leucine. (A) Total thickness (bars) and thickness of the post-modified layer (top white area) for brushes of different grafting densities; (B) absolute thickness ( $\Delta$ , left axis) and relative thickness ( $\blacksquare$ , right axis) of the post-modified layer for PHEMA brushes of different grafting densities.

All the post-polymerization modification experiments discussed so far have been carried out with D-10 leucine. To investigate the possible influence of the structure and chemical composition of the amino acid reagent on the post-polymerization modification, additional experiments were carried out with D-3 serine. Figure 4 compares the post-polymerization modification of PHEMA brushes of different grafting densities with D-10 leucine and D-3 serine. The results summarized in Figure 4 were obtained using PHEMA brushes of the same initial thickness and density, which were activated with NPC and subsequently exposed to a 1 mM solution of D-10 leucine and D-3 serine. The data in Figure 4 clearly illustrate that the extent to which post-polymerization modification proceed depends on the nature of the amino acid. For a dense brush, the thickness of the post-modified layer was three times larger when D3-serine was used instead of D-10 leucine. Whereas decreasing the brush density led to a strong increase in hydroxyl side chain modification in case of D-10 leucine, the relative thickness of the D3-serine post-modified top-layer of the PHEMA brush did not significantly vary with brush density. Comparison of the experimental and the theoretical SLD of D-3 serine post-modified PHEMA suggests a degree of conversion at the rim of the layer, of  $\sim 77\%$ . The results in Figure 4 reflect the differences in size and polarity between D-10 leucine and D-3 serine and the ability of these amino acids to penetrate the activated PHEMA brushes.



**Figure 4.** Influence of the nature of the amino acid on the post-polymerization modification of dense poly(2-hydroxyethyl methacrylate) brushes of various densities. (A) Total thickness (bars) and thickness of the post-modified layer (top white area) for brushes of different grafting densities modified with D-10 leucine and D3-serine; (B) relative thickness of the post-modified layer for PHEMA brushes of different grafting densities with different amino acids.

When investigating the post-polymerization modification of PHEMA brushes with between D-10 leucine and D-3 serine it is important to realize the observed results do not only reflect the size and polarity of the amino acid and steric crowding of the polymer brush but may also be due to non-homogeneous NPC activation, *i.e.* the presence of NPC concentration gradient through the brushes. To study the presence of possible NPC gradients, activated PHEMA brushes were analyzed with FTIR spectroscopy and UV-vis spectroscopy. FTIR spectra of the NPC activated brushes still revealed the OH vibrations around  $3300\text{cm}^{-1}$ , indicating incomplete hydroxyl group conversion (Figure 5). The influence of the brush thickness and density on the NPC activation was investigated by monitoring the UV-absorbance at 278 nm of a series of activated PHEMA brushes (Figure 6). For thin PHEMA brushes (up to  $400\text{ \AA}$ ), the absorbance at 278 nm was found to increase almost linearly (Figure 6A). After that, a plateau value was reached. When the absorbance is normalized with respect to the brush thickness, however, a continuous decrease intensity with increasing brush thickness is observed, which suggests that NPC activation is non-homogeneous and predominantly occurs at the top layer of the brush. UV-vis. analysis of a series of brushes of different densities (but prepared with an identical polymerization time) revealed a continuous increase in the UV-vis. absorbance at 278 nm but a continuous decrease in the normalized UV-vis. absorbance with increasing brush density (Figure 6B). These results reflect the increased accessibility of the side chain hydroxyl group with decreasing brush density. Taken together, the data in

Figure 6 indicate that post-polymerization modification of PHEMA brushes with D-10 leucine and D-3 serine is the result of a complex interplay of effects of steric crowding by the surface grafted polymer chains, size and polarity of the amino acid and NPC activation gradients.

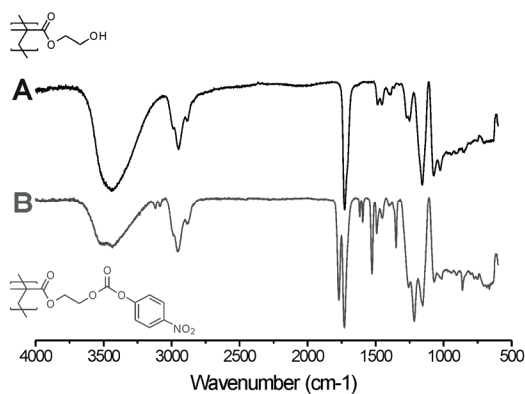


**Figure 5.** FTIR reflectance spectra (% transmittance) of (A) a PHEMA brush and (B) a NPC activated PHEMA brush (thickness ~ 1400 Å).

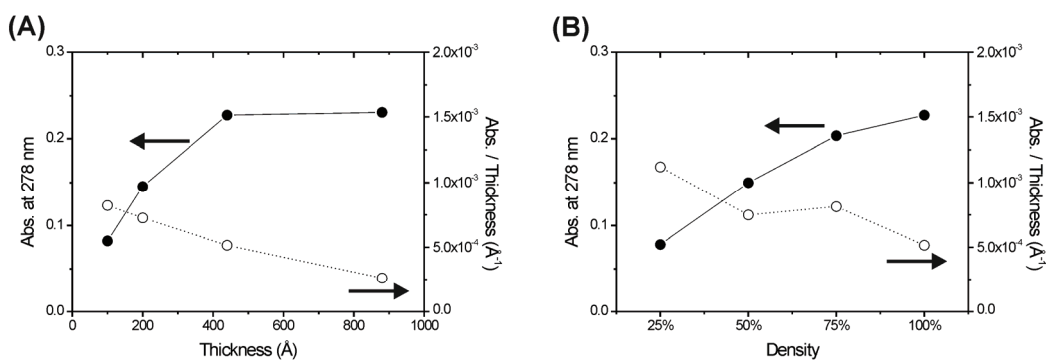


**Figure 6.** Intensity (●, left) and normalized intensity (○, right) of the UV absorbance band of: (A) NPC activated PHEMA brushes of different thickness and a grafting density of 100 %; (B) NPC activated brushes of different density (polymerization time 2 hrs).

### 6.3. Conclusions

This chapter has investigated the distribution of functional groups in polymer brushes obtained via NPC-mediated post-polymerization modification with deuterated amino acids. Neutron reflectivity experiments revealed that for dense PHEMA brushes, post-polymerization modification with D-10 leucine is restricted to the top  $\sim 200$  Å of the layer regardless of the brush thickness. Decreasing the grafting density from 100 % to 75 % or less significantly increased the extent of post-polymerization modification and results in brushes in which 75 % of the total thickness is post-modified with D-10 leucine. Experiments with D-3 serine demonstrated that the nature of the amino acid also plays a role; post-polymerization modification with this non-hydrophobic and sterically less demanding amino acid resulted in polymer brushes that were post-modified for 70 % independently of brush density. In addition to brush thickness and density and the nature of the amino acid, UV-vis. absorbance studied revealed that a non-uniform NPC activation also contributes to a non-homogeneous post-polymerization modification of the PHEMA brushes. For dense brushes, the NPC density was high near the brush-air interface but decreased with increasing brush thickness. Furthermore, at equivalent polymerization times, lower density brushes were activated to a larger extent than the former, which reflects the different accessibility. The results described in this chapter may be valuable not only since they provide guidelines for the preparation of homogeneous functional polymer brushes, but also as they point towards the possibility to deliberately, via judicious choice of the reaction conditions, prepare non-uniformly modified polymer brush, which may possess new and unexpected properties.

### 6.4. Experimental

#### 6.4.1. Materials

Deuterated amino acids (D-10 leucine and D-3 serine) were purchased from Cambridge Isotopes Laboratories, Inc. All other chemicals were obtained from Aldrich and used as received unless otherwise stated. The polymerization inhibitor in 2-hydroxyethyl methacrylate (HEMA) was removed by passing the monomer through a column of

activated basic aluminum oxide. Organic solvents were dried by passage through two columns of molecular sieves using a Pure Solv™ 400 solvent purification system. For neutron scattering experiments, rectangular silicon substrates with a thickness of  $525 \pm 25$   $\mu\text{m}$  and dimensions of  $50 \times 75$  mm were used. The ATRP initiator, (6-(2-bromo-2-methyl)propionyloxy)hexylchlorosilane, was synthesized and immobilized onto the substrates as previously described.<sup>17</sup> The ATRP inactive, 6-((chloro(dimethyl)silyl)hexyl) pivalate, was synthesized via the same method using pivaloyl chloride instead of  $\alpha$ -bromoisobutyryl bromide.<sup>17</sup>

### 6.4.2. Methods

Neutron reflectivity experiments were performed at the Swiss Spallation Neutron Source (SINQ) at the Paul Scherrer Institute (Villigen, Switzerland) using the AMOR time-of-flight reflectometer (neutron wavelength range from 2 to 12  $\text{\AA}$ ).<sup>18,19</sup> The reflectivity was recorded at three angles of incidence ( $0.3$ ,  $0.9$  and  $1.9^\circ$ ) in order to cover a wide scattering vector ( $q$ ) range. The data were fitted with the MOTOFIT package,<sup>20</sup> using a 5 layer model: bulk Si /  $\text{SiO}_2$  / PHEMA / post-modified PHEMA / air. The scattering length density (SLD) profiles were obtained by fitting the experimental reflectivity data. The scattering data were modelled assuming that the concentration of the deuterated groups is highest at the brush-air interface and that for a given amino acid this maximum concentration was the same for all samples. The thicknesses of the various polymer brushes were extracted from the fitted reflectivity data. The volume fraction of deuterated compound at a distance  $z$  from the surface  $\phi(z)$  was determined from the scattering length density profile using:

$$\phi(z) = [\rho(z) - \rho_{\text{PHEMA}}] / [\rho_{\text{D}} - \rho_{\text{PHEMA}}]$$

in which  $\rho(z)$  is the SLD determined from the fit at the distance  $z$  of the surface,  $\rho_{\text{PHEMA}}$  is the SLD of PHEMA ( $0.990 \times 10^{-6} \text{ \AA}^{-2}$ ) and  $\rho_{\text{D}}$  is the SLD of the post-modified PHEMA at the brush-air interface; namely  $1.700 \times 10^{-6} \text{ \AA}^{-2}$  for the PHEMA post-modified with D-10 leucine and  $1.7265 \times 10^{-6} \text{ \AA}^{-2}$  for the PHEMA post-modified with D-3 serine (these values were determined experimentally from the fitting). The theoretical SLD values for PHEMA, D-10 leucine and D-3 serine post-modified PHEMA were estimated to  $1.10 \times 10^{-6} \text{ \AA}^{-2}$ ,  $2.320 \times 10^{-6} \text{ \AA}^{-2}$  and  $2.240 \times 10^{-6} \text{ \AA}^{-2}$  using the National Institute of Standards and Technology (NIST) SLD online calculator.<sup>21</sup> Initial polymer brush thickness were



measured by AFM, with a Veeco Multimode Nanoscope IIIa SPM controller in tapping mode using NSC14/no Al Mikromasch cantilevers, on patterned polymer brushes that were prepared as previously described.<sup>22</sup> UV-Visible absorbance spectra were recorded using a Varian Cary 100 Bio UV-Visible spectrophotometer at room temperature on polymer brushes coated on quartz substrates. Fourier transform infrared (FTIR) reflectance spectroscopy was carried out on a Nicolet Magna-IR 560 spectrometer equipped with a Micro Specular Reflectance accessory (Specac Ltd., UK). AFM measurement were performed on a Veeco Multimode Nanoscope IIIa SPM controller (Digital instruments, Santa Barbara, CA) operating in tapping mode and using NSC14/no Al Mikromasch (Tallinn, Estonia) cantilevers.

### 6.4.3. Procedure

#### 6.4.3.1. Surface-initiated atom transfer radical polymerization

Surface-initiated atom transfer radical polymerization (SI-ATRP) of 2-hydroxyethyl methacrylate (HEMA) was performed as previously described,<sup>23</sup> using H<sub>2</sub>O/HEMA/CuCl/CuBr<sub>2</sub>/2,2'-bipyridyl in a 400/60/1/0.3/2.8 molar ratio. The grafting density of the PHEMA brushes was varied by modifying the silicon substrate with a mixture of the ATRP initiator (6-(2-bromo-2-methyl)propionyloxy)hexylchlorosilane) and an equivalent ATRP passive molecule (6-(chloro(dimethyl)silyl)hexyl pivalate), as reported before.<sup>24</sup> Grafting densities are given as the volume percentage of the ATRP initiator modified organosilane in the mixture of chlorosilanes that was used to modify the silicon substrate. Throughout this chapter, PHEMA brushes grafted from surfaces that are modified only with the ATRP initiator are referred to as dense brushes. For the FTIR measurement, the polymer brush thicknesses were measured by AFM on patterned polymer brush that were prepared as previously described.<sup>22</sup>

#### 6.4.3.2. Post-polymerization modification reactions

Post-polymerization modification reactions were carried out following a procedure reported earlier by Tugulu *et al.*<sup>14</sup> First, the polymer brushes were incubated for a period of 1 hr in a THF solution containing *p*-nitrophenyl chloroformate (35 mM) and triethylamine in a 1/1 molar ratio. After that, the substrates were left for a period of 16 hrs

in an anhydrous DMF solution containing 1 mM of deuterated amino acid (D-10 leucine or D-3 serine) and 2.5 mM of 4-(dimethylamino)pyridine (DMAP). Any remaining carbonate groups in the polymer brush were quenched by exposure to a 0.5 M solution of ethanolamine in anhydrous DMF for 30 min and the samples were subsequently thoroughly rinsed with ethanol and methanol and finally dried under nitrogen.

## 6.5. References

1. Barbey, R.; Lavanant, L.; Paripovic, D.; Schüwer, N.; Sugnaux, C.; Tugulu, S.; Klok, H.-A. *Chemical Reviews* **2009**, *109*, 5437-5527.
2. Zhao, B.; Brittain, W. J. *Progress in Polymer Science* **2000**, *25*, 677-710.
3. Edmondson, S.; Osborne, V. L.; Huck, W. T. S. *Chemical Society Reviews* **2004**, *33*, 14-22.
4. Pyun, J.; Kowalewski, T.; Matyjaszewski, K. *Macromolecular Rapid Communications* **2003**, *24*, 1043-1059.
5. Brittain, W. J.; Minko, S. *Journal of Polymer Science Part a-Polymer Chemistry* **2007**, *45*, 3505-3512.
6. Ell, J. R.; Mulder, D. E.; Faller, R.; Patten, T. E.; Kuhl, T. L. *Macromolecules* **2009**, *42*, 9523-9527.
7. Tran, Y.; Auroy, P.; Lee, L.-T. *Macromolecules* **1999**, *32*, 8952-8964.
8. Gao, X.; Kučerka, N.; Nieh, M.-P.; Katsaras, J.; Zhu, S.; Brash, J. L.; Sheardown, H. *Langmuir* **2009**, *25*, 10271-10278.
9. Geoghegan, M.; Ruiz-Perez, L.; Dang, C. C.; Parnell, A. J.; Martin, S. J.; Howse, J. R.; Jones, R. A. L.; Golestanian, R.; Topham, P. D.; Crook, C. J.; Ryan, A. J.; Sivia, D. S.; Webster, J. R. P.; Menelle, A. *Soft Matter* **2006**, *2*, 1076-1080.
10. Spiliopoulos, N.; Koutsioubas, A. G.; Anastassopoulos, D. L.; Vradis, A. A.; Toprakcioglu, C.; Menelle, A.; Mountrichas, G.; Pispas, S. *Macromolecules* **2009**, *42*, 6209-6214.
11. Raynor, J. E.; Petrie, T. A.; García, A. J.; Collard, D. M. *Advanced Materials* **2007**, *19*, 1724-1728.
12. Petrie, T. A.; Raynor, J. E.; Reyes, C. D.; Burns, K. L.; Collard, D. M.; García, A. J. *Biomaterials* **2008**, *29*, 2849-2857.
13. Tugulu, S.; Silacci, P.; Stergiopoulos, N.; Klok, H.-A. *Biomaterials* **2007**, *28*, 2536-2546.
14. Tugulu, S.; Arnold, A.; Sielaff, I.; Johnsson, K.; Klok, H.-A. *Biomacromolecules* **2005**, *6*, 1602-1607.
15. Trmcic-Cvitas, J.; Hasan, E.; Ramstedt, M.; Li, X.; Cooper, M. A.; Abell, C.; Huck, W. T. S.; Gautrot, J. E. *Biomacromolecules* **2009**, *10*, 2885-2894.
16. Daillant, J.; Gibaud, A., *X-ray and neutron reflectivity: principles and applications*. 2nd ed.; Springer: Berlin, 2009.

17. See Chapter 3: Tuning the pH Sensitivity of Poly(Methacrylic Acid) Brushes.
18. Gupta, M.; Gutberlet, T.; Stahn, J.; Keller, P.; Clemens, D. *Pramana-Journal of Physics* **2004**, *63*, 57-63.
19. Clemens, D.; Gross, P.; Keller, P.; Schlumpf, N.; Könnecke, M. *Physica B* **2000**, *276*, 140-141.
20. Nelson, A. *Journal of Applied Crystallography* **2006**, *39*, 273-276.
21. <http://www.ncnr.nist.gov/resources/sldcalc.htm> retrieved on 05/04/2011.
22. Tugulu, S.; Harms, M.; Fricke, M.; Volkmer, D.; Klok, H.-A. *Angewandte Chemie International Edition* **2006**, *45*, 7458-7461.
23. Huang, W. X.; Kim, J.-B.; Bruening, M. L.; Baker, G. L. *Macromolecules* **2002**, *35*, 1175-1179.
24. See Chapter 3: Tuning the pH Sensitivity of Poly(Methacrylic Acid) Brushes.

## 7. Conclusions and Perspectives

This Thesis explored the possibility to use responsive polymer brushes for sensing applications. The polymer layers investigated were synthesized using surface-initiated atom transfer radical polymerization, a versatile method to create polymer brush with well defined architecture. This study built upon previous work on responsive polymer brush and focused on the synthesis of sensitive and selective layers able to probe pH, potassium and mercury (II) ions. This work demonstrated that polymer brushes can be used as active coating associated with different sensing techniques.

The first chapter has displayed an introduction to the field of polymer brushes and the second chapter presented a detailed review of the work done in the field of solvent responsive, thermoresponsive, pH- and ion-sensitive polymer brushes.

In the third chapter results from a systematic series of QCM experiments that were aimed at further understanding and adjust of the pH-induced swelling properties of poly(methacrylic acid) brushes were presented. Due to the inherent strong interpolymer interaction within a polymer brush, the pKa value of the surface-tethered PMAA was found to occur at a pH that was different from that of the equivalent free polymer in solution. This study also revealed that the denser and the thicker the polymer film, the greater the absolute pH-induced QCM response. And the apparent pKa of the overall polymer film was found to decrease with decreasing grafting density of the PMAA brush. The second part of this section has demonstrated the possibility to finely tune the pH-responsiveness of PMAA based brushes post-polymerization modification reaction.

Chapter four has presented the synthesis and characterization of benzo-15-crown-5 containing polymer brushes. These layers could be successfully use as the active coating in QCM-D based ion sensors since they present a high sensitivity and selectivity toward potassium ions. It was demonstrated that the crown-ether functionalized polymer brushes were able to detect potassium ions even in presence of aqueous solutions that contain a high excess of a lower affinity ions. Interestingly the selectivity of the sensor was not influenced by the overall brush thickness. The sensitivity (*i.e.* magnitude of the system response), however, could be optimized by adjusting the thickness of the polymer layer.

A peptide functionalized polymer brush that can be efficiently used to probe heavy metal ions was presented in chapter five. This section demonstrated that polymer brushes can be employed not only for QCM based sensor but can also be associated with

voltammetric based detection. The peptide decorated polymer brush coated gold electrode was found to exhibit a higher mercury sensitivity than the bar gold electrode, and in the concentration range investigated a linear relation was observed between the system response and the heavy metal ions concentration. The peptide functionalized polymer brush coated microelectrodes allow the detection of ion via a reproducible electrochemical process and this system allowed the detection of mercury ions down to the nanomolar concentration range.

The last chapter addressed a more fundamental question, and provided answers to some questions raised by the post-polymerization modification chemistry used in the previous chapters. The efficiency of the incorporation of deuterated amino acid into a PHEMA brush, via the NPC mediated post-polymerization modification, was monitored using neutron reflectometry. For dense polymer brushes, the post-polymerization modification of PHEMA brushes with D-10 leucine was constrained to the top layer of the polymer coating. Nevertheless, the penetration of D-10 leucine could be drastically improved by decreasing the polymer chains grafting density. The polymer brush architecture was not the only limiting factor for an efficient post-polymerization reaction and the final distribution of the amine within the polymer layer results of the sum of various effects including the non-linear NPC activation, steric hindrance issues as well as amine chemical structure.

To conclude this Thesis work clearly highlighted some of the unique features offered by surface-initiated polymerization techniques for the fabrication of sensitive and selective layers that can be use for the selective surface modification of various sensing devices. The use of SI-ATRP allows access to responsive layers that are covalently attached to the surface and with enhanced receptor surface concentrations as compared to SAM. The polymer brushes presented here may not only be useful for the development of QCM-D of voltammetric based sensors, but could also be attractive active layers for field-effect transistor or surface plasmon resonance based devices.

Schüwer Nicolas

Date of birth: 17-08-1984

Place of birth: Besançon (F)

Nationality: Swiss and French

Marital status: Married, one child

## ***Curriculum vitae***

### ***Education & Professional Experience***

---

- Since May 2007: Ph. D. Thesis in the group of Prof. H.-A. Klok, Polymers Laboratory, École Polytechnique Fédérale de Lausanne (EPFL) (Switzerland).  
Ph. D. thesis: “*Synthesis of Polymer Brushes for Sensing Applications*”.
- 2005 - 2007: Master studies in Physical Chemistry at Åbo Akademi (Turku, Finland)  
Master thesis: “*Exotemplating – a flexible route towards porous transition metal oxide spheres*”.
- 2003 - 2005: Bachelor studies in Chemistry at the University of Franche-Comté (Besançon, France).

### ***Technical Skills***

---

- Synthesis: surface chemistry and thin film characterization, organic and polymer synthesis, surface-initiated radical polymerization, clean room environment and neutron reflectometry experience.
- Analytical methods: atomic force microscopy (AFM), ellipsometry, contact angle goniometry, Fourier-transform infrared spectroscopy (FTIR), Raman spectroscopy, UV/Vis spectroscopy, X-ray photoelectron spectroscopy (XPS), thermogravimetric analysis (TGA), mercury porosimetry, nitrogen physisorption,

wide angle X-ray scattering (WAXS) and small angle X-ray scattering (SAXS), nuclear magnetic resonance, quartz crystal microbalance with dissipation monitoring (QCM-D), neutron reflectometry, cyclic and square-wave voltammetry.

## Languages

---

French: mother tongue.

English: written and spoken fluently.

German: basic level.

## Publications

---

- Schüwer N., Barbey R., Klok H.-A.; “*Diagnostic and Sensory Polymer Brushes*”. *Chimia* (2011), 65(4), 276.
- Schüwer N., Klok H.-A.; “*Tuning the pH Sensitivity of Poly(methacrylic acid) Brushes*”. *Langmuir* (2011), 27(8), 4789-4796.
- Schüwer N., Klok H.-A.; “*A potassium-selective quartz crystal microbalance sensor based on crown-ether functionalized polymer brushes*”. *Advanced materials* (2010), 22(30), 3251-3255.
- Barbey R., Lavanant L., Paripovic D., Schüwer N., Sugnaux C., Tugulu S., Klok H.-A.; “*Polymer Brushes via Surface-Initiated Controlled Radical Polymerization: Synthesis, Characterization, Properties, and Applications*”. *Chemical Reviews* (2009), 109(11), 5437-5527.
- Riachi, C., Schüwer, N., Klok H.-A.; “*Degradable Polymer Brushes Prepared via Surface-Initiated Controlled Radical Polymerization*”. *Macromolecules* (2009), 42(21), 8076-8081.
- Smått J.-H., Schüwer N., Järn M., Lindner W., Linden M.; “*Synthesis of micrometer sized mesoporous metal oxide spheres by nanocasting*”. *Microporous and Mesoporous Materials* (2008), 112(1-3), 308-318.
  
- Schüwer N., Geue T., Hinestrosa J. P., Klok H.-A.; “*Neutron Reflectivity Study on the Post-Polymerization Modification of Poly(2-hydroxyethyl methacrylate) Brushes*”. in preparation.
- Schüwer N., Tercier-Waeber M.-L., Danial M., Klok H.-A.; “*Peptide Functionalized Polymer Brushes for Voltametric Based Mercury (II) Detection*”. in preparation.